FINITE ELEMENT ANALYSIS OF

SHEAR-LOCALIZATION IN HIGH-SPEED MACHINING

OF AISI 4340 STEEL

By

PARAG KONDE

Bachelor of Engineering

University of Pune

Maharashtra, India

2000

Submitted to the Faculty of the
Graduate College of the
Oklahoma State University
in partial fulfillment of
the requirements for
the Degree of
MASTER OF SCIENCE
December, 2004

FINITE ELEMENT ANALYSIS OF

SHEAR-LOCALIZATION IN HIGH SPEED MACHINING

OF AISI 4340 STEEL

Thesis approved:

Dr. Ranga Komanduri

Thesis Advisor

Dr. Samit Roy

Dr. Hong Bing Lu

Dr. Gordon Emslie

Dean of the Graduate College

ACKNOWLEDGEMENT

I wish to express my sincere thanks to my parents for their confidence in me. I would like to thank them for their encouragement at times of difficulty, love and understanding.

This project has been funded by a grant from the Division of Design, Manufacturing and Industrial Innovation (DMII) of the National Science Foundation (NSF). I would like to thank Dr. George Hezelrigg of NSF for his interest in and support of this work.

I would like to express my sincere appreciation to my advisor, Dr. Ranga Komanduri for his intelligent supervision, constructive guidance, financial support, inspiration, motivation, and friendship. I would also like to express my sincere appreciation to Dr. Samit Roy for his invaluable guidance, support and direct contribution toward the completion of this dissertation. I would like to express my gratitude to Dr. Hong Bing Lu for providing encouragement and technical guidance throughout this study. I would like to express my gratitude to Dr. Bo Wang for his timely technical guidance and invaluable discussions that helped me at my trying times. I would like to express my sincere gratitude to Dr. Hou for his guidance in understanding the machining concepts and for providing information on the experimental results. Without their great friendship, understanding, and encouragement, it would be hard to believe that I could

come this far. My graduate studies under them have been a wonderful and unforgettable period of time in my life.

I wish to express my sincere gratitude to my research partners Mr. Dhananjay Joshi and Mr. Syed Kareem for their invaluable contribution, constructive criticism, discussions, encouragement, and friendship throughout this study. Very special thanks for their contribution in deriving the equations for Recht's failure criterion and applying the same in the finite element theory. Special thanks are due to Mr. Nitin Daphalapurkar for his technical assistance and friendship throughout this project. I wish to extend my gratitude to Mr. Chris Brand and Mr. Luis Zamorano of AdvantEdge for helping me with the use of software. Special thanks are due to my home mates for their encouragement and friendship.

Special appreciation is due to all research colleagues of our group for their support and helpful conversations who have made these years a pleasant experience.

Finally, I would like to thank the Department of Mechanical and Aerospace Engineering for providing me with the opportunity to pursue M.S at Oklahoma State University.

SUMMARY

The nature of chip formation in the machining of AISI 4340 steel is investigated by combining the effects of material properties, cutting speed, and tool geometry. Finite element analysis of the chip formation process gives a better understanding of the process and plays an important role in optimization of the machining process. Shear-localized chip is one of the major types of chips produced in the machining of hardened AISI 4340 steel at high cutting speeds. Machining involves large strains, high strain rates, and high temperatures concentrated in the shear zone. In this study, a new method is presented to investigate the shear-localization process in the machining of hardened AISI 4340 steel of different hardness values, viz., 215 BHN, 325 BHN, and 520 BHN. The cutting speeds used are 65 m/min and 488 m/min to machine AISI 4340 steel (215 BHN), 40 m/min, 125 m/min, and 275 m/min to machine AISI 4340 steel (325 BHN), 15 m/min and 61 m/min to machine AISI 4340 steel (520 BHN). The tool rake angles used for all the simulations are -15°, -5°, 15°, and 30° and the depth of cut used is 0.5 mm.

The complex process of shear-localization involves large strains, high strain rates, and high temperatures. To accurately simulate this process with finite element method, continuous remeshing and adaptive meshing is used to sidestep the extensive distortion of elements. Johnson-Cook's constitutive model which gives flow stress at various strains,

strain rates, and temperature is used. Recht's classical model for catastrophic shear instability is employed as a failure criterion to simulate the shear-localization in the chip. *AdvantEdge*™, a commercial explicit finite element code, is used for the simulations in this investigation. A user-subroutine incorporating radial return method to update the stresses and Recht's failure criterion is linked to the main code.

The model validated by comparing the simulation results with the experimental results published in the literature [9] and also with the results from another finite element code, ABAQUS for which conventional method of Johnson-Cook's constitutive and damage model was used. Various stages involved in the shear-localization process are presented. Finally, the effects of material hardness values, cutting speed, tool rake angle, and contact length on the chip morphology are presented.

The results of the present investigation agree reasonably well with the experimental results published in the literature [9] (error less than 11%). Therefore, the model developed in the present investigation is thought to lend a strong justification for the analysis and its potential benefits in analyzing and/or remedying problems associated with the shear-localized chip formation, temperature generated, plastic strains involved in the machining of AISI 4340 steel with different hardness values.

TABLE OF CONTENTS

LIST OF TABLES

Table **Page**

LIST OF FIGURES

Figure No. **Page**

NOMENCLATURE

σ	Normal stress (Pa)
τ	Shear stress (Pa)
ε	Normal strain
γ	Shear strain
σ_y	Initial shear yield strength (Pa)
ε_y	Initial yield strain
T	Temperature (°C)
κ	Thermal conductivity (W/m.K)
ρ	Density (N/m^3)
c	Specific heat (J/Kg.K)
W	Work equivalent of heat (J)
ν	Poisson's ratio
E	Elastic modulus (Pa)
v	Cutting speed (m/min)
α	Rake angle (°)
doc	Depth of cut (mm)
A	Yield stress constant (Johnson-Cook's material constant) (Pa)
B	Strain hardening coefficient (Johnson-Cook's material constant) (Pa)
n	Strain-hardening exponent (Johnson-Cook's material constant)
C	Strain rate dependence coefficient (Johnson-Cook's material constant)

m	Thermal-softening constant (Johnson-Cook's material constant)
T_m	Melting temperature (°C)
T_r	Reference temperature (°C)
$\bar{\sigma}$	Flow stress (Pa)
$\bar{\varepsilon}^p$	Equivalent plastic strain
$\dot{\bar{\varepsilon}}$	Strain rate (s^{-1})
$\dot{\bar{\varepsilon}}_0$	Reference strain rate (s^{-1})
λ and μ	Lame's constants
σ_m	Mean stress (Pa)
δ_{ij}	Kronecker's delta
H	Hardness slope
Ep	Plastic Modulus (Pa)
R^k	Radius of von Mises yield surface
Δλ	Strain increment
$\dot{\bar{\gamma}}$	Shear strain rate (s^{-1})
$\dot{\bar{\gamma}}_0$	Reference shear strain rate (s^{-1})
A	Unit area (mm^2)
RC	Recht's Criterion

CHAPTER 1

INTRODUCTION

Manufacturing is the process of transforming raw materials or semi-finished products into new form or finished products whether the work is performed by hand or by power-driven machine.

The operations performed in manufacturing by power-driven machines will fall in either of the two basic categories viz., metal forming process and machining process. In metal forming process the final part is manufactured by deforming the raw material to final shape at the same time conserving the mass. In the machining process, material is cut to the desired shape i.e. by removing the unwanted material. The metal forming processes include forging, casting, deep drawing, etc., and the traditional machining processes include turning, milling, sawing, grinding, etc. The non-traditional machining processes include electro-discharge machining (EDM), electro-chemical machining (ECM), laser machining, in which the material is removed with electrical, chemical, or optical assistance.

The primary intent of this investigation is to study high-speed machining of AISI 4340 steel of different hardness values from a continuum perspective through finite

element method and more specifically the mechanism of shear-localized chip formation process. It is also intended to study the effect of material properties and machining conditions on the same, and to correlate the simulation results with the experimental results published in the literature [2, 9 and 12].

In orthogonal machining, a layer of workmaterial ahead of the tool is plastically deformed and is separated to form the chip and the finished surface. Large stresses (shear and compression) exceeding the yield strength are set up ahead of the tool resulting in large deformations (shear strains of 2-5), high temperatures (500°C-1200°C), and high strain rates (10^4 s^{-1}– 10^5 s^{-1}). The type of chip formed is greatly influenced by the type and condition of the workmaterial being cut and the machining conditions used. The types of chip formed are described in some detail in the following section.

1.1 Classification of Metal Cutting Chips

The classical description of the chip types for most materials, as the cutting speed is increased within the conventional range, begins initially with discontinuous chip (Type 1), then a continuous chip with a built-up edge (Type 3) and finally a continuous chip (Type 2) [1]. The chip formation process is often affected by instabilities in the cutting process (both in the primary and in the secondary shear zones) which are further augmented by the dynamic response of part(s) of the machine tool structure, yielding chip segmentation [2]. The source of such instabilities can be varied depending upon the metallurgical condition and thermo-mechanical properties of the workmaterial under the conditions of machining. The end result is a cyclic, or serrated chip. Such chips, formed under different conditions and with different work materials, may appear similar to the

naked eye but are distinctly different in their origin and form. Based on the foregoing considerations, Komanduri and Brown [3], classified serrated, or cyclic chips as follows:

- segmental chip,
- wavy chip,
- shear-localized chip, and
- discontinuous chip.

The main objective for such a classification is to be able to identify by metallurgical examination of chips alone, the sources of instability, the nature of chip formation under these conditions, and the mechanics of such chip formation. In this way, corrective steps can be taken, when possible, to minimize the effect of instability causing cyclic chip formation, the latter being undesirable from the point of tool wear, tool life, surface finish, and accuracy of the machined part. These types of cyclic chips listed above, their causes, and the mechanisms of their formation are described in following.

Segmental chip:

This is a continuous chip with periodic but asymmetric variation in chip thickness. It forms in an unstable speed range, primarily due to instabilities in the primary and secondary shear zones, with the dynamic response of the machine tool structure playing a secondary but nonetheless significant role. The cutting process can be characterized by large strains (up to 10); low, oscillating shear angles (6 to 11 deg); large cyclic variations in cutting and thrust forces; and stick-slip friction on the rake face.

Wavy chip:

This type of chip forms as a result of regenerative chatter or self-excited vibrations. It is accompanied by cyclic variations in undeformed chip thickness as well as shear, rake, and clearance angles. Limited rigidity and low damping of the tool and/or work supporting system(s) are mainly responsible for this type of chip. As the cutting process oscillates close to the natural frequency of part of the machine tool system, this causes resonance and consequently large amplitude of vibration. The resulting chip is wavy but symmetric, resembling a harmonic or sine wave.

Shear-localized chip:

This form of chip is observed with certain difficult-to-machine materials, such as hardened AISI 4340 steel at high speeds. It is also formed in materials with poor thermal properties and high strength at elevated temperatures, such as titanium alloys and nickel-base superalloys. FEM simulation of shear-localization in the machining of AISI 4340 steel of different hardness values and a range of cutting speeds is the subject of this study. This type of chip serration is primarily due to plastic instability, intense localized deformation in the primary zone leading to intense shear between the segments. With AISI 4340 steel at high cutting speeds, the concentration of thermal energy in the narrow shear bands can be due to insufficient time for the dissipation of heat from these bands. The concentrated shear band in titanium is formed due to concentration of thermal energy in those bands because of its poor thermo-mechanical properties. Most of the segment is formed under very low strain by a gradual flattening (upsetting) of an inclined wedge ahead of the advancing tool. During this stage the deformation in the primary zone is

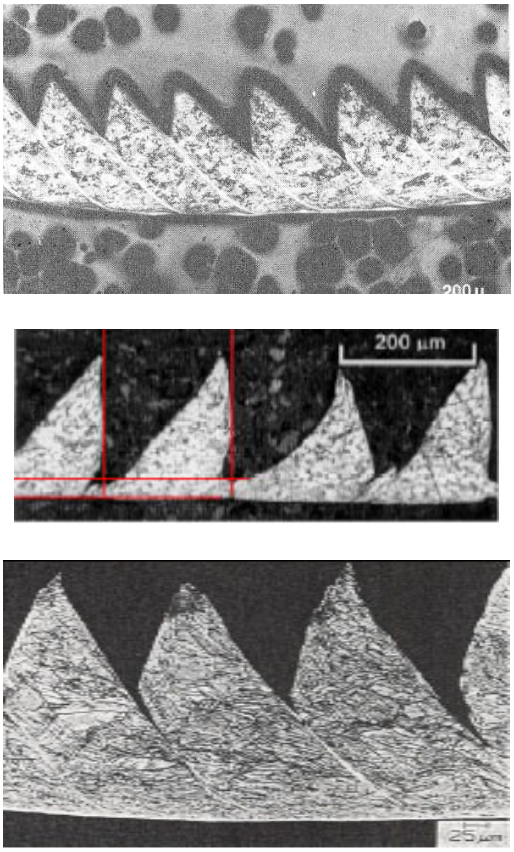

(a) AISI 4340 steel (325 BHN) (v = 275 m/min, doc = 0.5 mm, and α = -5°) [12]

(b) Ti-6Al-4V (v = 60 m/min, doc doc = 0.127 mm, and α = 15°) [50]

(c) Inconel 718 (v = 91.5 m/min, doc = 0.25 mm, and α = -15°) [61]

Fig. 1.1.1 Shear-localized chip formed in the machining of (a) AISI 4340 steel (325 BHN) [12], (b) Ti-6Al-4V [50], and (c) Inconel 718 [61] at different machining conditions.

highly localized. The initial contact of the chip with the tool face is very small and close to the apex of the tool. During the upsetting stage, intense shear takes place between the segment being formed and the one just formed. No secondary shear of the chip on the tool face seems to be operating. Consequently, no instability from the secondary shear zone arises or is expected for this type of chip formation. Also, the dynamics of the machine tool structure has very little influence on this type of chip formation, although a rigid system is recommended to avoid undue deflections and premature failure of the tool.

Discontinuous chip:

This type of chip is a special case of the catastrophic shear chip just discussed. In this case, complete separation of the segments occurs as a result of periodic rupture due to brittle fracture. Also, considerable deformation of the chip segment causes the maximum chip thickness to be quite large, unlike a catastrophic shear-failed chip, where most of the segment is relatively undeformed. This type of chip is more likely to form when machining brittle materials, such as cast iron, and with ductile materials at low cutting speed, large depths of cut, and low rake angles. The process of discontinuous chip formation is one of initial upsetting of the incoming work material ahead of the tool during which deformation is concentrated in a narrow band from the tool tip to the chip-workmaterial interface. This is followed by crack formation ahead of the tool tip due to tensile stress concentration followed by its rapid propagation leading to rupture along this shear surface. Unlike in catastrophic shear chips, there will be no rewelding of individual segments. Also, failure in the primary deformation zone is of brittle nature rather than ductile.

1.2 Brief Introduction to Metal Cutting

Metal cutting is a complex process involving large strains, high strain rates and high temperatures. The metal cutting mechanics involves forces, plastic deformation in the primary shear zone, and friction between the sliding chip and the tool face in addition to large strains, high strain rates, high temperatures, and tool wear. As the tool advances into the workmaterial, the workmaterial is plastically deformed in two regions viz., primary shear zone and secondary shear zone (Fig. 1.2.1). The primary shear zone

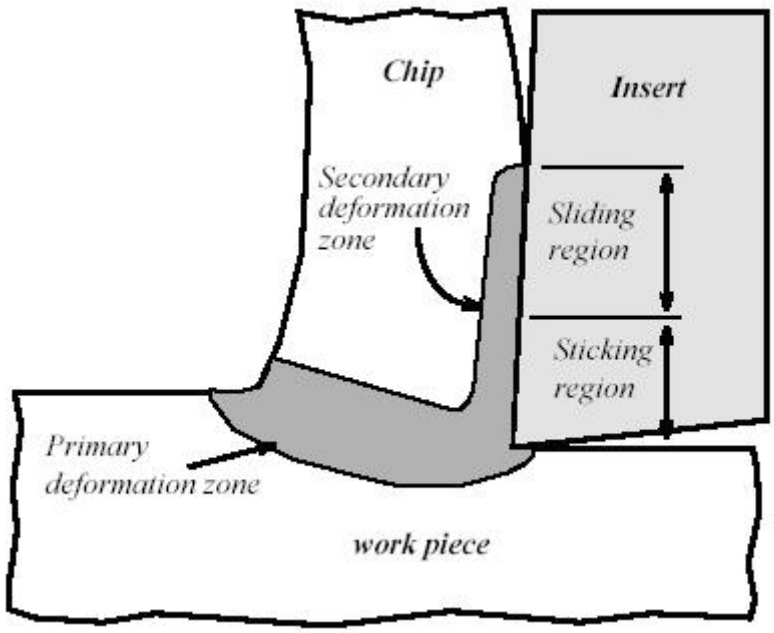

Fig. 1.2.1 Definition of primary and secondary shear zone and the sticking and sliding regions [4]

extends from the tip of the cutting tool to the junction between the deformed and undeformed workmaterial at the outer side. As the metal goes past the primary shear zone to form a chip, plastic deformation also occurs within the chip adjacent to the tool face in the secondary shear zone. This occurs when the frictional stress on the tool face reaches a value equal to the shear flow stress of the chip material. The secondary shear zone can be divided into sticking and sliding regions. In the sticking region the chip adheres to the cutting tool and internal shear takes place within the chip. In the sliding region there is a friction between the sliding chip and the tool face. In the primary shear zone, the heat generation is due to plastic deformation and in the secondary shear zone heat generation is due to friction between the chip and the tool face.

The chip formation process is similar in turning, milling, drilling, reaming, sawing, etc. So, the fundamental understanding of the chip formation process is

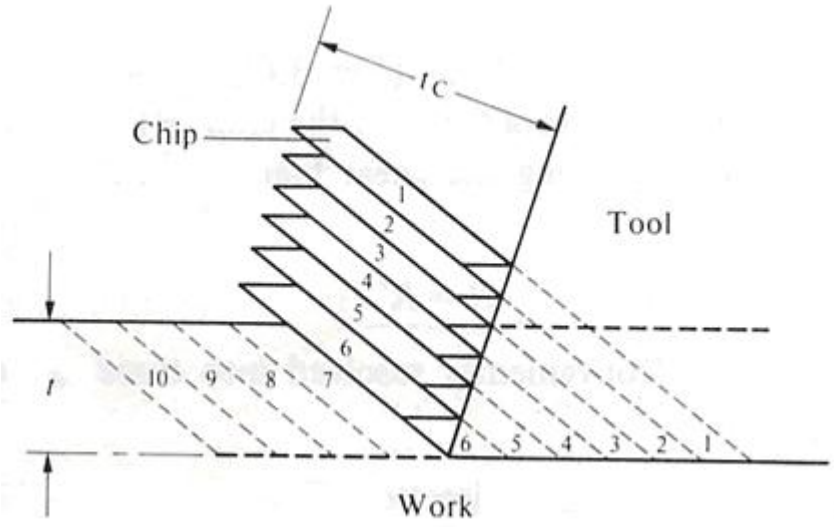

Fig. 1.2.2 Piispanen's idealized model of the cutting process [5]

paramount to increasing the efficiency of the process. Piispanen developed a card model [5] (see Fig. 1.2.2) which depicts the material cut as a deck of cards inclined to the free surface at an angle corresponding to the shear angle (φ). As the tool moves relative to the work, it engages one card at a time and causes it to slide over its neighbor. Although, this model does not give the exact picture it does contain the main concept in the chip formation process, namely, concentrated shear in a narrow region.

1.3 Introduction to the Finite Element Method

Finite element method (FEM) is a numerical analysis used for problems that may be too complex to solve by analytical methods. It breaks a complex structure into discrete components, resulting in an idealized structure that can be solved mathematically. These discrete components are called elements over which approximate functions are derived. These functions are derived using the idea that any continuous function can be expressed by a linear combination of algebraic polynomials, which are obtained by satisfying the governing equations, usually in a weighted integral sense over each element. Numerical

solution of the variables at specified points, called nodes, on each element and application of the calculated finite solutions to the entire geometry determines the solution to the problem.

After a CAD model is developed the material properties are defined. Then the next step in the finite element method (FEM) is discretization, a process of dividing the model into several small elements, connected with nodes. According to the requirements of the analysis, the type of element, such as triangular, brick or shell is selected. The stiffness matrix of the selected element describes the force-displacement relationship. The boundary conditions (mechanical and thermal constraints) are defined along with loading conditions, such as velocities, forces, pressure at the specified nodes. The boundary conditions and the loading conditions at the nodes, other than the specified nodes, are initially set to zero. Finally, the element descriptions, applied loads, and boundary conditions are assembled as a set of equations in matrix form. The form of a set of linear or non-linear equations for general static problem is as follows

$$\{F\} = \{U\}\,[K] \qquad 1.3.1$$

where U is nodal displacement vector, K is the stiffness matrix, and F is the force vector. However, for time dependent dynamic problems, the equation requires the form for a dynamic analysis, as represented in the following:

$$\{\mathrm{F}\} = [K]\{U\} + [M^1]\{\dot{U}\} + [M^2]\{\ddot{U}\} \qquad 1.3.2$$

where K is the stiffness matrix, U is the nodal displacement vector, which is updated as time changes, M^1 is the damping matrix, $\dot{U}$ are the nodal displacements with respect to first order time derivative (i.e. nodal velocity), M^2 is the mass matrix, and $\ddot{U}$ are the nodal displacements with respect to second order time derivative (i.e. nodal acceleration).

These set of equations are then solved numerically for the determination of unknown values. Then based on the resultant nodal displacements the stress, strain, and temperature rise are determined numerically.

The finite element formulation uses either the Lagrangian or the Eulerian formulation [6]. In the Lagrangian formulation attention is focused on how the velocity of a particular element varies with time and in Eulerian formulation attention is drawn to how velocities vary from element to element at the same time. In other words, in a Lagrangian referential, the computational grid deforms with the material where as in an Eulerian referential it is fixed in space.

In case of severe distortion of elements in high straining analysis, remeshing and adaptive meshing technique (discussed in detail in Chapter 5) can be used. This technique also helps in resolving fine-scale features in the solution.

1.4 Thesis Outline

The primary intent of this investigation is to study high-speed machining of AISI 4340 steel of different hardness values from a continuum perspective through finite element method and more specifically the mechanism of shear-localized chip formation process. It is also intended to study the effect of material properties and machining conditions on the same, and to correlate the simulation results with the experimental results published in the literature [2, 9, and 12].

In order to obtain an accurate prediction of the metal cutting process, the finite element model should be able to deal with the following physical phenomenon:

- Extremely large and localized deformation

- Contact conditions and friction
- Material exhibiting thermal softening effects
- Material exhibiting strain hardening effects
- Correctly identify the transition from continuous to shear-localized chip with change in the machining conditions.

In Chapter 2, literature pertaining to the experimental and analytical investigation is conducted by various researchers in the machining of AISI 4340 is reviewed. This is followed by a review of literature on finite element analysis of the machining of AISI 4340 steel. Finally a brief discussion is made of some important finite element analysis approaches for possible application to this investigation.

In Chapter 3, the objectives and approach of the present investigation are presented.

In Chapter 4, the thermo-mechanical properties of AISI 4340 steel which are responsible for the type of chip formed under different machining conditions are compared with respect to other materials. The thermo-plastic instabilities generated in the machining of AISI 4340 steel at high cutting speeds, effect of material hardness on the chip formation, and finally, the mechanism of shear-localized chip formation are discussed.

In Chapter 5, the development of finite element model along with the assumptions made and the user-subroutine are presented. Features, such as adaptive meshing and contact generation are discussed. Johnson-Cook constitutive model and the stress update model used in the user-subroutine are discussed. The derivation of the terms in Recht's

classical model of catastrophic shear instability in metals, used here as a failure criterion, is given along with the user-subroutine.

In Chapter 6, material properties and machining conditions used for all the simulations are given. The model validation is done by comparing the simulation results with the experimental results published in the literature [9] and also by comparing with the results from conventional model developed in ABAQUS. Catastrophic shear instability observed in the simulation of the machining of AISI 4340 steel is discussed. This is followed by a discussion on the influence of material hardness, cutting speed, and rake angle on the chip formation process in the machining of AISI 4340 steel. A discussion on the influence of contact length on the chip morphology is also presented.

In Chapter 7, the conclusions drawn from the simulation results as well as the future work are presented.

CHAPTER 2

LITERATURE REVIEW

2.1 Introduction

Chapter 1 gave an overview of the machining process and the finite element method as applied to machining. Machining involves large strains, high strain rates, and high temperatures concentrated in the primary shear zone. To understand this complex process, considerable experimental work has been done. The most common methods used are *in situ* machining inside a SEM, high-speed photography under actual cutting conditions, use of quick stop device while cutting is in progress and metallurgical analysis of the chips formed in cutting using optical microscope. Considerable progress has been made in understanding the metal cutting process with these methods. An alternate tool to investigate the machining process is finite element analysis (FEA), which has proven to be an effective technique. However, the FEA results have to be validated with the results published in the literature or by selective experimentation to gain confidence in the simulation results. The subsequent sections in this chapter provide a brief literature review of the analytical, experimental, and finite element method pertaining to orthogonal metal cutting process.

2.2 Analytical Studies on Shear-localization in Machining

To predicted onset of the shear-localization in machining, several analytical studies have been done. Analytical models were developed on the basis of the thermo-mechanical properties of material and machining conditions used. The first to do this was Recht [8] who recognized shear-localization as a process of 'catastrophic thermo-plastic shear' driven by softening effects of deformation heating.

Recht [8] proposed that in the machining of ductile metals, the plastic deformation is slow at low cutting speeds compared to high cutting speeds. Therefore, the material strain-hardens and the process is essentially isothermal. Initially, plastic shear strain is restricted to a few weak shear planes within the material. Strain-hardening strengthens the weak material in these zones and the burden of strain is distributed throughout the material. If strain-hardening did not occur, deformation would remain localized. He further explained the cause of the catastrophic slip in the chip at high cutting speeds. When the cutting speed is high, the plastic deformation is rapid which causes the heat to generate locally establishing temperature gradients. If the rate of weakening of material due to temperature increase exceeds or equals the rate of increase in strength of material due to the effects of strain-hardening, the material continues to deform locally. This process leads to catastrophic thermo-plastic shear in the machining of hardened AISI 4340 steel and other difficult-to-cut materials. He developed a criterion for catastrophic slip considering the shear strength of material to be a function of strain and temperature. This criterion is used in this investigation to simulate shear-localized chip formation process.

Semiatin and Rao [10] proposed an analytical model which was capable of a quantitative prediction of the cutting speeds at which shear-localization begins in the machining. The model incorporates the material properties and machining conditions which influence heat transfer within the chip and the remainder of the workpiece. The model is given as follows

$$\alpha = -\sqrt{3}\left\{\frac{1}{\tau}\left(\frac{\partial \tau}{\partial \gamma}\right)_{\dot{\bar{\gamma}}} + \left(\frac{\partial \tau}{\partial T}\right)_{\gamma,\dot{\bar{\gamma}}} \frac{1}{\tau}\frac{dT}{d\gamma}\right\} \Big/ m \qquad (2.1.1)$$

where, the numerator denotes the normalized flow softening rate and the denominator '*m*' denotes the strain rate sensitivity. Here, α is the flow-localization parameter. According to this model the shear-localization in the metal cutting is imminent if the value of the flow-localization parameter (α) is equal to or greater than 5. They applied this model in predicting the critical cutting speed in the machining of AISI 4340 steel (325 BHN). The critical cutting speed obtained with this model was 60 m/min when the tool rake angle of -5° and depth of cut of 0.5 mm was used. The resultant critical cutting speed obtained with this model is different from the critical cutting speed (275 m/min) obtained in experiments as reported in the literature [2]. Semiatin and Rao [10] took material properties and heat generation, heat conduction, and heat transport into consideration. But, they excluded the dynamics of the machine tool structure, and in particular the compatibility between the rate at which the cutting forces decreases during instability and flow-localization in the chip and rate at which the machine tool itself can unload. Therefore, the estimates of the critical cutting speeds obtained from the model are approximate. They also explain that, in view of its success in predicting flow-localization in forging, it was attempted to apply to the problem of shear-localization in the metal

cutting. But, the results obtained with this model when applied to metal cutting, are found to be unreasonable.

Xie *et al*. [11] used the flow-localization criterion developed by Semiatin and Rao [10] to predict the onset of instability in the chip. They established a relationship between the flow-localization parameter, α, and the cutting conditions. They proposed that a critical value of the combination of cutting speed (v) and feed rate (f) can be found with respect to a corresponding flow-localization parameter value that may lead to the onset of shear instability in the machining process. They referred the value of 'vf' as 'chip load'. According to Semiatin and Rao [10], the shear-localization in the metal cutting is imminent if the value of the flow-localization parameter (α) is equal to or greater than 5. To verify this, Xie *et al*. [11] conducted experiments on AISI 4340 steel, AISI 1020 steel, AISI 304 stainless steel, and Ti-6Al-4V and determined the value of chip load. They used this value of chip load in the flow-localization criterion to determine the value of flow-localization parameter. The value of flow-localization parameter obtained for AISI 4340 steel, AISI 1020 steel, AISI 304 stainless steel, and Ti-6Al-4V was 5.23, 5.12, 4.60, and 4.41, respectively. This shows that the flow-localization value slightly varies around 5.0 for different materials, which reasonably agrees with the proposition made by Semiatin and Rao [10]. But, as explained by Semiatin and Rao [10] the prediction of cutting speed by this criterion is approximate.

Komanduri and Hou [12] analyzed the cyclic chip formation in machining to identify the possible heat sources contributing to the temperature rise in the primary shear

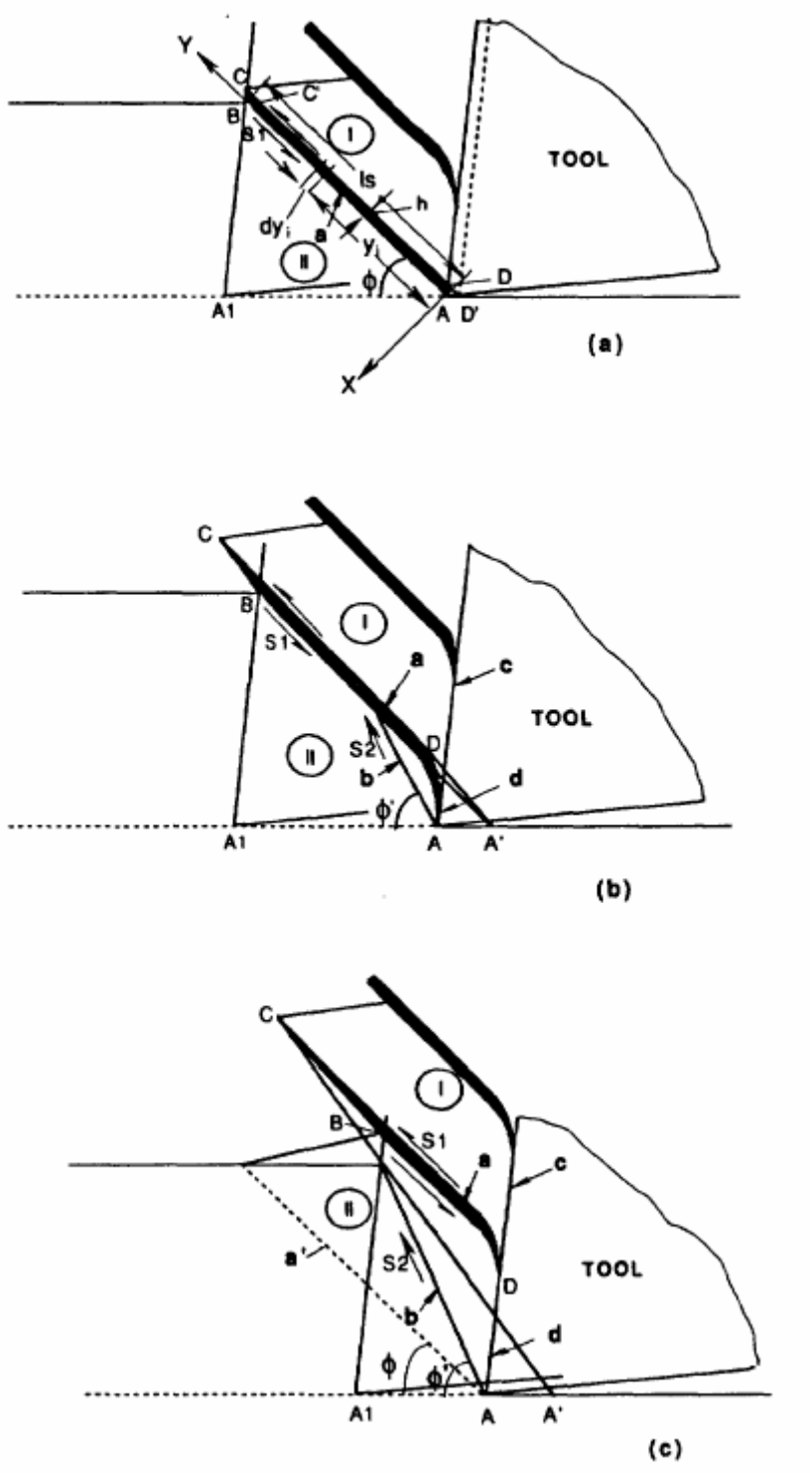

Fig 2.2.1 Schematic of the different stages of shear-localization in machining showing various heat sources responsible for the temperature rise in the shear band [12]

zone. The temperature rise in the shear band due to each of the heat sources was calculated using Jaeger's classical theory for stationary and moving heat sources. They identified temperature rise in the shear band due to four primary and preheating effects of these four heat sources. The four primary heat sources identified are (1) the shear band heat source, *a*, where intense shear takes place between the segments [Fig. 2.2.1(a)]. This heat source is the predominant contributor to the temperature rise in the shear band especially at the higher cutting speeds; (2) the secondary shear band heat source *b* [Figs. 2.2.1(b) and (c)] which forms during the upsetting stage of the cyclic chip formation; (3) the frictional heat source, *c* [Figs. 2.2.1(b) and (c)] between the segment already formed and the rake face of the cutting tool, and (4) frictional (intense shear) heat source *d* [Fig. 2.2.1(c)] between the segment just being formed and the tool face during the upsetting stage of the following segment. They pointed out that the first primary shear band heat source is the major contributor (~ 81%) at a cutting speed of 500 m/min, followed by its image heat source (~ 6.5%) and the rest of the heat sources contributing ~ 12.5%. They showed that the influence of each of the heat source will be different depending on the cutting speed. Based on this temperature rise, Recht's classical model of catastrophic shear instability was applied by predicting analytically the conditions for the onset of shear-localization. Under the combined effect of thermal softening and strain hardening, the strength of material is calculated in the shear band. This is compared with the yield strength of the material to predict the thermal softening initiation and dominance. If the strength in the shear band is lower than the yield strength of the material, the thermal softening predominates and the shear-localization is imminent. Based on this model they reported that cutting speed for the onset of shear-localization can be predicted.

Komanduri and Hou [12] suggested that serrations in chip while machining difficult-to-cut material is due to the onset of thermal instability in the cutting process which results from competing thermal softening and strain-hardening in the primary shear zone. They explained that the shear-localization mechanism in machining AISI 4340 steel at high cutting speeds and titanium alloy at low to moderate cutting speeds is similar, but with a basic difference. They suggested that the formation of adiabatic shear bands in AISI 4340 steel at high cutting speeds is due to less time available to dissipate the heat generated in the shear zone. Whereas, in titanium alloys the adiabatic shear bands are formed due to its poor thermal properties (low thermal conductivity and low specific heat) because of which there is concentration of thermal energy in these bands.

2.3 Experimental Studies on Shear-localization in Machining

Advances in the mechanics of shear-localization in the machining of titanium alloys (Ti-6Al-4V) is due to the pioneering work of Shaw *et al*. [7]. This research has led to a better understanding of the chip formation process in the machining of some other difficult-to-machine materials, such as hardened steels (e.g. AISI 4340 steel) and nickel-base superalloys (e.g. Inconel 718) yielding cyclic chips.

Matsumoto *et al.* [13] conducted machining studies on AISI 4340 steel with different hardness values. The aim of their study was to investigate the effect of change in the material hardness value on the chip morphology. They used cutting speed of 91.4 m/min, depth of cut of 0.15 mm, and feed rate of 0.89 mm/rev for all the experiments. The used AISI 4340 steel with hardness values ranging from 29 HRC to 57 HRC. Chip morphology study using scanning electron microscopy (SEM) showed that continuous

chip was produced when machining AISI 4340 steel (29 HRC) and segmented chip was produced when machining AISI 4340 steel of hardness above 50 HRC. They attributed the transition in the chip morphology from continuous to segmental phenomenon to the two conflicting factors affecting the cutting mechanism. One is the increase in yield strength due to the increase in steel hardness and the other is the reduction in the yield strength due to the cutting heat generated. This effect of material hardness of AISI 4340 steel on the chip morphology is investigated in the present study.

Lemaire and Backofen [14] also studied the differences between the segmental chip and the shear-localized chip while cutting Fe-0.52C-18.5Ni martensitic steel. Even though they used the work material other than AISI 4340 steel and machined at low cutting speed (0.333 in/sec) which is not in the interest of the present study, the observations done by them are note worthy. In the tests they conducted the rake angle was varied from 0 to 20°, cutting speeds from 0 to 0.333 in/sec, and depths of cut from 0 to 0.012 in. At lower depths of cut (~ 0.012 in) and at very low cutting speeds (~ 0.096 in/sec) continuous chip were produced. Whereas, at remaining cutting conditions, the chips produced was referred to as discontinuous chip with three subtypes of chip. The first subtype was segmental chip, which was characterized by irregular fracture along sheared edge of the chip accounted for chip separation. The second subtype of chips was irregular in the lower portion of the sheared edge, near the cutting tool, but was smooth and followed a thin band of austenite along the remainder of the sheared edge. Subtype three chips was shear-localized chip containing a band of austenite along the complete length of the sheared edge and no separation of segments was observed. Lemaire and Backofen attributed the formation of shear-localized chip to the thermal softening during

the machining. They explained that the flow stress of the material drops with increase in temperature in the shear zone, causing the material to shear easily locally.

Komanduri *et al.* [2] conducted extensive high-speed machining studies and investigated the mechanism of shear-localization in high-speed machining of some difficult-to-machine materials. They conducted machining tests on AISI 4340 steel (325 BHN) at various speeds (up to 2500 m/min) and examined the longitudinal midsections of the chips using optical microscopy. They found the chips to be discontinuous below 30 m/min and continuous from 30 to 60 m/min. At a speed of 125 m/min, the deformation of the chip was found to be inhomogeneous on a gross level with two wide regions, one where the deformation is very high (i.e., between the segments) and the other where the deformation is relatively low (i.e., within the segments). At cutting speeds above 275 m/min, they observed fully developed catastrophic shear bands in the chips separated by large areas of relatively less deformed material, similar to that when machining titanium alloys. Also, as the cutting speed increases, the extent of contact between the segments was found to decrease rapidly. At speeds of 1000 m/min and above, due to rapid intense, localized shear between the segments, these segments were found to separate completely as isolated segments instead of being held intact as a long chip. The speed at which this decohesion occurs was found to depend upon the metallurgical condition of the steel machined and its hardness. This will be reconfirmed in this investigation using numerical simulations.

Komanduri, Flom and Lee [15] reported important observations made at high and ultra high-speed machining of AISI 4340 steel. Their main goals were to increase the productivity through higher metal removal rates and examine the effect of increase in

cutting speed on chip morphology. They showed that temperature at the tool-chip interface increases with speed approaching the melting point of the workpiece material. They pointed out that the cutting forces decrease with increasing speed to a minimum at a speed characteristic of AISI 4340 steel for a given metallurgical condition; beyond which the forces tend to increase slowly. In the case of AISI 4340 steel (215 BHN), the forces decrease with increasing speed until about 1500 m/min at which point the forces begin to increase with speed. Whereas, for AISI 4340 steel (275 BHN), the forces tend to increase slowly with speed above 6400 m/min. They also pointed out that decrease in force with speed observed does not mean a lowering of horsepower requirements. However, one can take advantage of the lower forces at higher speeds (especially with higher chip loads). At very high speeds, momentum forces become significant. They found from the experiments that although the shear-localized chip is preferable for easier chip disposal, especially at higher speeds where individual segments of a chip are completely separated, formation of the shear-localized chip has not generally been accompanied by reduction of tool wear at high speeds. They concluded that higher speeds are limited by rapid tool wear, but higher removal rate can be achieved by increasing the depth of cut instead of cutting speed.

2.4 Finite Element Analysis of Shear-localization in Machining

Advancement in the computer technology and finite element method has enabled the prediction of chip formation, tool wear, and distribution of residual stresses in the machining of various materials numerically. The literature available on finite element analysis of chip formation process, tool wear, and distribution of residual stresses in

machining is vast. So, as the focus of the present investigation is limited to the shear-localization in the machining of AISI 4340 steel of different hardness values, the literature pertaining only to the finite element analysis of the machining of AISI 4340 steel is discussed, followed by a discussion of some important finite element analysis approaches referred to in the present investigation.

Eu-Gene Ng *et al.* [16] presented a 3D model of high-speed machining of AISI 4340 steel (52 HRc) using ABAQUS/Explicit. They used eight node reduced integration 3D elements (C3D8RT) to model the tool and the workpiece. For the separation of chip from the workpiece, a shear failure criterion was employed. Here, two-node element link is used at the predefined separation path, and these elements are deleted when the effective plastic strain reaches the damage plastic strain value. The material model used was Johnson-Cook's constitutive model. They also made a first attempt to employ Recht's criteria to simulate catastrophic chip segmentation. They also took the crack initiation at the free surface of the chip when machining hardened steels up to 62 HRc

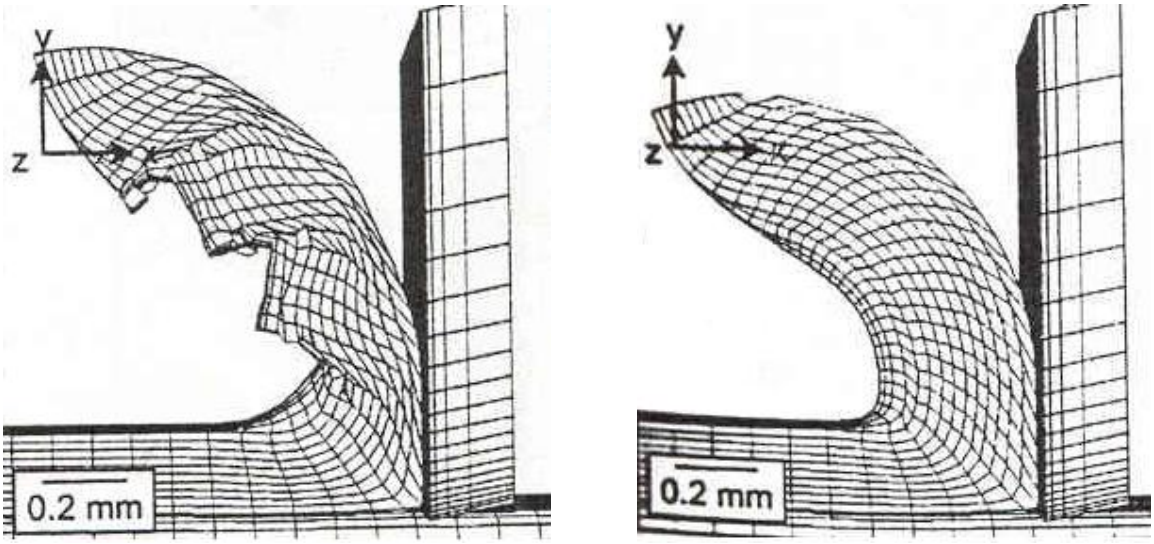

(a) (b)

Fig. 2.3.1 Resultant chips observed (a) with, and (b) without the catastrophic slip and crack propagation module [16]

into consideration. The Johnson-Cook's damage model is used to predict the crack propagation in the chip. Due to frictional instability at the tool-chip interface, regions of high and low plastic strain were observed. AISI 4340 steel (52 HRc) was machined at a cutting speed of 400 m/min and depth of cut of 0.2 mm with a tool rake angle of 0°. The width of cut used was 1 mm. When the authors simulated the machining process with the catastrophic slip and crack propagation module, shear-localized chip was observed to form [see Fig. 2.3.1(a)] and when simulated without this module, continuous chip was observed to form [see Fig. 2.3.1(b)].

The idea of simulating with and without the catastrophic slip and crack propagation modules was to examine the suitability of the developed module to result into correct chip morphology for the given machining conditions. The difference in results with and without the catastrophic slip and crack propagation module as compared to experimental results was found to be 13% and 36%, respectively. Temperature difference on the workpiece surface observed was less than 50°C for both continuous and segmental chip formation, even when a higher temperature was generated in the shear zone with segmental chip. This was attributed to the steeper shear angle in segmental chip than in continuous chip, which reduced the proportion of heat energy flowing into the workpiece. The simulations were also carried out for oblique metal cutting with tool inclination angle of 5° with the same machining conditions as used for orthogonal metal cutting. The temperature generated during oblique cutting was observed to be higher compared to orthogonal machining, which was due to larger width of cut requiring more energy input to shear the workpiece material and higher plastic strain magnitude.

The use of Recht's criterion in conjunction with Johnson-Cook's damage model is more suitable for simulating discontinuous chip rather than shear-localized chip. Because in the discontinuous chip formation process the initial upsetting of the incoming workmaterial ahead of the tool during which deformation is concentrated in a narrow band (similar to an elastic hinge) from the tool tip to the chip-workmaterial interface [3]. This is followed by crack formation ahead of the tool tip due to a tensile stress concentration followed by its rapid propagation leading to rupture along this shear surface, which is simulated by Johnson-Cook's damage model. Therefore, as in the present investigation the shear-localization is assumed take place only due to thermal softening and shear concentration in the primary shear zone with no crack formation, only Recht's criterion is employed.

Marusich and Ortiz [17] developed a Lagrangian finite element model of orthogonal high-speed machining of AISI 4340 steel. They developed an algorithm which incorporated features, such as adaptive meshing and continuous remeshing, fracture model for crack initiation and propagation in the regime of shear-localized chip. The predetermined line of node separation used by many researchers was not considered, which made this model more realistic. Here, the transition in chip morphology was analyzed with change in cutting speed, rake angle, and depth of cut. A continuous chip was reported when a tool (analytically rigid) with rake angle 30° is used at a cutting speed of 1800 m/min with 0.25 mm depth of cut (see Fig. 2.3.2). By changing the tool rake angle to -5°, cutting speed to 600 m/min, and depth of cut to 0.5 mm, shear-localized chip was reported. Further, by changing the cutting speed to 1200 m/min and keeping rest of the parameters the same as for the shear-localized chip, the formation of isolated

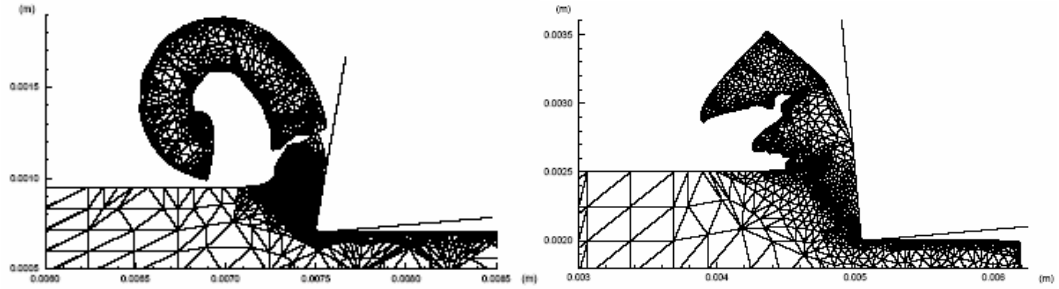

(a) α = 30°, v = 1800 m/min, doc = 0.5 mm (b) α = -5°, v = 600 m/min, doc = 0.5 mm

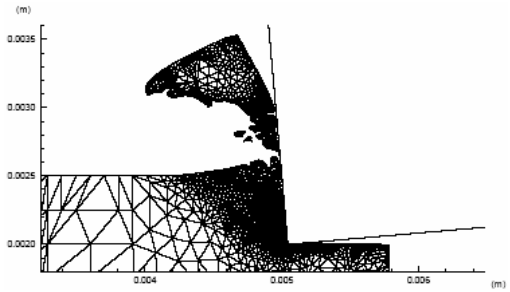

(c) α = -5°, v = 1200 m/min, doc = 0.5 mm

Fig. 2.3.2 Transition in chip morphology observed in the machining of AISI 4340 steel at different cutting speeds and rake angles. The chip observed is (a) continuous, (b) shear-localized, and (c) isolated segments [17]

individual segments of the chip was reported. Here, the chip morphology results are in good agreement with the experimental results (Komanduri *et al.* [12]), but the machining parameters used are different from those reported in the experiments [12]. The cutting speeds used by Komanduri *et al.* [12] are 31-61 m/min for continuous, 244 m/min for fully developed shear-localized chip, and 976 m/min for isolated individual segments of chip. Also, the tool rake angle used for all types of chips was -5°.

Guo and Yen [18] investigated high-speed machining of AISI 4340 steel (325 BHN) forming isolated individual segments. They refer to this kind of chip as discontinuous chip, whereas in the literature this kind of chip morphology has been referred to as isolated individual segments produced at high-speed machining [2, 12 and

19]. The material was cut at a cutting speed of 1000 m/min and with a rake angle of -5°. Johnson-Cook's material and damage model were used in combination to simulate the crack initiation and propagation. A difficulty from the FEM point of view is the definition of the tool-chip contact for the discontinuous chip formation process, where frequent breakage of segments produce new elements to expose to the tool rake face. To solve this problem they tracked the location of the element during the simulation process to establish contact between the tool and the chip. They applied Coulomb's friction law and shear stress limit to model the sticking and sliding of the chip on the tool rake face. The coefficient of friction used was 0.1, which seems to be too low for high-speed machining. The shear stress limit used was 457 MPa. Arbitrary Lagrangian-Eulerian (ALE) approach was employed. They used the element deletion method to initiate and propagate a crack when the Johnson-Cook's damage failure criterion is met. ALE adaptive meshing was used during machining simulations to maintain high-quality mesh and prevent the analysis to terminate due to high element distortion. When the failed element is deleted, the method of converting adaptive nodes to non-adaptive at the interface between failed and non-failed elements is a note worthy aspect of this simulation. The authors have done only qualitatively comparison with the chip found in the literature [2]. They attribute discontinuous chip formation at high cutting speeds (1000 m/min) to adiabatic shearing and crack formation in the primary shear zone. Whereas, in the literature, this type of chip was observed to form due to catastrophic shear instability with no crack formation in the primary shear zone [2]. The primary reason for the formation of this type of chip was explained in Ref. 2 as due to rapid

intense, localized shear between the segments, where the segments are found to separate completely as isolated segments instead of being held intact as a long chip.

In finite element simulation of machining, the most challenging part is to separate the chip from the workpiece. Several chip separation criteria have been advanced in the literature to facilitate the simulation of the metal cutting processes [20-30]. Strenkowski and Carroll [20] developed an element-separation criterion based on effective plastic strains applied at the tool tip region of the workpiece. They used a general purpose finite element code NIKE2D and employed an updated Lagrangian formulation to model the orthogonal metal cutting process. They used a parting line along the anticipated cut surface of the workpiece. This was to allow the upper surface of the workpiece to separate and form a chip as the tool advanced through the workpiece. This parting line capability compares effective plastic strain at the node closest to the tool tip with a specified rupture value for the workpiece material. When the effective strain exceeds the failure criterion, those nodes are allowed to separate from the workpiece. In this way, these nodes are free to move up the tool rake face. Strenkowski and Carroll [20] employed this technique to analyze machining of 2024-T4 aluminum alloy with a tool angle of 20° and a friction coefficient of 0.3. They varied the separation criteria over the range of 0.25 to 1.0, which had a little effect on the chip geometry and tool forces, but had significant effect on the residual stresses in the workpiece. The authors pointed out that, an effective plastic strain criterion for separation is not readily available for most materials. However, the mean shear stress on the shear plane can be approximated from the computed tool forces and by comparing the estimated mean shear stress with the yield shear strength of the material, a determination can be made as to whether the correct

value of the separation criterion has been made. The authors pointed out that with increase (within the range of 0.25 to 1.0) in the value of the separation criterion, larger residual stresses in the workpiece surface were reported. The reason for the sensitivity of the residual stresses to the separation criterion is that this criterion is applied to only to the node closest to tool tip. Later on this very node becomes part of the machined surface once the tool tip has passed by. By constraining this node to remain tied to the workpiece for a longer time, cutting tool forces are transmitted to the sub-surface of the machined workpiece, resulting in the observed residual stresses. In contrast, the tool forces were unaffected by the separation criterion because the tool forces were found by averaging nodal forces over the entire rake face and due to which the effect of the tool tip node is significantly lessened. A similar criterion was used by Carroll and Strenkowski [21] for ultraprecision machining of aluminum 2024-T361 using single point diamond tool material.

Shi *et al.* [22] used parting line chip-separation criterion similar to that used by Strenkowski and Carroll [20] with the basic difference that they used stress-based criterion available in ABAQUS code to effective plastic strain criterion used by the latter. They used this to study the effect of friction on thermo-mechanical quantities, such as the maximum temperature, the contact length, the shear angle, and the cutting force in orthogonal machining of AISI 4340 steel. Tool rake angles ranging from 15° to 30° and friction coefficients ranging from 0.0 to 0.6 were considered for the simulation. The stress-based criterion states that chip separation occurs when the stresses along the cutting path reach a critical combination at a specified distance in front of the tool tip. Pairs of nodes were initially bonded along the predetermined cutting line defined by

contact surfaces. When the chip separation criterion is met at the specified distance (size of an element: 50.8 µm) in front of the tool tip, the pair of finite elements above and below the contact surface immediately before the tool tip will separate. To simulate the sticking-sliding interaction of chip along the tool rake face, modified Coulomb's friction law was implemented [23]. According to modified Coulomb's friction law, there will be no relative motion between the chip and the tool rake face when the chip shear stress parallel to the tool rake face is less than the critical friction stress (549 MPa for AISI 4340 steel), i.e. the contact point is in the sticking region. On the other hand, if the chip shear stress exceeds the critical friction stress, then relative motion occurs between the chip and the tool, i.e. the contact point is in the sliding region. The resultant chip observed was continuous when machined at 152.4 m/min. Tool-chip contact length, shear angle, cutting force, and maximum temperature rise were all observed to be dependent on the coefficient of friction and rake angle. With fixed rake angle and with an increase in friction coefficient, the chip curvature and the shear angle were reported to decrease, while the contact length, the cutting force, and the maximum temperature were reported to increase. Also, for a fixed friction coefficient and with an increase in the rake angle, the shear angle was reported to increase, while the cutting force and the maximum temperature were reported to decrease.

Although, the parting line technique in conjunction with the comparison of effective plastic strain at the node closest to the tool tip [20 and 21] or with the stress-based criterion at the specified distance ahead of the tool tip [22] is relatively easy to simulate, they are completely arbitrary and possess a few short comings [16]. The use of parting line limits the modeling of the tool rake angle i.e. large negative rake angle

cannot be used. The node separation on the parting line at a small distance from the cutting edge results in a small crack in the workpiece material ahead of the tool. The presence or absence of the crack ahead of the cutting edge is questionable since the hydrostatic stress close to the cutting edge is compressive, and cannot produce tensile rupture of the workpiece material. Also, the values of stress and strain are determined as the tool moves against the workpiece. Also, with the use of these criteria, the characteristic of the finished surface will be decided by the criterion and not by the machining conditions, due to which the effect of cutting conditions, and consequently of residual stress will be eliminated.

Shih and Yang [24], Shih [25-27], and Komvopoulos and Erpenbeck [29] used a chip separation criterion based on the distance in the cutting direction between the tip of the cutting tool and the finite element nodal point located immediately ahead of the tip. During the cutting process, distance between the tool tip and the finite element nodal point (D_S) located immediately ahead of the tip is checked with the predefined value (D_{SL}) after every incremental movement of the cutting tool [see Fig. 2.3.3(a)]. The elements in front of the tool separate when the distance measured (D_S) is less than the predefined distance value (D_{SL}); thus the criterion is said to meet. The value of D_{SL} selected by Shih [25-27] was 3 μm, which is arbitrarily determined from trial runs which is one of the shortcomings of this criterion. This value of D_{SL} must be small enough to simulate the cutting condition and high enough to avoid numerical instability. Shih [25-27] has developed an elastic-viscoplastic finite element formulation to implement large strain and high strain-rate plastic deformation in the machining of AISI 1020 carbon

steel. He also developed an unbalanced force reduction method and sticking-sliding friction modeling

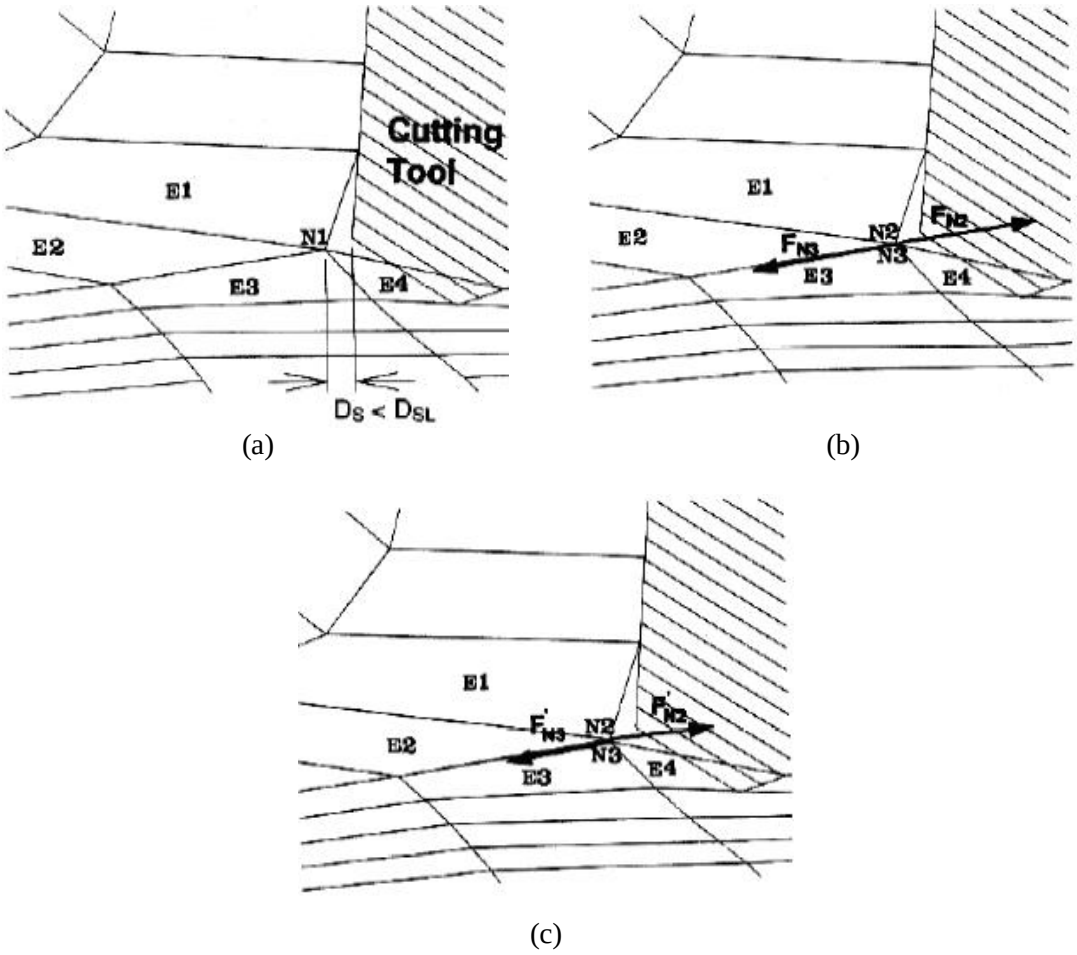

Fig. 2.3.3 Illustration of the distance based chip separation criterion and the unbalanced forces reduction method to improve the stability during the separation of elements for chip formation modeling, (a) the cutting tool at the position which satisfies the element separation criterion, (b) the separation of node N1 into nodes N2 and N3, (c) the reduction of unbalanced forces at nodes N2 and N3 [24]

technique. During simulation the resultant force at node N1 [see Fig. 2.3.3(b)] ahead of the tool tip prior to satisfaction of the criterion is close to zero, i.e. the node N1 is in equilibrium. But as soon as the criterion is satisfied, the elements E2 and E3 are separated, and the common node N1 shared by the separating elements is replaced by two

new nodes, namely, N2 and N3. Because of the separation of the elements E2 and E3, the original equilibrium condition is no longer satisfied, and the non-zero resultant forces F_{N2} and F_{N3} are generated at the newly formed nodes N2 and N3. If the tool is incremented with these unbalanced forces F_{N2} and F_{N3}, numerical instability may occur in the analysis. Therefore, the unbalanced force reduction method is adapted to reduce these forces. This is done by applying external forces F'_{N2} and F'_{N3} [see Fig. 2.3.3(c)] of equal magnitude and similar orientation after the separation of the elements. Then, the magnitudes of these externally applied forces F'_{N2} and F'_{N3} are reduced incrementally, after which the tool again advances incrementally.

The technique used by Strenkowski and Carroll [20], Carroll and Strenkowski [21], and Shi *et al.* [22] does not require implementation of the unbalanced force reduction method as used by Shih [25-27] in the code. This is because they have pair of nodes bonded together before the chip is separated from the workpiece. Thus, no replacement with new nodes is necessary after the criterion is met. But the disadvantaged discussed earlier regarding parting line crack in the workpiece ahead of the tool tip can be reduced by using distance-based chip separation criterion.

Shirakashi and Maekawa [31], Shirakashi and Obikawa [32], and Obikawa and Usui [33] developed a new concept for computational machining simulations called iterative convergence method (ICM). The ICM uses flow lines which consist of trajectories of particles or a series of finite elements. Though in ICM, each cycle does not correspond to real tool advancement, the successive modification of the flow field leads to a quick convergence. Here the tool is loaded onto an already formed chip. It provides a way, by iteration, of finding the formed chip shape that is consistent with the materials

flow properties and friction interaction with the tool. Here, the finite elements are structured to follow the stream lines of the steady state chip flow as observed in the

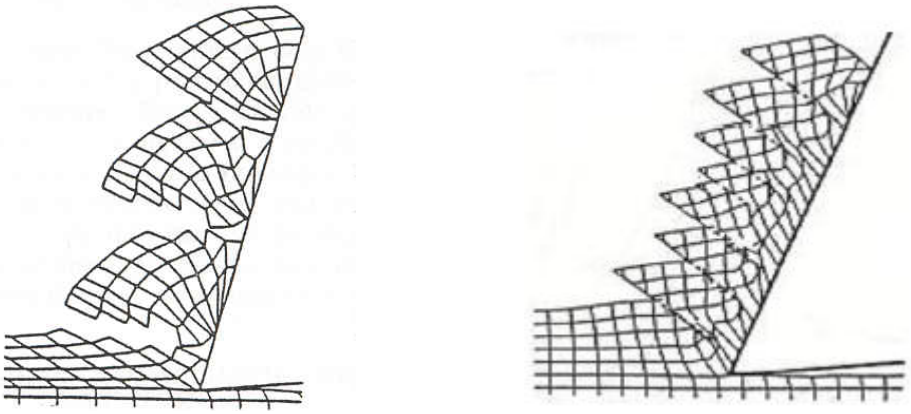

(a) (b)

Fig. 2.3.4 Predicted chip shape in the machining of (a) β-brass (v = 13 mm/min, f = 0.25 mm, d = 1 mm and α = 15°), and (b) titanium alloy Ti--6Al-4V (v = 30 m/min, f = 0.25 mm, d = 1 mm and α = 20°) [31]

continuous chip. Therefore, ICM scheme cannot be directly applied to the analysis of non-steady machining producing shear-localized chip. For the formation of fracture at the tool tip, geometric criterion (of predefined distance variable) somewhat similar to that employed by Shih [25-27] was used. To simulate the separation within the chip and not at the tool tip, a strain criterion introduced by Obikawa *et al.* [34] was used.

The above model was applied to analyze machining of β-brass and a titanium alloy (Ti-6Al-4V). During the machining simulation of β-brass, cracks were observed to initiate at the tool side within the highly deformed workpiece and propagates towards the free surface side, resulting in a periodic segmentation of the chip [see Fig. 2.3.4(a)]. Whereas, during the simulation of the machining of titanium alloy, fracture was observed to occur in the chip at the free surface side only, and not along the rake face [see Fig. 2.3.4(b)]. The authors attributed the segmentation of the chip in titanium to the small

fracture strain of the alloy followed by the propagation of a crack and the localization of deformation. They discarded shear-localization as a cause, but elucidated as a result giving large deformation in the chip. Unfortunately, this is not how titanium chips are formed in machining. The model proposed by Obikawa and Usui [33] is more like discontinuous chip formation. The conditions between the tool face and chip are entirely different.

The formation of shear-localized chip in the machining of some of the difficult-to-cut material is a known fact. The shear-localization is a result of strain hardening, strain rate sensitivity, and thermal softening. Taking these into consideration, Lemonds and Needleman [39] formulated the effects of these factors on shear-localization. Although, their formulation was intended for any general shear-localization problem, such as high rate forming, explosive welding, armor penetration, and crash-worthiness of vehicles, it can be used in the finite element simulation of high-speed machining. Here, the authors have taken finite geometrical changes into account and have neglected the inertial effects. To accomplish this they have confined their attention to a strain rates from 10^{-3} to 10^{3} sec^{-1}, where material rate sensitivity is the main time effect, and higher strain rates, where inertial effects play an important role are excluded from consideration. They used both isothermal hardening as well as kinematic hardening model to examine their effect on the shear band development. They reported that localization occurs sooner or more abruptly in a kinematic hardening solid than in an isotropic hardening solid. Detailed discussion of the analytical formulation of the shear-localization and implementation in the finite element method can be found in Ref. 39. This formulation is applied to the iterations in *AdvantEdge*™ code for the calculation of mechanical and thermal state variables [17].

Baker *et al.* [43-46] assumed pure adiabatic shearing with no cracks occurring in the chip segmentation in the finite element analysis of high-speed machining of titanium alloy. They used ABAQUS/Standard, an implicit code with C++ code, for the preprocessing of the model. They preferred to use quadrilateral elements to triangular elements because of better convergence properties. As with these elements, the strains are continuous over element boundaries, high mesh density is needed in regions of intense plastic deformations in order to resolve large strain gradients. Remeshing is done when either the convergence problems due to strongly deformed elements occur or when the tool is advanced by a certain predefined distance. The simulations require the positions of the new nodes on the contact surface to coincide exactly with the old position to avoid divergence of the solution. To ensure the size of the problem remains within the calculable limits, the refinement of the elements was confined to the region around the shear zone, where maximum plastic deformation was expected. This mesh refinement zone was moved with the shear zone during machining. Baker *et al.* [43-46] used two techniques to simulate the material separation, namely, node separation on the predefined parting line (as used in Ref. 20-22 and 30) and pure deformation process similar to forging. As there are some disadvantages with the parting line technique (as discussed earlier), they used the pure deformation method in the simulation to compare the results. In the pure deformation method, node separation is not necessary; instead as the tool advances, all the nodes move on the tool surface and the elements may deform strongly. The elements that overlap with the tool are removed during remeshing. Advantage with this method is that it converges more easily and no material separation line has to be prescribed. The disadvantage with this method is that elements are removed only when

remeshing is done. Therefore, they can carry load between the tool and the workpiece which is aphysical. ABAQUS uses residual force and compares with the average force within the model in order to check for convergence. But this method is not appropriate for metal cutting, as the average force in the model is small compared to the maximum forces occurring in the shear zone. Therefore, Baker *et al.* [43-46] adjusted the convergence controls accordingly and compared the force value within the shear zone. In order to achieve this, artificial dampening (less than 0.1%, for negligible influence on overall results) was introduced for the first $5.0e^{-11}$ sec. of the simulation.

Baker *et al.* [43] simulated machining of a titanium alloy (Ti-6Al-4V) with the above described methods. They machined the material at a cutting speed of 3000 m/min, depth of cut of 0.04 mm with a tool rake angle of 10°. In this study, the authors assumed no friction at the chip-tool interface and heat flow into the tool was also neglected. These properties were incorporated later on to check their effect. The resultant chip morphology with the node separation method and with pure deformation method was shown in

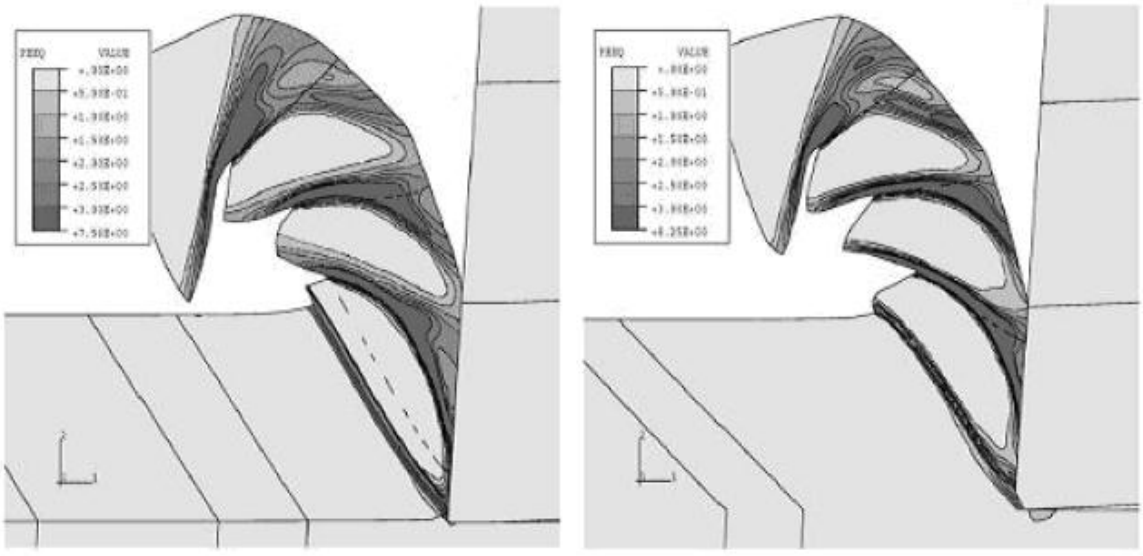

(a) (b)

Fig. 2.3.5 Chip morphology with (a) node separation method, and (b) pure deformation method, when machining titanium alloy (Ti-6Al-4V) at cutting speed of 3000 m/min, depth of cut of 0.04 mm with a tool rake angle of 10° [43]

Fig. 2.3.5, which is observed to be almost similar. However, the difference in forces was reported to be 10% by these methods. The absence of narrow shear bands was attributed to the lower refinement of the elements. Baker *et al.* [43] have compared the simulation results with the experimental results from the literature [47]. The observed difference in the chip morphology was attributed to different machining conditions used in simulations and experiments (cutting speed of 2400 m/min, rake angle of 0°, and depth of cut of 0.042 mm was used). The absolute values of the forces reported in the simulation were not in agreement with the experimental values and are less by a factor of about two. The authors attribute this difference to the uncertainties in the plastic flow curves and also to the different rake angles used. Parametric study was also done by varying the elastic modulus (between 57.5 MPa and 575 MPa) and the cutting speed (between 6000 and 30 m/min). They concluded that, by lowering the elastic modulus, higher degree of segmentation, and increase in frequency of segmentation is observed. Whereas, with the reduction in cutting speed, no shear-localization in the machining of titanium alloy was reported. But, according to the literature, shear-localization is observed even at the lower cutting speed of 0.5 m/min when machining titanium alloys [33]. The authors conclude that shear-localization does not seem to be the only reason for chip segmentation and crack formation and propagation may also plays an important role especially at the low cutting speeds.

Baker *et al.* [44] studied the influence of thermal conductivity on shear-localization in the machining of titanium alloy (Ti-6Al-4V). The same model and

machining conditions were used as in Ref. 43. The thermal conductivity of the material was increased from the correct value to ten times the value in the simulation. The chip morphology showed a transition from shear-localized to continuous chip. An increase in force is observed when the chip changes from shear-localized to continuous with an increase in thermal conductivity of the material. Also, with increase in the thermal conductivity, the time between the formation of two shear bands was reported to be increased.

Hua and Shivpuri [49] investigated segmented chip formation based on implicit, Lagrangian, non-isothermal rigid-viscoplastic finite element simulation in which a dynamic flow stress model is used as the basis for high strain rates and high temperatures. They applied ductile fracture criterion based on strain energy for the crack initiation process during chip segmentation. They proposed that the primary reason of the chip transition from discontinuous to serrated is due to change of stress state near the tool tip, which is caused by the change of the cutting speed which influences the crack initiation (void coalescence) and propagation. They concluded that a crack initiates in the primary deformation zone and propagates to the free surface in the direction away from the tool surface. This results in chip separating from the workpiece in the free surface side and connecting each at the tool rake face side. Here, the authors propose that as the cutting speed increases, the crack initiation site moves towards the free surface (or away from the rake face), and eventually at a certain higher cutting speed (600 m/min for titanium) continuous chip results. This crack initiation theory within the primary shear zone conflicts with both shear-localization theory (proposed by Komanduri *et al.* [19]) and periodic crack formation at free surface (proposed by Nakayama *et al.* [51]).

Shivpuri and Hua [50] extended the model reported in Ref. 49 by incorporating material changes into the phenomenological behavior of the chip. The model predicted that at lower cutting speeds the temperature in the primary and secondary shear zone is below the β-transus temperature. This indicates that there is no phase transformation occurring during the chip formation. Therefore, the fracture propagates in the α – β phase towards the cutting tool face resulting in a discontinuous chip as discussed earlier. At higher cutting speeds, temperature in the secondary shear zone reaches β-transus. Therefore, there is a phase transformation in the secondary shear zone leading to increase in material ductility. Therefore, fracture propagates towards the outer surface resulting in a segmented chip but held together at the tool side of the chip.

Eu-Gene Ng and Aspinwall [52 and 53] developed a model using ABAQUS/Explicit to simulate continuous and segmental chip formation when machining AISI H13 tool/die steel. They used shear failure criteria and element deletion/adaptive remeshing techniques and Johnson-Cook's material model. They analyzed two models, one with crack nucleation module and the other without. Machining parameters used for both the cases were: cutting speed 200 m/min, depth of cut 0.25 mm, and width of cut 2 mm. The crack nucleation module when incorporated in the model produced serrated chip while the other model produced continuous chip for the same machining parameters. Temperature fields observed were different for different types of chips produced. For the continuous chip formation, the chip-tool interface temperature observed was higher than in the shear zone. While for the segmental chip, the temperature in the shear zone was observed to be higher. The stress magnitude observed was higher in the continuous chip due to lower shear angle which resulted in higher cutting forces. For the segmental chip,

the magnitude of stress field in the shear zone was higher than with the continuous chip and was confined to narrow region. Whereas, in the continuous chip formation process, the magnitude of the stress field was lower and was observed to be distributed over a wide area.

CHAPTER 3

PROBLEM STATEMENT

It can be understood from the previous two chapters the complexities involved in the high-speed metal cutting process. Various approaches, such as analytical, slip-line field, experimental, and finite element analysis have been used to study the chip segmentation phenomenon. Each of these approaches has certain advantages and shortcomings. The main advantage in using the finite element method is that various material models and complex boundary conditions can be incorporated in the simulations. It also aids in both qualitative and quantitative understanding of the material behavior in high-speed machining. Simultaneously the finite element model provides detailed information on the nature of chip formation, strain and strain rate distributions, temperature distribution and heat generation, and principle stress distribution. It can also provide vital information on cutting and thrust forces induced in the cutting process, which facilitates in the design of cutting tools and selection of the machine tools.

The objectives of the proposed investigation are as follows:

1. Develop a finite element model to investigate shear-localization phenomenon in high-speed machining of AISI 4340 steel. Incorporate Johnson-Cook material model coupled with Recht's failure criterion for high temperatures, large strains and high strain rates in this model. To accomplish this, a subroutine is developed and incorporated in commercially available finite element software, namely *AdvantEdge*™.
2. Validate the results of finite element model with the experimental data reported in the literature [9]. Also, validate the results of finite element model with the results of a conventional approach used for machining simulations using ABAQUS.
3. Apply the newly developed model to investigate the effect of different hardness values of AISI 4340 Steel, different cutting speeds and different tool rake angles on the nature of chip formation.
4. Compare shear-localization in machining of AISI 4340 steel observed in the simulations with the shear-localization process elucidated by Komanduri *et al.* [2, 3, 12 and 19].

CHAPTER 4

SHEAR-LOCALIZATION IN THE MACHINING OF AISI 4340 STEEL

4.1 Thermo-mechanical Properties of AISI 4340 Steel

As discussed in Chapter 1, the instabilities in the cutting process occur due to thermo-mechanical response of the workmaterial under the conditions of cutting. The consequence is localized shear and consequent cyclic chip formation [12]. Continuous chips are likely to form in the machining of materials with extensive slip systems (e.g. fcc/bcc crystalline structure), good thermal properties, and low hardness, such as conventional aluminum alloys (e.g. Al 6061-T6) and low carbon steels (e.g. AISI 1018 steel). However, the material of our investigation, viz., AISI 4340 steel, and other materials, such as titanium alloys and nickel-base superalloys have limited slip systems due to their hcp crystalline structure, poor thermal properties, or high hardness and so are likely to form shear-localized chip when machined. While there may be a transition from a continuous to a shear-localized chip with increase in cutting speed for materials such as AISI 4340 steel and nickel-base superalloys, there may not be any transition for some materials. For example, only a continuous chip is observed in the machining of aluminum

alloys (e.g. Al 6061-T6) upto very high cutting speeds and only shear-localized chip is formed even at low speeds in the case of titanium alloy (e.g. Ti-6Al-4V).

Table 4.1.1 Density and thermal properties of some workmaterials [12].

Material	Thermal conductivity λ		Density ρ (g/cm^3)	Specific heat c, (cal/g °C)	Thermal diffusivity		Product of ($\lambda\rho c$)	
	λ (cal/cm s°C)	(α of AISI 1018 steel = 1)			α (cm^2/s)	(α of AISI 1018 steel = 1)	$\lambda\rho c$ (cal/g °C)	($\lambda\rho c$ of AISI 1018 steel =1)
Titanium 6Al-4V	0.0160	0.1135	4.43	0.14	0.0258	0.1585	0.0099	0.0816
Inconel 718	0.0290	0.2057	8.19	0.104	0.0340	0.2081	0.0247	0.2031
AISI 4340 Steel	0.0797	0.5652	7.83	0.11	0.0925	0.5663	0.0686	0.5641
AISI 1018 Steel	0.141	1	7.85	0.1099	0.165	1	0.1216	1
Al 2024	0.3917	2.778	2.78	0.2109	0.666	4.0388	0.2286	1.88
Al 6061-T6	0.4228	3.00	2.71	0.2131	0.733	4.4418	0.2442	2.00

Table 4.1.1 gives the thermo-mechanical properties of some of the difficult-to-cut materials (Ti-6Al-4V, Inconel 718, and AISI 4340 steel) as well as some of the easy-to-cut materials (low carbon steel AISI 1018 and aluminum alloys Al 6061-T6 and Al 2024). Also, given in the table is a comparison of the groups of thermal properties, viz. thermal diffusivity ($\lambda/\rho c$), and the product of thermal properties ($\lambda\rho c$) (also termed as thermal contact coefficient), as well as the ratio of these values considering the values for a low carbon steel (AISI 1018 steel) as unity. It can be seen that the thermal diffusivity of AISI 4340 steel is only about 56% that of AISI 1018 steel. The thermal diffusivity of other difficult-to-cut materials viz., titanium 6Al-4V and Inconel 718 are 16% and 21% that of AISI 1018 steel, respectively. In contrast, the thermal diffusivity of Al6061-T6 and Al 2024 are 400% and 444% that of AISI 1018 steel, respectively. Similarly, the

thermal contact coefficient of AISI 4340 steel is only about 56% that of AISI 1018 steel and of

titanium 6Al-4V and Inconel 718 are 8% and 20% that of AISI 1018 steel, respectively. In contrast, the values are 188% and 200% for Al6061-T6 and Al 2024, respectively. Consequently, much of the heat generated in machining of these materials, which have good thermal properties or have extensive slip systems, will be dissipated without concentrating in a narrow band. Consequently, only continuous chips yield with these materials. Whereas, in the case of difficult-to-cut materials, the heat generated is concentrated in a narrow shear band without dissipating to the surrounding material, leading to a shear-localized chip formation.

The speeds at which shear-localized chip is formed in titanium alloys and nickel-base superalloy are much lower than for AISI 4340 steel. The reason for this can also be attributed to the thermal properties of these materials. The difference in thermal diffusivity of titanium 6Al-4V and Inconel 718 compared to AISI 4340 steel are 40% and 35%, respectively, as that of AISI 1018 steel. Also, the difference in thermal contact coefficient of titanium 6Al-4V and Inconel 718 compared to AISI 4340 steel are 48% and 35%, respectively, as that of AISI 1018 steel. This shows that the heat dissipation in AISI 4340 steel is higher than Ti-6Al-4V and Inconel 718. Therefore, the speed at which the shear-localized chip forms in AISI 4340 steel should be much higher than the other two difficult-to-cut materials. When AISI 4340 steel is machined at conventional speeds, there is comparatively good heat dissipation resulting in continuous chip formation (see Section 4.3 for details on transition speed) but when machined at higher speeds, the chip formed is shear-localized.

4.2 Thermo-plastic Shear Instability in the Machining of AISI 4340 Steel at High Speed

As discussed in the previous section, the thermal properties of the workmaterial play a significant role in setting up the internally generated temperature gradients. These gradients influence the dynamic plastic behavior of the materials and are functions of thermo-physical properties as well as strain rate and shear strength [8]. Thus, the fundamental difference in the nature of chip formation with shear-localized chip and that with continuous chip may be attributed to the thermo-plastic shear instability (strain hardening versus thermal softening) involved in the processes.

When AISI 4340 steel is machined at low cutting speeds, strain-hardening predominates over thermal softening and hence resulting in a continuous chip formation. For low deformation rate, the process is essentially isothermal. Once shear takes place along the main shear plane, the stress required for further deformation is higher than before, so the weakest plane will be shifted to the next plane. In other words, initially, plastic shear strain is restricted to a few weak shear zones within the material. Strain-hardening strengthens the weak material in these zones and the burden of strain is distributed throughout the material. This leads to a uniformly distributed deformation in the chips on a macroscale. Hence, in the case of a continuous chip, strain hardening always predominates over thermal softening. This process also applies to materials with good thermal properties when machined at conventional speed.

But when AISI 4340 steel is machined at higher cutting speeds, the plastic deformation is rapid. Also, as the thermal properties of this material are moderately poor, it leads to local heat generation in the shear plane. Once shear takes place along the main shear plane, the strength there becomes lower than before. So, the main shear plane is still the weakest plane and hence shear continues on the same plane. In other words, during rapid deformation, heat generated locally establishes local temperature gradients; maximum temperature exists at the points of maximum heat generation. Here, the rate of decrease in strength due to temperature rise equals to or exceeds the rate of increase in strength due to strain hardening. Thus the material continues to deform locally and fails catastrophically at the shear zone and forms shear-localized chip. Hence, in the case of shear-localized chips, the thermal softening predominates over strain hardening. Detailed mechanism of shear-localization is given the Section 4.4.

4.3 Effect of Material Hardness on the Chip Formation in the Machining of AISI 4340 Steel

The purpose of this study is to investigate the catastrophic shear instability in high-speed machining of AISI 4340 steel. The term “high speed machining” is relative from a materials viewpoint, because of the vastly different speeds at which different materials can be machined with acceptable tool life. According to Komanduri *et al.* [15], high-speed machining may be defined as the speed at which the chip morphology is markedly different than the conventional continuous chip. When machining AISI 4340 steel, the morphology of the chip formed depends on factors such as material hardness, cutting speed, and the depth of cut. The speed at which catastrophic shear completely

develops depends on the hardness of this material. With increase in hardness, the cutting speed at which shear-localized chip is formed decreases (see Table 4.3.1). For an AISI 4340 Steel (325 BHN), discontinuous chips are formed at speeds below 31 m/min and continuous chip is found to develop in the speed range of 31 – 61 m/min. At speeds higher than 61m/min, the deformation of the chip is inhomogeneous on a gross level with two regions, one narrow band where deformation is very high (i.e. between the segments) and the other where deformation is relatively low (i.e. within the segments). An inhomogeneous shear-localized chip is produced at a speed of 125 m/min and fully developed shear-localized chip at 244 m/min for AISI 4340 Steel (325 BHN). With further increase in speed, the shear-localized chip persist without transition to any other chip form or reversal to continuous chip, but the extent of contact between the segments is found to decrease rapidly. At speeds of 976 m/min and above, individual segments are completely isolated instead of being held together as a long chip.

Table 4.3.1 Effect of AISI 4340 steel hardness on shear-localization [12].

AISI 4340 Steel Hardness (BHN)	Cutting speed at with catastrophic shear completely developed (m/min) (ft/min)	Cutting speed at which individual segments were completely isolated (m/min) (ft/min)
520	61 (200)	305 (1000)
325	244(800)	976 (3200)
215	488(1600)	1952 (6400)

Table 4.3.1. gives the speed at which catastrophic chip is completely developed and the speed at which individual segments are completely isolated for different hardness values of AISI 4340 steel. With 520 BHN AISI 4340 steel, the speed at which the catastrophic shear completely developed is 61 m/min and the segmentation into

individual segments is 305 m/min. as the hardness of steel decreases, these speeds increase. For example at 215 BHN, shear-localized chips are developed at a speed of 488 m/min and isolated individual segments at 1952 m/min.

4.4 Mechanism of Shear-localization in the Machining of AISI 4340 Steel

A brief description on shear-localized chip formation process was given in Section 1.1 of Chapter 1. Fig. 4.4.1 is a schematic of the shear-localized chip formation process, showing various surfaces that participate in the process according to Komanduri *et al.* [12]. As the workmaterial approaches the tool, it experiences a cyclic and asymmetric stress state that changes with time. The chip segment enclosed in 1, 3, 4, and 5 in Fig. 4.4.1 is being upset (plastically deformed) by the advancing tool. Appropriate stress, strain, and temperature fields are thus being set up in the workmaterial. As the material begins to shear along line 5, these fields develop conditions which lead to thermo-plastic instability, as governed by the thermo-mechanical response of the workmaterial under the conditions of cutting. The strain in the bulk of the segment due to upsetting, however, is rather small as can be seen by the very little deformation of the grains within the segment in Fig. 4.4.2. A very thin band between the segments accepts the burden of further strain, thus localizing shear. The chip segment then moves up the ramp formed by the workmaterial on the workpiece side of 5. As the tool moves into the ramp, a new segment begins to form. Its upper surface, represented by line 5, becomes the surface through which the tool upsets the material ahead. As upsetting progresses, this surface becomes that identifies by line 3 and 4, the

latter of which is pressed against the tool face. Until a new localized shear zone forms again due to thermo-mechanical instability, the increasing portion of line 4 [a hot, freshly sheared (nascent) surface] that lies on the rake face remains at rest. Shearing between the segments along line 3 ceases when the next localized shear band is forming along line 5.

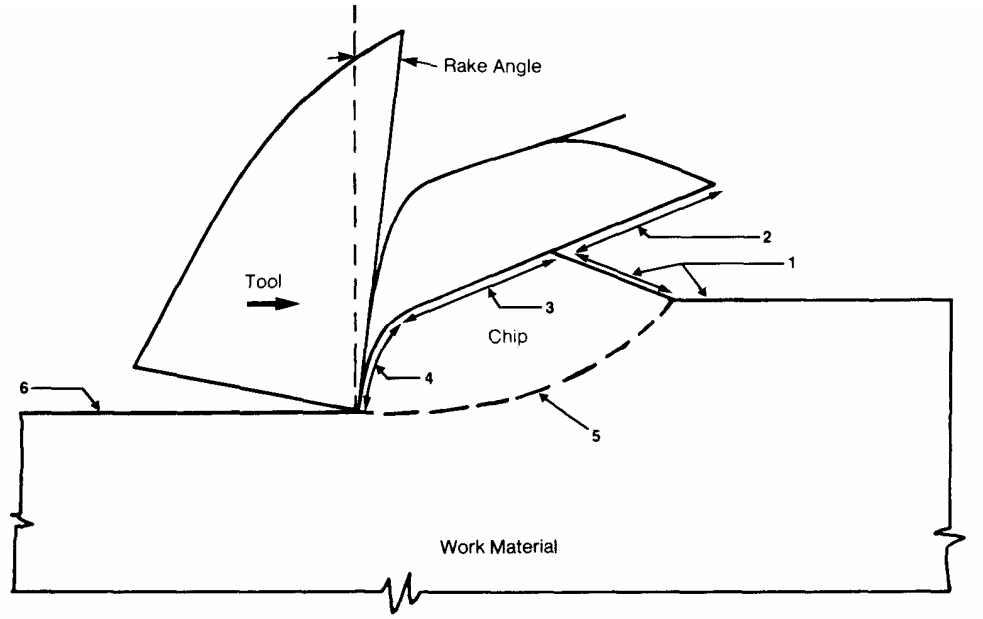

1. Undeformed surfaces
2. Part of the catastrophically shear failed surface separated from the following segment due to intense shear
3. Intense shear band formed due to catastrophic shear during the upsetting stage of the segment being formed
4. Intensely sheared surface of a segment in contact with the tool and subsequent slid on the tool face
5. Intense localized deformation in the primary shear zone

6. Machined surface

Fig 4.4.1 Schematic diagram of a shear-localized chip formation process, such as the case with AISI 4340 steel, showing various faces that take part in the process [2]

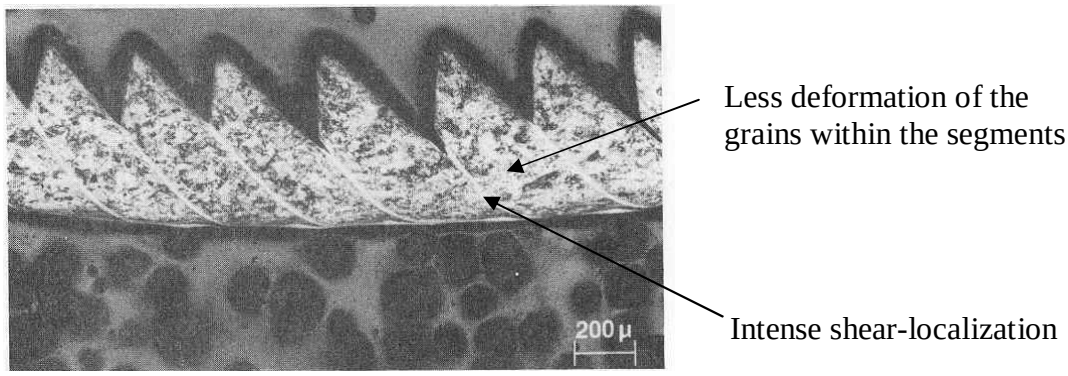

Fig 4.4.2 Fully developed shear-localized AISI 4340 steel (325 BHN) chip. Cutting speed 245 m/min [15]

Once upsetting in the segment and shear between the segments have ceased, the chip segment moves up the tool face.

The sliding of the chip segment on the tool face is, therefore, characterized by a stick-slip motion. The sliding resistance at the chip-tool interface is very severe in case of shear-localized chip than for a steady state continuous chip. During shear-localization, the region between the segments undergoes shear separation followed by partial sliding between the chip segment and the tool face.

CHAPTER 5

FINITE ELEMENT ANALYSIS OF HIGH-SPEED MACHINING OF AISI 4340 STEEL

5.1 Introduction

In Chapter 1, we discussed the basics of the finite element analysis. As described earlier, machining is a complex process involving large plastic strains, high strain rates, and high temperatures. Therefore, the finite element code needs special handling for a successful analysis of this process. In this investigation various technique used are contact generation defined by master and slave surfaces, continuous remeshing and adaptive meshing to sidestep the extensive distortion of elements, Johnson-Cook's constitutive model (which gives flow stress at various strains, strain rates, and temperatures), and Recht's classical model for catastrophic shear instability used as a failure criterion for shear-localization in the chip. *AdvantEdge*™, a commercial explicit finite element code, is used for the simulations in this investigation. A user-subroutine incorporating radial return method to update the stresses and Recht's failure criterion is

linked to the main code. These techniques are discussed in detail in subsequent sections in this chapter.

For finite element analysis of machining, the following assumptions are made:

1. Cutting speed is constant.
2. Orthogonal or 2D machining.
3. Cutting velocity vector is normal to the cutting edge.
4. Workpiece material is homogeneous polycrystalline, isotropic, and incompressible solid.
5. Workpiece is at a reference temperature of 20° C at the beginning of simulation.
6. Adiabatic temperature boundary conditions are assumed. No cutting fluid is assumed in the cutting.
7. Machine tool is perfectly rigid and machine tool dynamics have no influence on machining.
8. Coefficient of friction is constant at the tool-chip and the tool-work interfaces.

5.2 Adaptive Meshing

Adaptive meshing is increasingly recognized as a crucial part of the finite element modeling in areas, such as ballistic penetration, crashworthiness, and of primary interest to us here, namely, the machining process, to mention some [38]. Machining process involves large unconstrained plastic flow in areas, such as shear band and chip-tool interface. So, in finite element modeling these areas may get severely distorted which result in an inaccurate solution. Therefore, in machining, adaptive mesh refinement provides a powerful tool for systematically increasing the accuracy of solution and for

alleviating element distortion and resolving sharp gradients in finite deformation problems.

AdvantEdge™ uses six-noded quadratic triangular elements [54]. The element has three corner and three midside nodes providing quadratic interpolation of the displacements within the element. The element is integrated with three-point quadrature interior to the element as shown in Fig.5.2.1 (a). The constitutive response of the material is computed at the integration points. Consequently, the element provides a linear pressure distribution within the element.

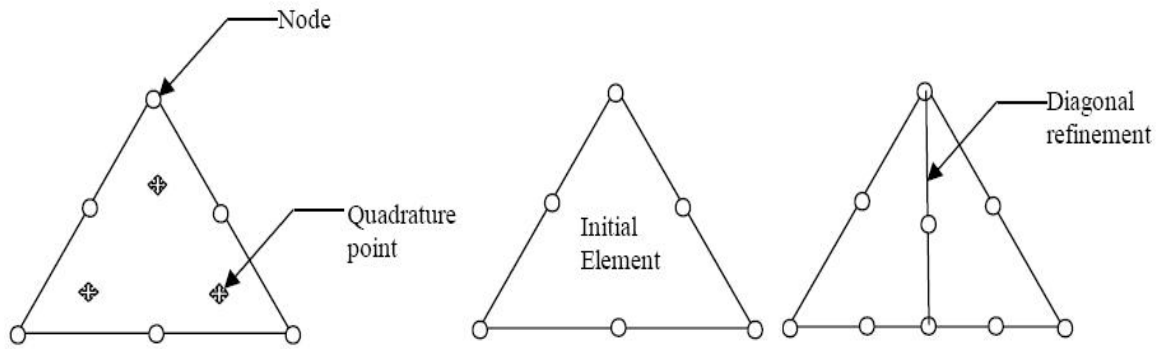

(a) (b) (c)

Fig. 5.2.1 Six-noded quadratic triangular element used in *AdvantEdge*™ (a) the integration points, (b) element before refinement, and (c) element after refinement [54]

The method for adaptation begins with a model of the solid to be analyzed. The model contains relevant boundary information such as that required to automatically generate a first mesh over the solid. As the solution proceeds, the mesh follows the deforming boundary. This is done by refining large elements, remeshing distorted elements, and coarsening small elements. For instance, if the element is in need of

refinement, the diagonal of the element is split, a midside node becomes a new corner node and new midside nodes are added to both elements [see Fig. 5.2.1 (b)]. With this, the connectivity of the finite element mesh is redefined at regular intervals by triangulating the nodes at their spatial locations. This process of continuous remeshing, by itself, is capable of eliminating the bulk of the deformation-induced element distortion. If, despite this continuous remeshing, the aspect ratio of some of the elements becomes unacceptable, the mesh is subjected to Laplacian smoothing. Coarsening of small elements is done in areas where the elements have become inactive. This is done to keep the size of the problem within manageable bounds.

5.3 Contact

In machining, complicated contact situations are developed between deformable bodies, i.e., tool and workpiece. *AdvantEdge*™ uses the predictor-corrector method (used in PRONTO2D explicit dynamic code) for contact development [17]. In this code, the bodies in contact can be deformable or rigid, depending on the selection. These

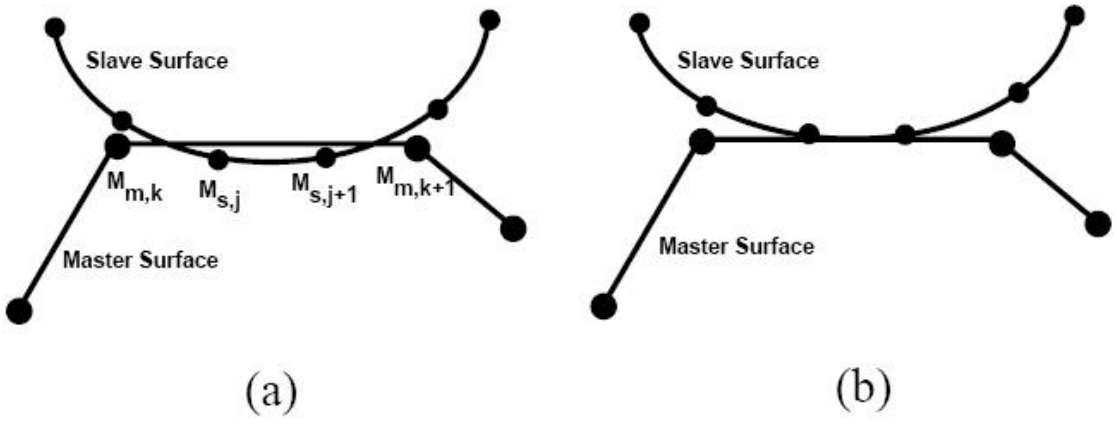

Fig. 5.3.1 Schematic showing contacting surfaces (a) predictor configuration of surfaces (b) Kinematically compatible surfaces [17]

contacting surfaces are designated as master and slave surfaces as shown in the Fig. 5.3.1 For deformable bodies, a balanced master-slave approach in which surfaces alternatively act as master and slave is employed. However, rigid surfaces are always treated as master surfaces [38]. In predictor configuration [Fig. 5.3.1 (a)], nodal accelerations are calculated from out-of-balance forces and assuming no contact has occurred, the predictor nodal positions, velocities, and accelerations are calculated. A Coulomb's friction model is used to define stick-slip friction at the chip-tool interface. Corrector method is applied to calculate the nodal acceleration from the forces. Subsequently, the nodal velocity and displacements are calculated [Fig. 5.3.1 (b)].

5.4 Johnson-Cook's Constitutive Model

An ideal plasticity model for machining should be able to describe the material's properties, such as strain-hardening behavior, thermal softening behavior, and strain-rate dependence. Also, to accurately model the deformation process of materials in high-speed machining over wide range of strain rates (10^3 to 10^6 s^{-1}) and temperatures (300°-1200° C), a reliable constitutive description of the stress-strain behavior is required. Several physically and phenomenologically based models have been developed for use in computational mechanics. But the most widely and successfully implemented constitutive model that can be applied for high-speed machining process is the one proposed by Johnson and Cook [55]. This model takes into consideration the influence of large strains, high strain rates, and high temperatures on flow stress of the material. Its success can be attributed to its simplicity and the availability of parameters for various materials of interest. This constitutive model is intended primarily for computations and is well suited

because it uses variables that are readily available in most solid mechanics computer codes [56]. The Johnson-Cook's constitutive model is given as follows

$$\bar{\sigma} = \left[A + B \left(\bar{\varepsilon}\right)^{n} \right] \left[1 + C \ln\left(\frac{\dot{\bar{\varepsilon}}}{\dot{\varepsilon}_0} \right) \right] \left[1 - \left(\frac{T - T_r}{T_m - T_r} \right)^{m} \right] \qquad (5.4.1)$$

where, the material constants in the above equation are as follows:

A Yield stress constant

B Strain hardening coefficient

n Strain-hardening exponent

C Strain rate dependence coefficient

m Thermal-softening constant

The material constants are experimentally found by Split Hopkinson Pressure Bar (SHPB) test or ballistic impact test.

The first term in the brackets gives the dependence on strain, which represents strain-hardening effect. The second term gives instantaneous strain-rate sensitivity which represents strain-rate hardening and the third term gives the temperature dependence of stress i.e. thermal-softening effect. Although, this model does not represent any history effects of temperature or strain-rate, it's been widely used in machining applications and is successful as well. Hence, this model is used in this investigation.

5.5 Stress Update

AdvantEdge™ does not provide Recht's thermo-plastic shear instability criterion in the code. So, a user-subroutine defining Johnson-Cook's material model and Recht's

thermo-plastic shear instability criterion were developed. This user-subroutine was linked dynamically (.dll) to the main finite element code. The user-subroutine is called for every integration point in the finite element model for each time step. Elastic predictor, radial return algorithm is used to determine the stress state of the material and isotropic hardening is considered. This model uses the solution-dependent state variables, such as stress, strain, and strain rate to compute the flow stress by Johnson–Cook's constitutive equation. Further, these solution dependent state variables are updated and Recht's thermo-plastic shear instability criterion is checked.

The initial conditions of stress tensor σ_{ij}^{k-1} and strain tensor ε_{ij}^{k-1} are known from the last equilibrium state [$(k-1)^{th}$ time step]. We calculate the measures σ_{ij}^{k} and ε_{ij}^{k} at the updated state (k^{th} time step) from the strain increment passed in the user-subroutine through the main finite element code.

First, the elastic predictor, the trial stress tensor is obtained from the strain increments

$$\sigma_{pq}^{k(tr)} = \sigma_{pq}^{k-1} + \lambda\, tr\,(d)^{k} + 2\,\mu\, d^{k}_{pq} \tag{5.5.1}$$

where, μ and λ are Lame's constants, given as,

$$\mu = \frac{E}{2\,(1+\nu)} \qquad \lambda = \frac{\nu\, E}{(1-2\,\nu)\,(1+\nu)} \tag{5.5.2}$$

where, E is Young's modulus, and υ is Poisson's ratio.

The iterations (i^{th} step) for radial return method starts with decomposing the total trial stress tensor into hydrostatic (or mean stress tensor) $\sigma_m^{i(tr)}$ and deviatoric stress tensor $\sigma_{pq}^{\ i(div)}$.

The hydrostatic (or mean stress) component is given by

$$\sigma_m^{i(tr)} = \frac{\delta_{ij}\sigma_{rr}^{\ i(tr)}}{3} \tag{5.5.3}$$

The decomposition of trial stress tensor is given by

$$\sigma_{pq}^{\ i(tr)} = \sigma_{pq}^{\ i(div)} + \sigma_m^{i(tr)} \tag{5.5.4}$$

Therefore, the deviatoric stress tensor is given by

$$\sigma_{pq}^{\ i(div)} = \sigma_{pq}^{\ i(tr)} - \sigma_m^{i(tr)} \tag{5.5.5}$$

The magnitude of the deviatoric stress tensor is given by

$$\sigma_N^{\ i(div)} = \sqrt{\sigma_{pq}^{\ i(div)}\sigma_{pq}^{\ i(div)}} \tag{5.5.6}$$

The von Mises yield stresses are determined by applying Johnson-Cook's material model for flow stresses

$$\overline{\sigma}^{\,k} = \left[A + B \left(\overline{\varepsilon^{(k-1)}}\right)^n \right] \left[1 + C \ln \left(\frac{\dot{\overline{\varepsilon^{(k-1)}}}}{\dot{\varepsilon}_0} \right) \right] \left[1 - \left(\frac{T^{(k-1)} - T_r}{T_m - T_r} \right)^m \right] \tag{5.5.7}$$

The radius of von Mises yield surface in deviatoric stress space is given by

$$R^k = \sqrt{2/3}\ \overline{\sigma}^{\,k} \tag{5.5.8}$$

For isotropic hardening, the radius of the von Mises yield surface is not constant.

Hardening slope H^k depends on both elastic and plastic moduli. Plastic modulus $E^k{}_{\mathrm{p}}$ is computed as change in flow stress with change in equivalent plastic strain.

$$E^k{}_{\mathrm{p}} = \frac{\partial \bar{\sigma}^{\,k}}{\partial \varepsilon_{pl}{}^{k}} \qquad \& \qquad H^k = \frac{E E^k{}_P}{E - E^k{}_P} \tag{5.5.9}$$

Increment in equivalent plastic strain for i^{th} iteration is computed as

$$\Delta\lambda^{\mathrm{i}} = \frac{\sigma_N{}^{i(div)} - R^k}{2\mu\left(1 + \frac{H^k}{3\mu}\right)} \tag{5.5.10}$$

The next step is to check the yield condition. If the deviatoric stress does not exceed the von Mises yield stress (i.e. the increment in equivalent plastic strain is negative), then there is no yield and the new stress is set equals to the trial stress. But, if the yield stress is exceeded (i.e. the increment in equivalent plastic strain is positive), then plasticity occurs in the increment and the new stress is computed taking the plastic stress into consideration. Then the plastic corrector is applied as follows,

$$\sigma_{pq}{}^{(i+1)(tr)} = \sigma_{pq}{}^{(i)(tr)} - 2\,\mu\,\Delta\lambda^{\mathrm{i}}\,\frac{\sigma_{pq}{}^{(i)(div)}}{\sigma_N{}^{(i)(tr)}} \tag{5.5.11}$$

And the strain increment for all iterations is summed as follows

$$\Delta\lambda_{Total}{}^{\mathrm{i}} = \Delta\lambda_{Total}{}^{\mathrm{i}} + \Delta\lambda^{\mathrm{i}} \tag{5.5.12}$$

Thus corrected trial stress state computed for the $(i+1)^{th}$ iteration in Eqn. (5.5.11) is again decomposed into hydrostatic and deviatoric stress state. The iteration again starts from Eqn. (5.5.3). This procedure repeats till the corrected trial stress state converges to

the yield condition. After the convergence of trial stress state, the equivalent plastic strain, plastic strain rate, plastic work rate, and the stress are updated.

5.6 Recht's Failure Criterion

As discussed in Section 4.3 of Chapter 4, the dynamic plastic behavior of the materials is influenced by the internally generated temperature gradients. These internally generated temperatures are function of thermophysical properties of the material and its shear strength and the strain rate.

Recht [8] took the thermo-physical response into consideration and developed a simple criterion for catastrophic shear in the primary shear zone. According to him, the catastrophic shear occurs at a plastically deforming region within a material when the slope of the true stress-true strain curve becomes zero. The criterion is given as follows

$$0 \le \frac{\dfrac{\partial \tau}{\partial \gamma}}{-\dfrac{\partial \tau}{\partial T}\dfrac{dT}{d\gamma}} \le 1.0 \qquad (5.6.1)$$

where, τ, ε, and θ refer to the shear stress, shear strain, and temperature, respectively. Accordingly, material will shear catastrophically when this ratio lies between 0 and 1; catastrophic shear will be imminent when the ratio is equals to 1. No catastrophic slip occurs when the ratio is greater than 1, in which case the material will strain-harden more than it will thermal-soften.

In this investigation, Recht's catastrophic slip criterion is used as the failure criterion. As *AdvantEdge*™ does not provide this criterion, a code was written for this and incorporated in the user-subroutine and linked to the main finite element program.

The terms in the criterion are derived by modifying the original Johnson-Cook's material model given in Eqn. (5.5.7). This work was done in collaboration with Mr. Dhananjay Joshi and Mr. Syed Kareem.

From the relation

$$\bar{\tau} = \frac{\bar{\sigma}}{\sqrt{3}} \quad \text{and} \quad \bar{\gamma} = \bar{\varepsilon}\sqrt{3} \tag{5.6.2}$$

The Johnson-Cook's model can be modified as

$$\bar{\tau} = \frac{1}{\sqrt{3}} \left[A + B \left(\frac{\bar{\gamma}}{\sqrt{3}} \right)^n \right] \left[1 + C \ln \left(\frac{\dot{\bar{\gamma}}}{\dot{\gamma}_0} \right) \right] \left[1 - \left(\frac{T - T_r}{T_m - T_r} \right)^m \right] \tag{5.6.3}$$

the strain-hardening ($\partial\bar{\tau}/\partial\bar{\gamma}$) term and the thermal-softening ($\partial\bar{\tau}/\partial\bar{T}$)v term can be directly determined by partial differentiation of Eqn. (5.6.3) with respect to shear strain and temperature, respectively, as follows:

$$\frac{\partial\bar{\tau}}{\partial\bar{\gamma}} = \left[\frac{\mathrm{n}\, B}{3} \left(\frac{\bar{\gamma}}{\sqrt{3}} \right)^{n-1} \right] \left[1 + C \ln \left(\frac{\dot{\bar{\gamma}}}{\dot{\gamma}_0} \right) \right] \left[1 - \left(\frac{T - T_r}{T_m - T_r} \right)^m \right] \tag{5.6.4}$$

$$\frac{\partial\bar{\tau}}{\partial T} = \frac{1}{\sqrt{3}} \left[A + B \left(\frac{\bar{\gamma}}{\sqrt{3}} \right)^n \right] \left[1 + C \ln \left(\frac{\dot{\bar{\gamma}}}{\dot{\gamma}_0} \right) \right] \left[\frac{-\mathrm{m}}{(\mathrm{T}-\mathrm{T_r})} \left(\frac{T - T_r}{T_m - T_r} \right)^m \right] \tag{5.6.5}$$

Second denominator term of Recht's criterion is the rate of change of temperature with strain. Recht developed a model [8] to determine temperature gradient with strain in the catastrophic shear zone.

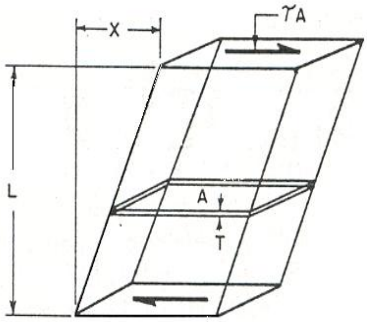

Fig. 5.6.1 Model used to determine temperature gradient with strain in catastrophic shear zone [8]

The thin zone identified by unit area *A* in Fig. 5.6.1 is of thickness *T* and is assumed to be the weakest zone within the length *L* of the specimen. If the catastrophic shear is achieved, the zone will remain confined to this thickness *T*. If a high enough constant rate of average strain x/L is applied on the specimen, catastrophic shear in area *A* is produced. As zone *A* is very thin, it is assumed to be a plane of uniform heat generation. Plastic deformation is confined to this zone. Heat generation rate over unit area *A* can be calculated as

$$q = \frac{\tau L}{W} \dot{\gamma} \tag{5.6.6}$$

Temperature in the area *A* can be calculated as

$$T_A = q \sqrt{\frac{t}{\pi \kappa \rho C}} = \frac{\tau_y L \dot{\gamma}}{W} \sqrt{\frac{t}{\pi \kappa \rho C}} \tag{5.6.7}$$

For constant strain rate

$$dT_A = \frac{1}{2} \frac{\tau_y L \dot{\gamma}}{W} \sqrt{\frac{1}{\pi \kappa \rho C t}} \, dt \qquad (5.6.8)$$

$$\frac{d\gamma}{dt} = \dot{\gamma} \qquad \& \qquad \gamma = \dot{\gamma} t + \gamma_y \qquad (5.6.9)$$

Substituting Eqn. (5.6.9) in Eqn. (5.6.8), gives

$$\frac{dT_A}{d\gamma} = \frac{1}{2} \frac{\tau_y L}{W} \sqrt{\frac{\dot{\gamma}}{\pi \kappa \rho C (\gamma - \gamma_y)}} \qquad (5.6.10)$$

Specimen length L can be considered as depth of cut *f* in orthogonal machining. Substitution of Eqns. (5.6.4), (5.6.5), and (5.6.10) into Eqn. (5.6.1), gives

$$RC = \frac{\left[\frac{n B}{3} \left(\overline{\varepsilon_{pl}} \right)^{n-1} \right] \left[1 - \left(\frac{T - T_r}{T_m - T_r} \right)^m \right]}{\frac{1}{\sqrt{3}} \left[A + B \left(\overline{\varepsilon_{pl}} \right)^n \right] \left[\frac{-m}{(T - T_r)} \left(\frac{T - T_r}{T_m - T_r} \right)^m \right] \left[\frac{1}{2} \frac{\tau_y f}{W} \sqrt{\frac{\dot{\overline{\varepsilon_{pl}}}}{\pi \kappa \rho C (\overline{\varepsilon_{pl}} - \varepsilon_y)}} \right]} \qquad (5.6.11)$$

where, *RC* is the Recht's failure criterion. Eqn. (5.6.11) can be easily incorporated in the user-subroutine.

If Recht's criterion is satisfied i.e. the value of *RC* is between 1 and 0 at all the integration points in an element, the stress state of the element is set to zero. The element is said to be deleted when the stresses are set to zero. Once the element is flagged as deleted, it is discarded from further calculations and cannot be reactivated.

CHAPTER 6

FEM SIMULATION OF THE MACHINING OF AISI 4340 STEEL UNDER DIFFERENT MACHINING CONDITIONS

6.1 Material Properties and Process Parameters

The objective of the present investigation is to study the formation of shear-localized chip when machining AISI 4340 steel of different hardness values. Shear-localization is considered to be the main cause in chip segmentation when machining AISI 4340 steel at high speed. As discussed in Chapters 1, 2, and 4 the chip morphology depends on the thermo-mechanical properties of AISI 4340 steel as well as process parameters in machining. Sections 4.1 and 4.3 of Chapter 4, discuss the influence of thermal and mechanical properties on chip morphology. Simulations are carried out for hardness values of 215 BHN, 325 BHN, and 520 BHN of the work material as given in Table 6.1.1 [58]. The thermal and mechanical properties of AISI 4340 steel used in the simulations are given in Table 6.1.2 [12]. To take the influence of temperature, strain, and strain rate in to consideration the Johnson-Cook's constitutive model was employed to predict the plastic behavior of the material. Table 6.1.3 gives values of the constants used in the Johnson-Cook's constitutive model. These constant are obtained from the literature [16 and 55] and are based on split Hopkinson pressure bar test. Recht's failure

criterion [8] is used to predict the shear-localization. To incorporate Johnson-Cook's material model and Recht's failure criterion a user subroutine was developed. *AdvantEdge*™, a commercially available 2D Lagrangian finite element code is used in this study. The simulations are carried out for different machining conditions to study the chip formation, more specifically the transition from continuous chip to shear-localized chip. The quantitative validation of the simulation results is done with the experimental results from the literature [9]. The qualitative validation of the simulation results is done by comparing the chip morphology of the chip generated experimentally [2 and 12] and by simulation.

Table 6.1.1 Yield strength of AISI 4340 steel of different hardness values [58]

Hardness (BHN)	*Yield Stress (MPa)*
215	675
325	950
520	1675

Table 6.1.2 Mechanical and thermal properties of AISI 4340 steel [12]

Property	*Value*
Young's Modulus (GPa)	200
Poisson's ratio	0.3
Density (kg/mm^3)	7850
Thermal conductivity (W / m °C)	33.346
Heat capacity (J / Kg °C)	460
Melting Temperature (°C)	1500

The Johnson-Cook's constants used in the simulation were available in the literature for material hardness of 520 BHN and 325 BHN (Table 6.1.3) [16 and 55]. As the Johnson-Cook's constants were not available for material hardness of 215 BHN, they were obtained by extrapolation which gave reasonable results.

Table 6.1.3 Johnson-Cook's constants used in the simulations [16 and 55]

Hardness (BHN)	*A (MPa)*	*B (MPa)*	*C*	*n*	*m*	$\dot{\varepsilon}_0$ *(1/s)*	T_r *Room Temperature (°C)*	T_m *Melting Temperature (°C)*
520	950	725	0.015	0.375	0.625	1	20.0	1500
325	792	510	0.014	0.26	1.03	1	20.0	1500
215	712	452	0.014	0.26	1.03	1	20.0	1500

Table 6.1.4 Cutting conditions used in the simulations

Process Parameter	*Value*	*Hardness*
Cutting Speed (m/min)	65, 125 and 488	215 BHN
	40, 125 and 275	325 BHN
	15, 61, and 125	520 BHN
Rake Angle (°)	-15, -5, 15 and 30	All
Depth of Cut (mm)	0.5	All

The cutting conditions used in the simulation are taken from the literature [2 and 12] to compare the results and thus verify the suitability of the material model and the failure criterion for metal cutting simulation applications (see Table 6.1.4). The friction

coefficient used in the study was 0.5. Simulations were run on an Intel Pentium 4 CPU (2.3 GHz) with 1 GB of RAM.

6.2 Model Validation

Section 5.1 of Chapter 5 enlists several assumptions made in the numerical model. Along with these assumptions the newly developed user subroutine incorporates Johnson-Cook's material model and Recht's failure criterion which needs to be validated. The model was verified by comparing finite element predictions with experimental results available in the literature [9]. Barry *et al.* [9] conducted turning cutting tests on AISI 4340 steel (520 BHN) at cutting speeds of 60, 120, and 180 m/min, rake angle -6° and depth of cut 2 mm. The depths of cut used were 0.02, 0.04, 0.06, and 0.08 mm for all combinations of cutting speeds with a constant value of rake angle and depth of cut.

Fig. 6.2.1 shows the variation of the average cutting forces for different depth of cut and cutting speeds. The cutting force tends to decrease slightly with increase in cutting speed in both experiments and numerical simulations. The maximum difference in the average cutting force between experimental and simulations is less than 11% for all the depths of cut. Thus, a reasonable agreement in the prediction of the cutting forces at different cutting speeds and depths of cut validates the numerical model and the assumptions of the material behavior.

As the experimental data for temperature and plastic strain is not available, a numerical model was developed in ABAQUS, another commercially available finite

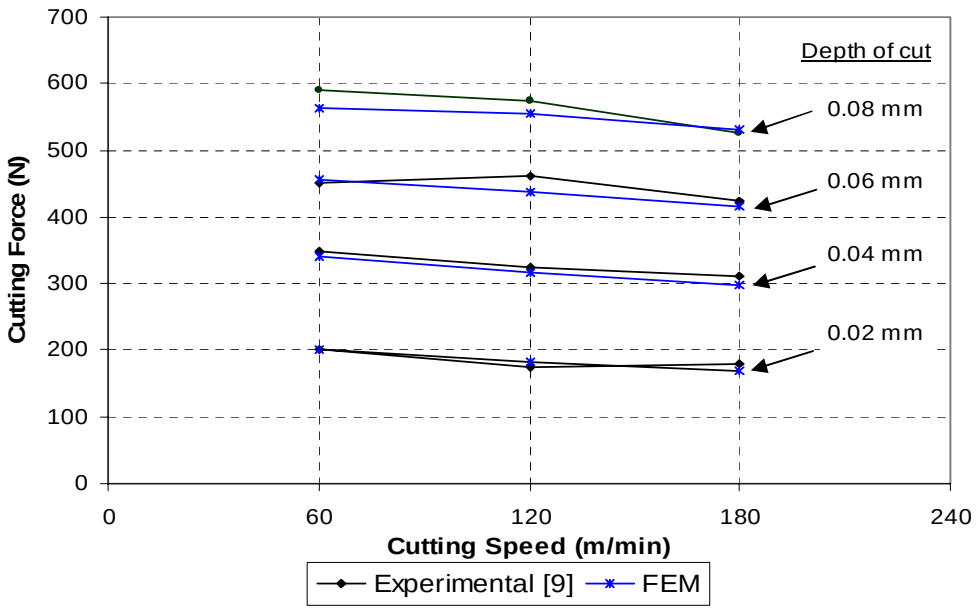

Fig. 6.2.1 Comparison of FEM and experimentally available cutting forces for different values of cutting speed and depth of cut [9]

element code. Johnson-Cook's material model and Johnson-Cook's damage model (shear failure) which are commonly used in the metal cutting simulations [16, 18 and, 59] was used in this investigation. Though, Johnson-Cook's damage model was used specifically for the saw-tooth chip formation simulations [16, 18 and, 59], it can be used here with the selection of machining parameters such that it will result in either a continuous chip or wavy chip without any discontinuation. The machining parameters used here are as follows: depth of cut 0.15 mm, rake angle 0°, and cutting speed 1000 m/min. Large depth of cut was not used to avoid extreme distortion of elements. Analysis of metal cutting was also done in *AdvantEdge*™ with similar machining conditions. Average temperature and average equivalent plastic strain in the shear zone and in the chip along the tool rake face were compared (Figs. 6.2.2 and 6.2.3).

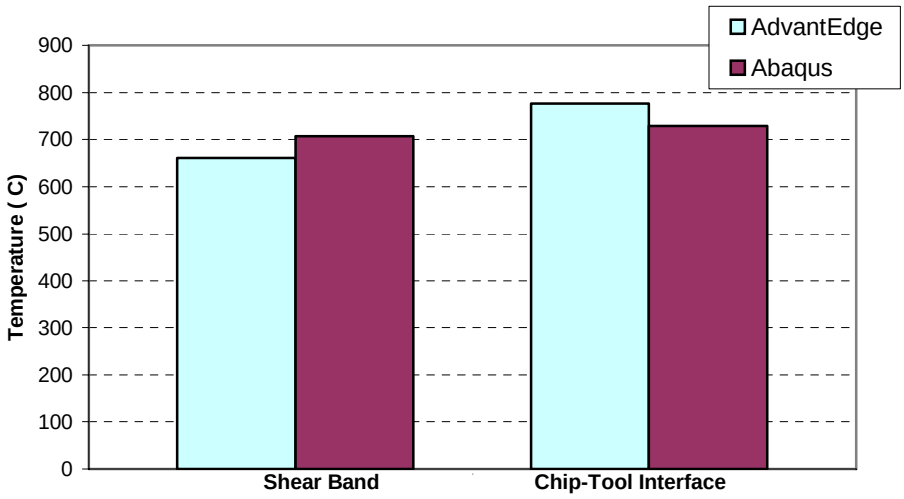

Fig. 6.2.2 Average temperatures obtained with *AdvantEdge*™ and ABAQUS in the shear band and at the chip-tool interface

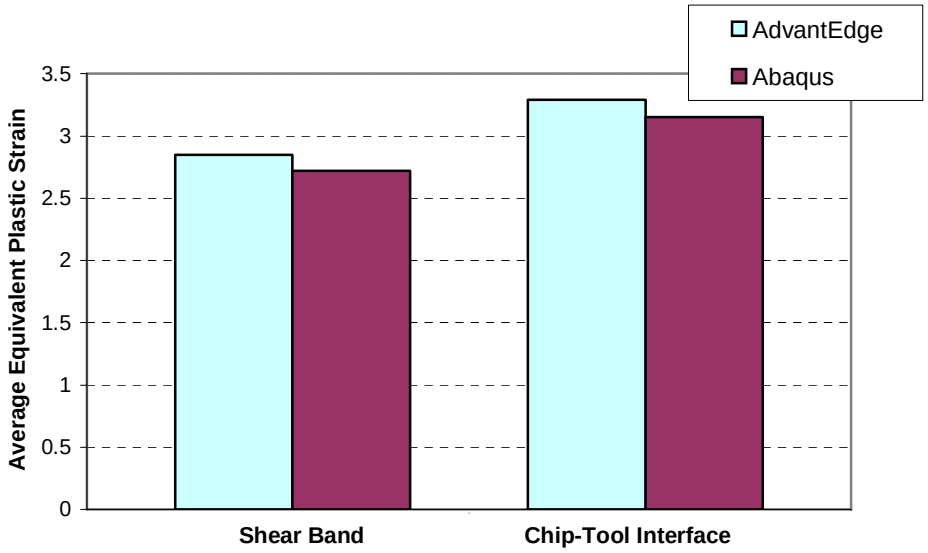

Fig. 6.2.3 Average equivalent plastic strain obtained with *AdvantEdge*™ and ABAQUS in the shear band and at the chip-tool interface

The chips produced in both simulations were continuous with some waviness on the back. The average temperature in the shear band was taken when steady state was reached. The average temperature in ABAQUS was taken at the centroid of the elements both along the shear band and the chip-tool interface. Approximately similar locations

were selected for the chip along the tool face in *AdvantEdge*™ and ABAQUS for comparison. Average equivalent plastic strain was also compared for the same locations. The error in the results obtained was in the range of 6.5% for the temperatures and equivalent plastic strains. Thus, the new failure criterion used in *AdvantEdge*™ shows reasonable agreement with the conventional failure criterion used in metal cutting simulations.

6.3 Catastrophic Shear Instability in the Machining Simulations of AISI 4340 Steel

When hardened AISI 4340 steel is machined at high cutting speeds, shear-localized chips are formed. This is primarily due to plastic instability, intense localized deformation in the primary zone leading to intense shear between the segments. Thermal energy is concentrated in the narrow shear band due to insufficient time for the dissipation of heat from these bands. The shear-localization observed in the simulations is similar to that explained in Section 4.5 of Chapter 4.

Various stages involved in the shear-localized chip formation process are shown in Fig. 6.3.1(a)-(f). Here, machining of AISI 4340 steel (325 BHN) is simulated at a cutting speed of 275 m/min, a tool rake angle of –15° and a depth of cut of 0.5 mm. Fig 6.3.1(a) shows a segment already formed and the beginning of the next segment as the tool approaches the work material. Appropriate stress, strain, and temperature fields begin to set up in the work material when the work material is upset with the advancement of the tool [see Fig 6.3.1(b)]. The shear surface begins to appear with

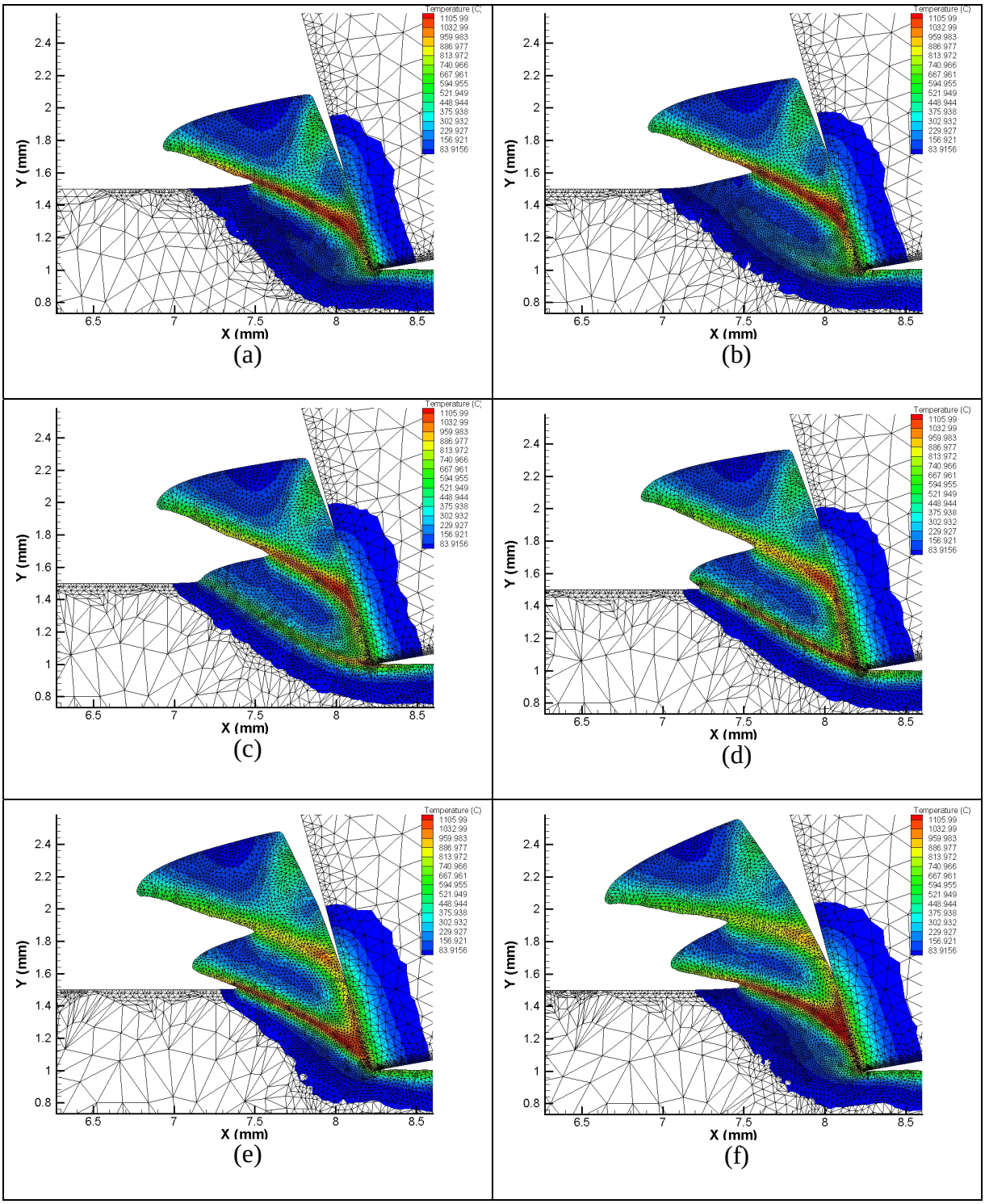

Fig. 6.3.1 Various stages involved in the shear-localized chip formation in the machining of AISI 4340 steel (325BHN) at 275 m/min

increased density of elements in the region. The element refinement in this region is due to the adaptive meshing technique used in the simulations. The shear surface originates from the tool tip almost parallel to the cutting velocity vector. The material begins to shear along this shear band as can be seen in Fig 6.3.1 (b). As the tool advances further [Fig 6.3.1 (c)], the stress, strain, and temperature fields in the shear surface develop conditions leading to thermoplastic instability. The shear surface gradually curves with concave surface upwards until it meets the free surface. High temperatures are generated in the shear surface. The instability is governed by the thermo-mechanical response of the work material under the conditions of cutting. Material ahead of the tool is upset forming the segment and shear-localization takes place simultaneously between the segments. The strain in the bulk of the segment is rather small which is also evident in the micrographs of the chips. The burden of further strain is accepted by a very thin band between the segments, thus localizing shear. As the tool advances further, the chip segment moves up the ramp formed by the workmaterial on the workpiece side of the shear band [Fig. 6.3.1(d)]. As the tool moves into the ramp, the segment is upset further [Fig. 6.3.1 (e)]. The segment is pressed against the tool rake face. The shearing between the segment and workpiece ceases when a new segment begins to form [Fig. 6.3.1(f)]. When the upsetting and shearing between the segments ceases, the segment moves up the tool face. This procedure is repeated again for the next segment.

Very high strains and temperature are seen at the chip-tool interface. This was observed to be due to the sliding of the segment on the tool rake face as was characterized by stick-slip motion. During shear-localization, the region between the

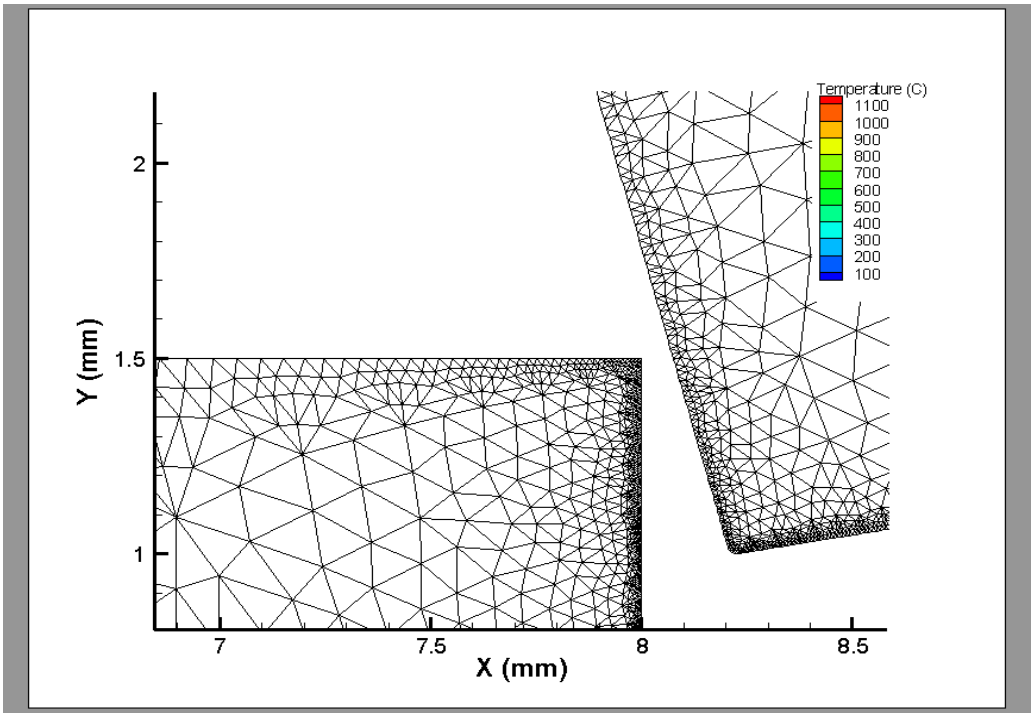

Animation of machining of AISI 4340 Steel (325 BHN) at cutting speed of 275 m/min, rake angle of -15°, and depth of cut of 0.5 mm

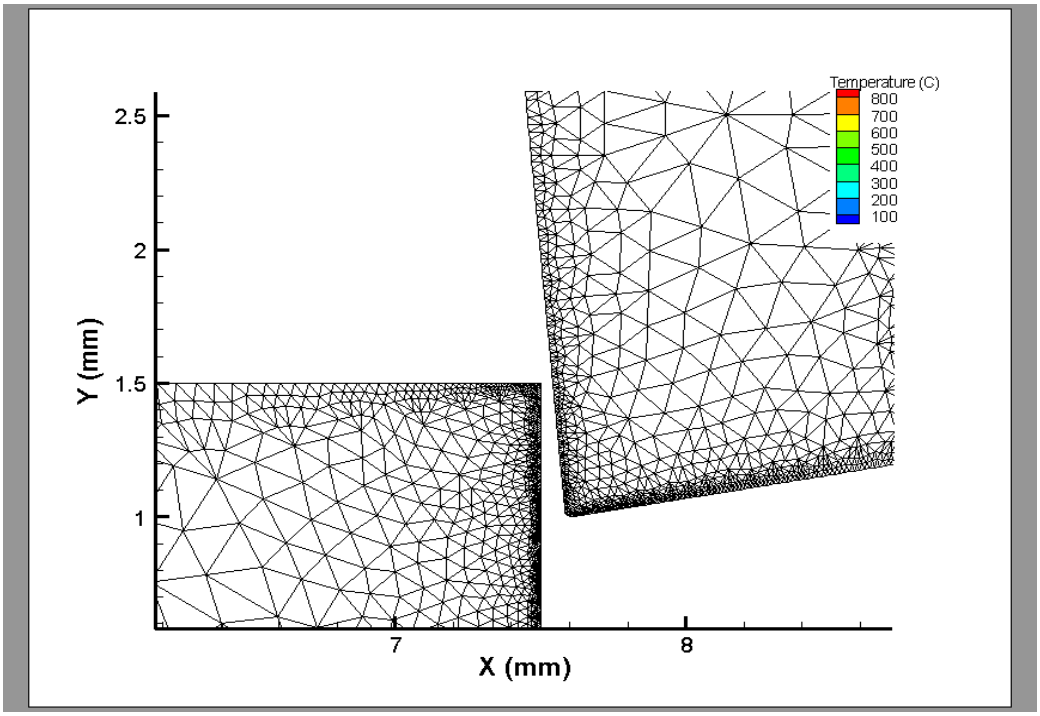

Animation of machining of AISI 4340 Steel (325 BHN) at cutting speed of 40 m/min, rake angle of -5°, and depth of cut of 0.5 mm

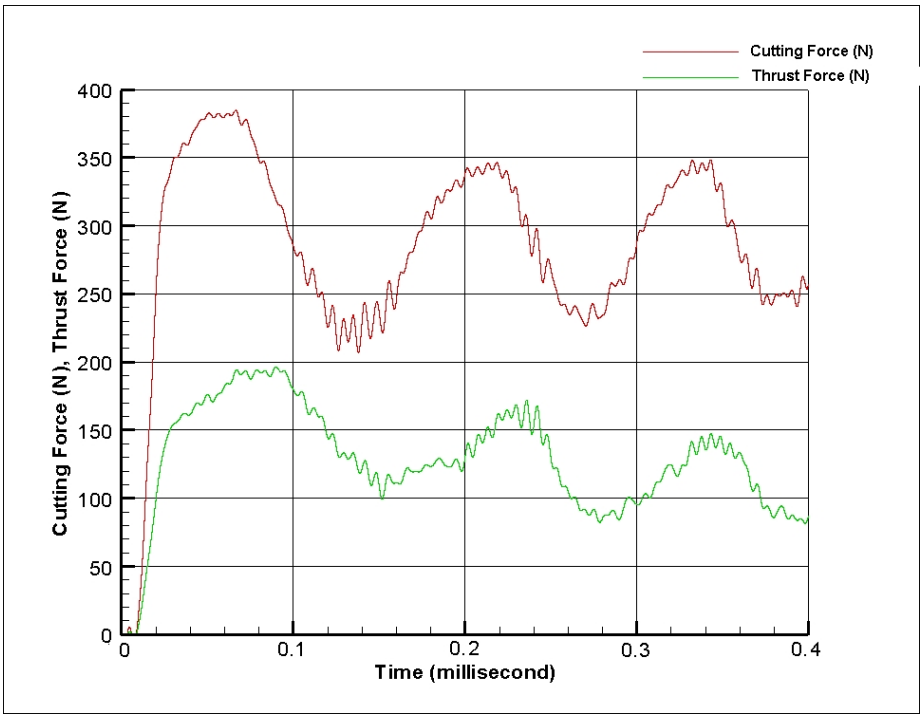

Fig 6.3.2 Dynamic components of the cutting and thrust forces in the machining of AISI 4340 steel (325 BHN) at cutting speed of 275 m/min and depth of cut 0.5 mm with a –15° rake angle

segments is seen to undergo shear separation between the segments followed by partial sliding between the chip segment and the tool face.

Fig. 6.3.2 shows that cutting and thrust forces fluctuate significantly from the mean when shear-localized chip is formed. The cutting and thrust force gradually rise during the upsetting of the segment and drops rapidly when the segment undergoes catastrophic shear. The periodic variation of forces causes undue vibrations in the machine system. Due to this, the tool also experiences deflections in a cyclic manner as described by Komanduri and von Turkovich [19]. The tool is pushed away from the workpiece during the upsetting stage and springs back on workpiece as the catastrophic shear takes place. This can cause tool fatigue and hence a reduction in tool-life.

6.4 Effect of Material Hardness on Chip Segmentation in the Machining of AISI 4340 Steel

In machining AISI 4340 steel, the chip morphology depends on many factors, such as microstructure and material hardness, cutting speed, tool rake angle, and the depth of cut. Komanduri *et al.* [19] and Komanduri and Hou [12] reported the effect of material hardness on shear-localization. They observed that with increase in material hardness, the cutting speed at which the shear-localized chip is formed reduces. They reported cutting speeds of shear-localized chip for material hardness of 215 BHN, 325 BHN, and 520 BHN (see Table 4.2.1 for details). For all the machining conditions, they used a tool rake angle of -5° and a depth of cut of 0.5 mm. These conditions were used here for the simulation of metal cutting process for comparison.

Figs. 6.4.1 (a)-(f) shows the temperature and equivalent plastic strain contours obtained in the simulations at different cutting speeds and different material hardness values. They show intense localization of high temperatures and plastic strains in the shear band. It can be seen from the figure that cutting speed at which shear-localization occurs for different hardness values of the work material is different. Shear-localized chip is observed at a cutting speed of 61 m/min for the material hardness of 520 BHN, 275 m/min and 488 m/min for material hardness of 325 BHN and 215 BHN, respectively. While machining AISI 4340 steel (325 BHN) at a cutting speed of 125 m/min (keeping all the other machining conditions constant), the chip formed was observed to be inhomogeneous on the gross level with two wide regions, one where deformation was very high (i.e., between the segments) and the other where deformation was relatively

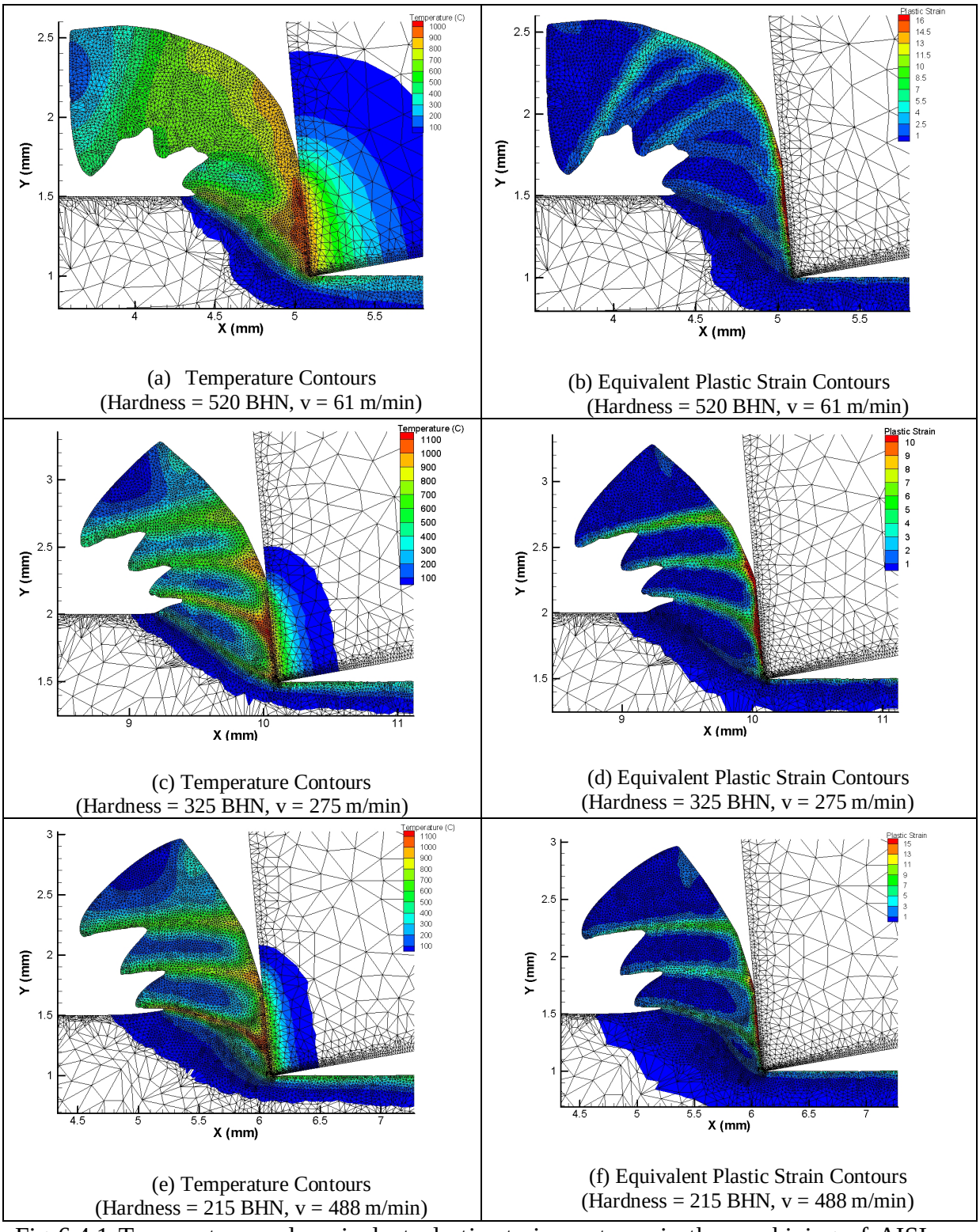

(a) Temperature Contours
(Hardness = 520 BHN, v = 61 m/min)

(b) Equivalent Plastic Strain Contours
(Hardness = 520 BHN, v = 61 m/min)

(c) Temperature Contours
(Hardness = 325 BHN, v = 275 m/min)

(d) Equivalent Plastic Strain Contours
(Hardness = 325 BHN, v = 275 m/min)

(e) Temperature Contours
(Hardness = 215 BHN, v = 488 m/min)

(f) Equivalent Plastic Strain Contours
(Hardness = 215 BHN, v = 488 m/min)

Fig 6.4.1 Temperature and equivalent plastic strain contours in the machining of AISI 4340 steel of different hardness values

low (i.e., within the segments). Whereas, with further reduction in cutting speed from 125 m/min to 40 m/min, continuous chip was observed to be formed. To verify the effect of material hardness on shear-localization, another set of simulations were performed at a constant cutting speed of 125 m/min for all the material hardness values. Rest of the machining parameters were kept constant as in previous set of simulations, i.e. the tool rake angle of -5°and a depth of cut of 0.5 mm.

Intense shear-localization was observed in the chip with material hardness of 520 BHN. Due to high material hardness and high speed, thermal softening was always observed to predominate over strain hardening in the shear zone. Once the shear had taken place along the main shear plane, the strength there becomes lower than before. So, the main shear plane is still the weakest plane and hence shear is observed to continue in the same plane. For the same machining condition and material hardness of 325 BHN, shear-localization was observed to be of less intense nature and the degree of segmentation was less than observed in the machining of the material hardness of 520 BHN. A smaller segment was observed between two bigger fully formed segments. When machining AISI 4340 (215 BHN) chip with relatively smaller segments were observed than with material hardness values of 520 BHN and 325 BHN. Here, the thermal energy was not observed to concentrate in the shear band as much as it did in material hardness of 325 BHN. It was observed to dissipate more within the chip. The thermal softening was not observed to be much dominating in the shear zone.

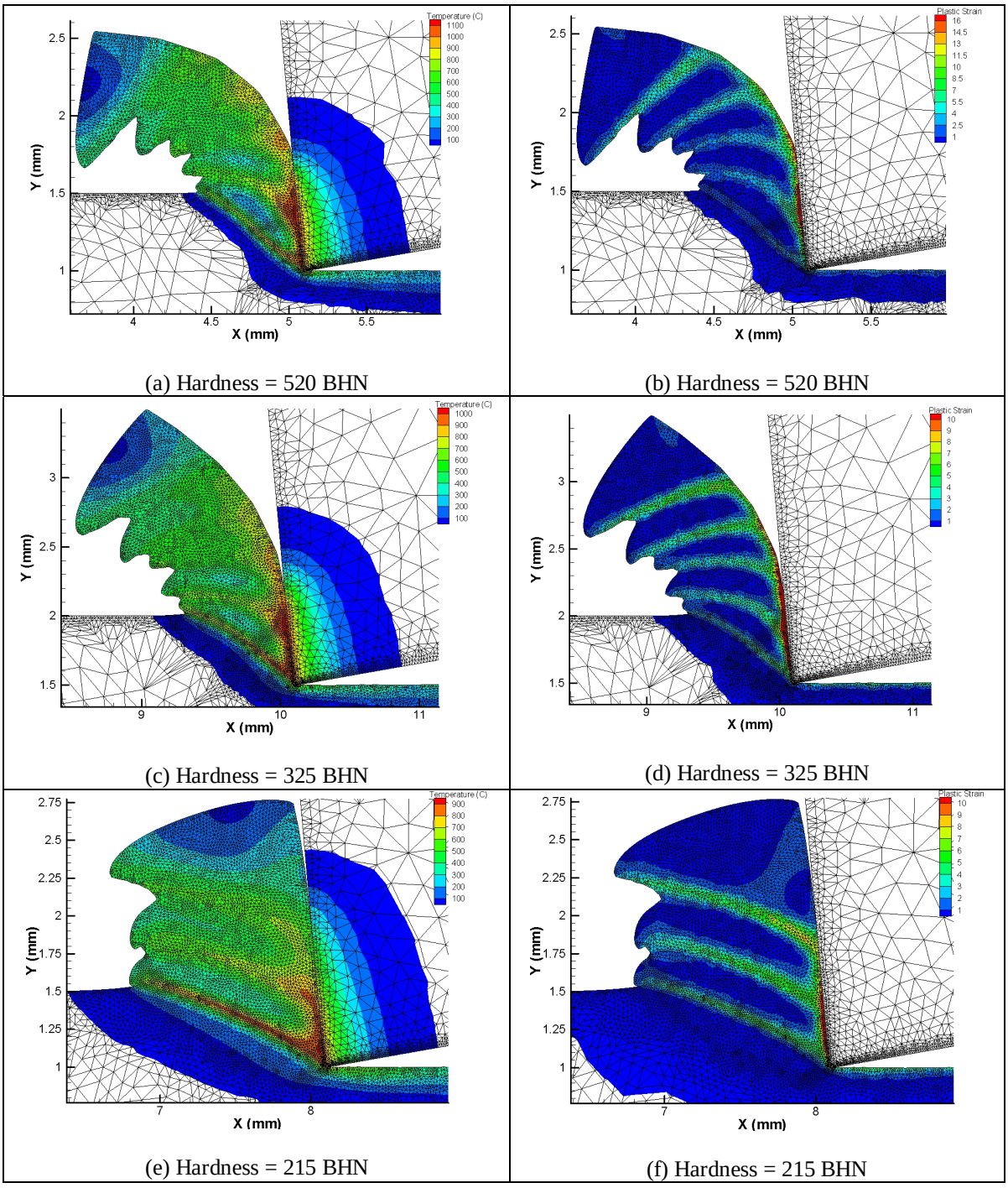

(a) Hardness = 520 BHN

(b) Hardness = 520 BHN

(c) Hardness = 325 BHN

(d) Hardness = 325 BHN

(e) Hardness = 215 BHN

(f) Hardness = 215 BHN

Fig. 6.4.2 Temperature contours and equivalent plastic strain contours in the machining of AISI 4340 steel of hardness 520 BHN (a and b), 325 BHN (c and d) and 215 BHN (e and f) at 125 m/min

6.5 Effect of Cutting Speed on Chip Segmentation in the Machining of AISI 4340 Steel

It has been reported in the literature that cutting speed plays an important role in metal cutting and subsequently in the resultant chip morphology [2, 12, and 17]. It is shown in Section 4.4 of Chapter 4 that with increase in the cutting speed, the chip morphology changes from continuous to shear-localized in AISI 4340 steel. The finite element analysis of machining AISI 4340 steel of different hardness values and at different cutting speeds revealed the effect of cutting speed on temperature and equivalent plastic strain in the shear zone, cutting and thrust forces, and power consumed. The cutting speeds used in the simulations were 15 and 61 m/min, for hardness 520 BHN; 40, 125, and 275 m/min, for hardness 325 BHN; and 65 and 488 m/min, for hardness 215 BHN. The tool rake angle used was -5° and depth of cut used was 0.5 mm. Fig. 6.5.1(a)-(f) gives the comparison of the micrographs of the chips formed in the experimental and simulations of the machining of AISI 4340 (325 BHN) at cutting speed of 40 m/min, 125 m/min, and 275 m/min.

Fig. 6.5.1(a) shows the resultant chip when AISI 4340 steel of hardness 325 BHN was machined at a cutting speed of 40 m/min. At this speed, the plastic deformation rate of the material was observed to be lower. The temperature distribution within the chip was seen to be evenly distributed throughout the chip except at the tool-chip interface where the temperature was highest. Strain-hardening strengthens the material at the shear zone. Similar to the temperature distribution, the strain was also evenly distributed throughout the chip except at the tool-chip interface. Strain-hardening in the process always dominates over thermal softening. These factors contribute towards the generation

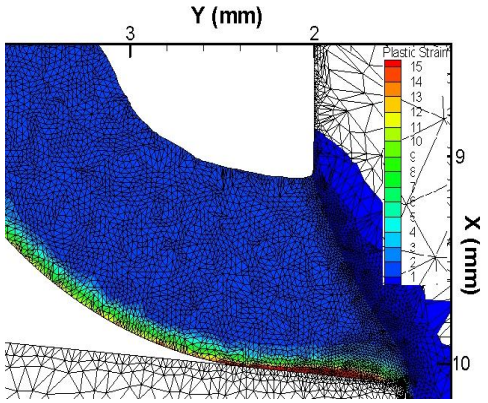

(a) v = 40 m/min, plastic strain contours

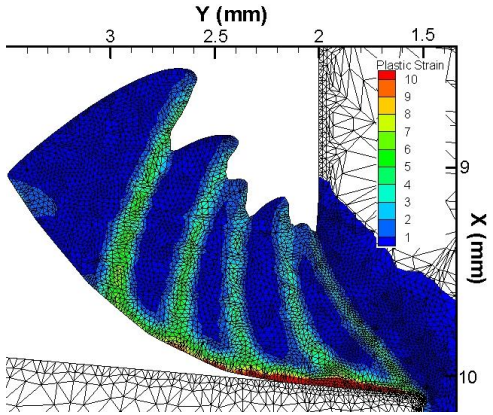

(c) v = 125 m/min, plastic strain contours

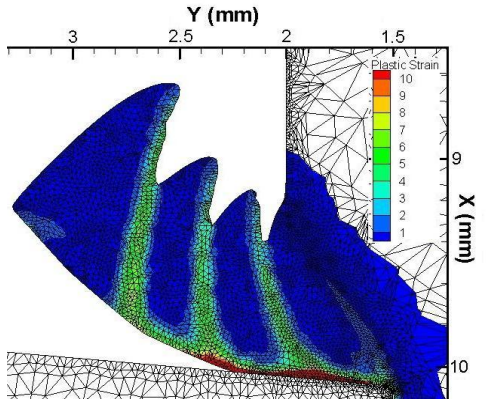

(e) v = 275 m/min, plastic strain contours

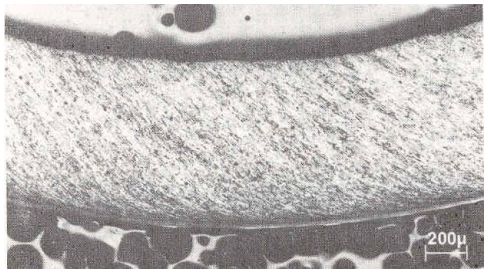

(b) v = 40 m/min

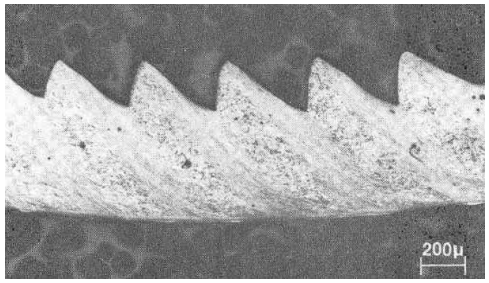

(d) v = 125 m/min

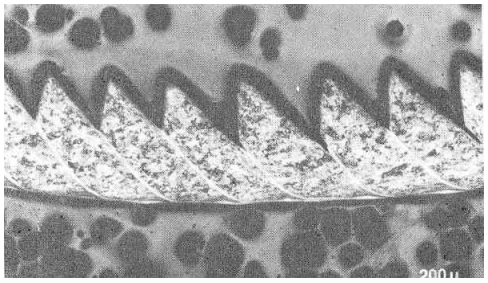

(f) v = 275 m/min

Fig. 6.5.1 Comparison of the micrographs of the chips formed in the machining and in simulation of AISI 4340 (325 BHN) at cutting speed of 40 m/min (a,b), 125 m/min (c,d) and 275 m/min (e,f)

of a continuous chip. When the cutting speed was changed to 125 m/min (keeping all other parameters constant), the deformation of the chip was found to be inhomogeneous on the gross level with two wide regions, one where deformation was very high (i.e., between the segments) and the other where deformation was relatively low (i.e., within the segments) [Fig. 6.5.1(b)]. With further increase in cutting speed to 275 m/min, the catastrophic shear appeared to set in completely in the primary shear zone. Due to higher cutting speed, the rate of deformation was observed to be high. The temperature was localized in the shear zone making the material softer locally. Recht, in his model, explains this behavior of the material as when thermal softening exceeds strain-hardening in the shear band, it results in catastrophic failure of the material. The chip morphology obtained by finite element method is in reasonable agreement with the experimental results reported in Ref. 12.

The tool nose radius has a significant effect on the chip formation process. In the

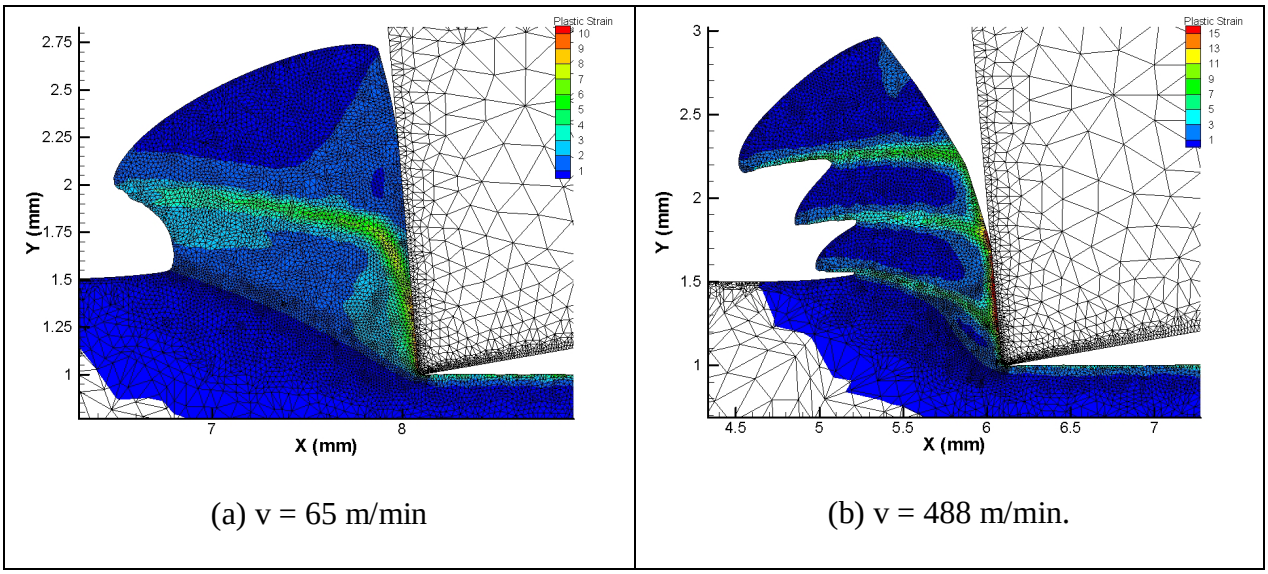

(a) v = 65 m/min

(b) v = 488 m/min.

Fig. 6.5.2 Chip morphology observed in the machining of AISI 4340 Steel (215 BHN) at cutting speeds of (a) v = 65 m/min, (b) v = 488 m/min

present investigation one-tenth value (0.05 mm) of the depth of cut was selected to avoid any major effects on chip formation. If the tool nose radius is increased beyond the depth of cut, the tool with positive rake angle essentially acts as negative rake angle tool, thus changing the cutting conditions and hence the chip formation process. The tool nose radius along with feed rate and cutting speed plays a vital role on the surface finish of the machined surface of the workmaterial. With larger tool nose radius, lower feed rates, and higher cutting speeds the very fine surface finish can be achieved [62].

Transition in the chip morphology from continuous to shear-localized chip was also observed when machining AISI 4340 steel (215 BHN) at cutting speeds of 65 m/min [Fig. 6.5.2 (a)] and 488 m/min [Fig. 6.5.2 (b)]. Similar results were observed for AISI 4340 steel (520 BHN) when machined at cutting speed of 15 m/min [Fig. 6.5.3 (a)] and 61 m/min [Fig. 6.5.3 (b)].

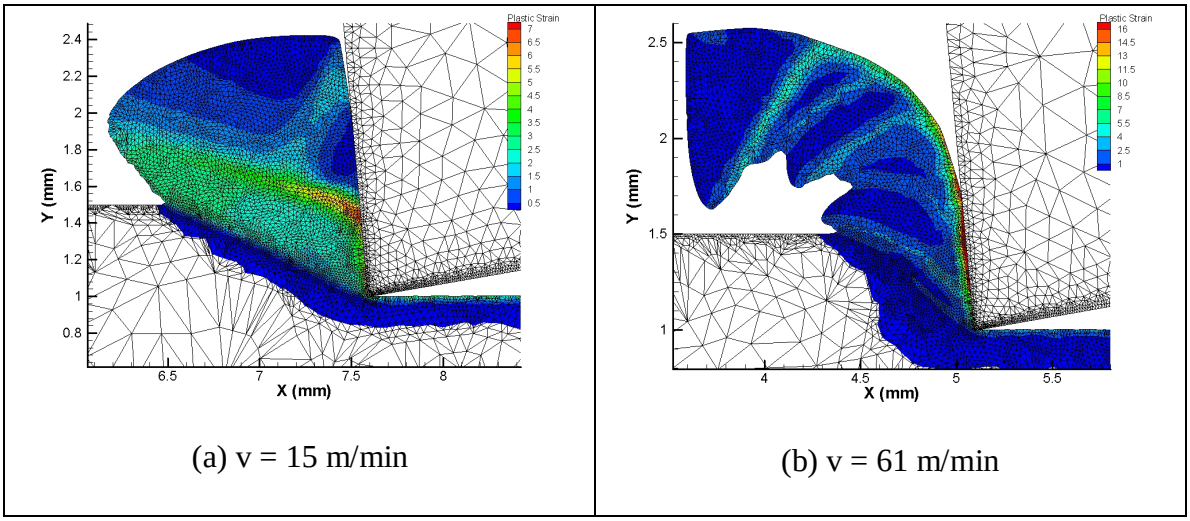

(a) v = 15 m/min

(b) v = 61 m/min

Fig. 6.5.3 Chip morphology observed in the machining of AISI 4340 Steel (520 BHN) at cutting speeds of (a) v = 15 m/min, (b) v = 61 m/min

The temperature and equivalent plastic strain in the shear zone were found to be different for different cutting speeds and material hardness values. The trend of the

temperature in the shear zone followed by materials with different hardness at different cutting speed was more or less identical [Fig. 6.5.4 (a)]. When machining AISI 4340 steel (215 BHN) at a cutting speed of 65 m/min, the temperature in the shear zone was observed to be 550°C. It rose steeply to 850°C at a cutting speed of 125 m/min and then slowly to 1040°C at 488 m/min. For 325 BHN hardness, it was observed to be 545°C at 40 m/min and steeply rose to 984°C at 125 m/min and then slowly to 957°C at 275 m/min. For hardness of 520 BHN, it was observed to be 700°C at 15 m/min, steeply rose to 880°C at 61 m/min and then slowly to 970°C at 125 m/min. Thus, the temperature in the shear zone was observed to be lower for continuous chip, then rise fast when the shear instability in the shear zone is set in. Once the shear instability is set in, the increment in the shear zone temperature is slower for the rest of the incremental cutting speeds.

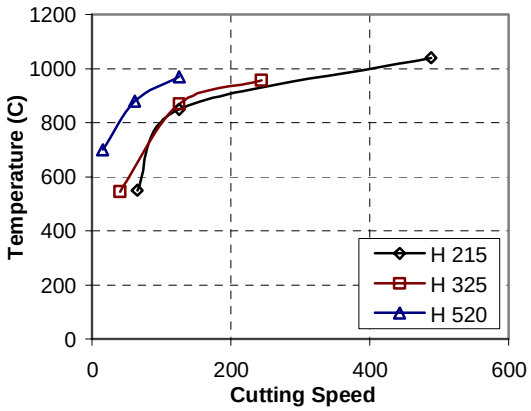

(a) Temperature

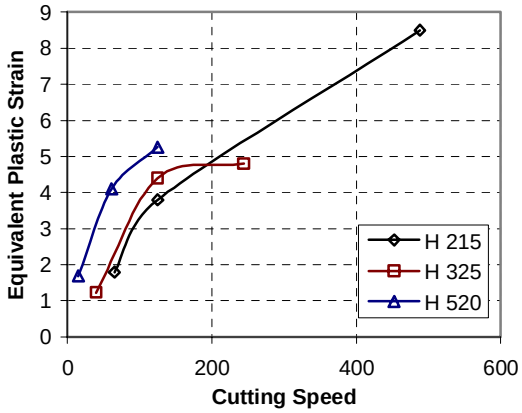

(b) Equivalent plastic strain

Fig. 6.5.4 (a) Temperature and (b) equivalent plastic strain in the shear zone in the machining of AISI 4340 steels of different hardness values

The equivalent plastic strain in the shear zone also follows, more or less, in a similar manner as does the shear zone temperature for material with different hardness

values [Fig. 6.5.4 (b)]. The equivalent plastic strain in the shear zone was found to be between 100% and 200% for all the material hardness values when machined with their respective lower speeds at which continuous chip is produced. The plot for material hardness of 215 BHN does not show the normal trend as others because of the intermediate cutting speed of 125 m/min, which is too close to the cutting speed at which continuous chip is formed. If a cutting speed higher than 125 m/min but lower than 488 m/min is used, this usual trend could be noted.

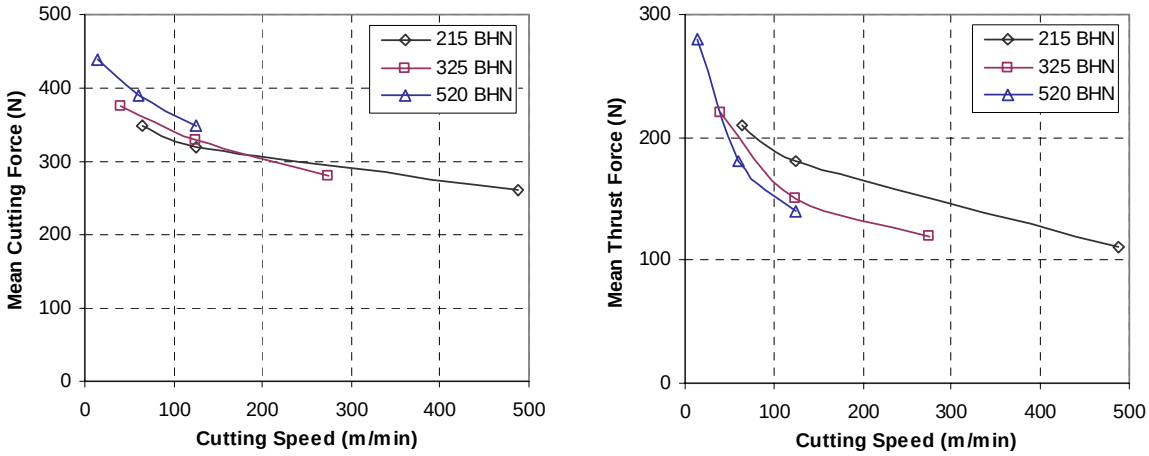

(a) Mean cutting force (b) Mean thrust force

Fig. 6.5.5 (a) Mean cutting force and (b) mean thrust force in the machining of AISI 4340 steels of different hardness values, depth of cut = 0.5 mm

Fig. 6.5.5 shows the variation in cutting and thrust forces for all the material hardness values. Both cutting and thrust forces show a decreasing trend as the chip morphology changes from continuous to shear-localized with increase in cutting speed. This trend is consistent with the observations by various researchers [15, 24, and 25]. This decreasing trend can be attributed to the localized adiabatic heating in the shear-localized chips. At lower cutting speeds, strain hardening dominates all the time in the

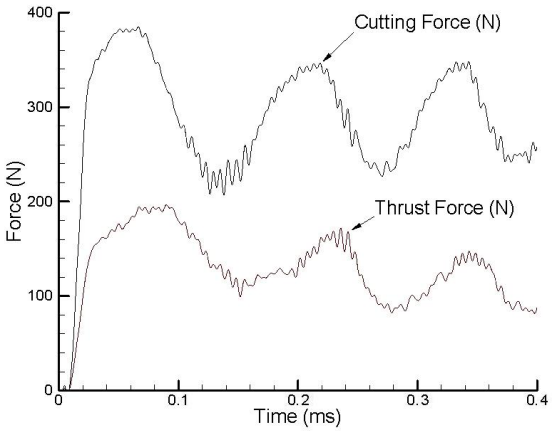

(a) Forces when shear-localized chip is produced (v = 275 m/min, α = -5°)

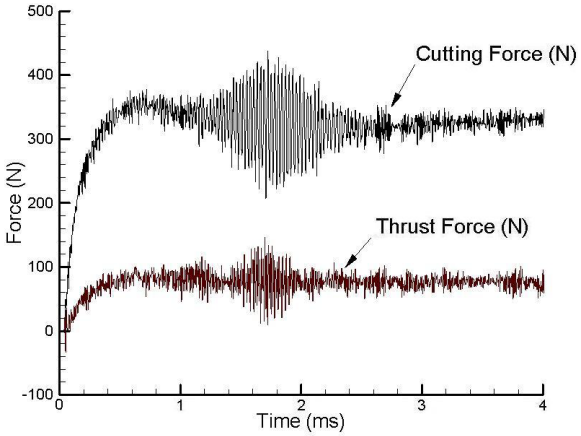

(b) Forces when continuous chip is produced (v = 40 m/min, α = 15°)

Fig. 6.5.6 Cutting and thrust forces trend when the shear-localized and continuous chip is produced in the machining of AISI 4340 steel (325 BHN)

chip formation process which increases the strength of the material, resulting in a continuous chip. While at higher cutting speed, thermal softening exceeds the strain hardening and generates higher temperatures in a very thin area (shear zone). This

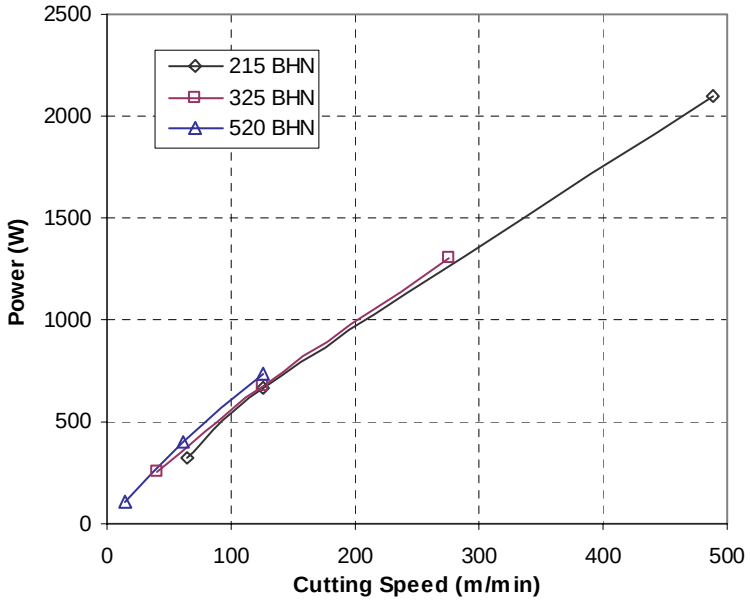

Fig. 6.5.7 Power required to machine AISI 4340 steel of different hardness values at different cutting speeds

weakens the material in the shear zone rapidly due to which the force required in less. Although, the cutting force in the shear-localized chip formation process is less than that in the continuous chip formation process, it is of fluctuating nature (see Fig. 6.5.6). This fluctuation gives rise to vibrations in the machine tool making the process unstable.

Fig 6.5.7 shows the power required for machining AISI 4340 steel of different hardness values at different cutting speeds. It can seen from the plot that power is directly proportional to the cutting speed i.e., it increases almost linearly with increase in cutting speed. It does not depend on the type of chip formed in machining.

6.6 Effect of Rake Angle on Chip Segmentation in the Machining of AISI 4340 Steel

The effect of rake angle on the temperature and equivalent plastic strain in the shear zone, cutting and thrust forces, and power required to machine AISI 4340 steel of different material hardness values at different cutting speeds is studied in this investigation. Tools with rake angles of -15°, -5°, 15°, and 30° are used.

The tool rake angle showed a significant effect on the chip morphology for all the material hardness values. Fig. 6.6.1 shows the rake angle effect for AISI 4340 steel (325 BHN) at different cutting speeds. Although, the rake angle of -15° produced shear-localized chip for all the cutting speeds, the intensity of shear-localization differed with cutting speed. At a cutting speed of 40 m/min and a rake angle -15°, waviness is observed in the chip.

As explained in the previous section, with a rake angle of -5° at a cutting speed of 40 m/min, the chip produced was continuous. With further increase in rake angle, the

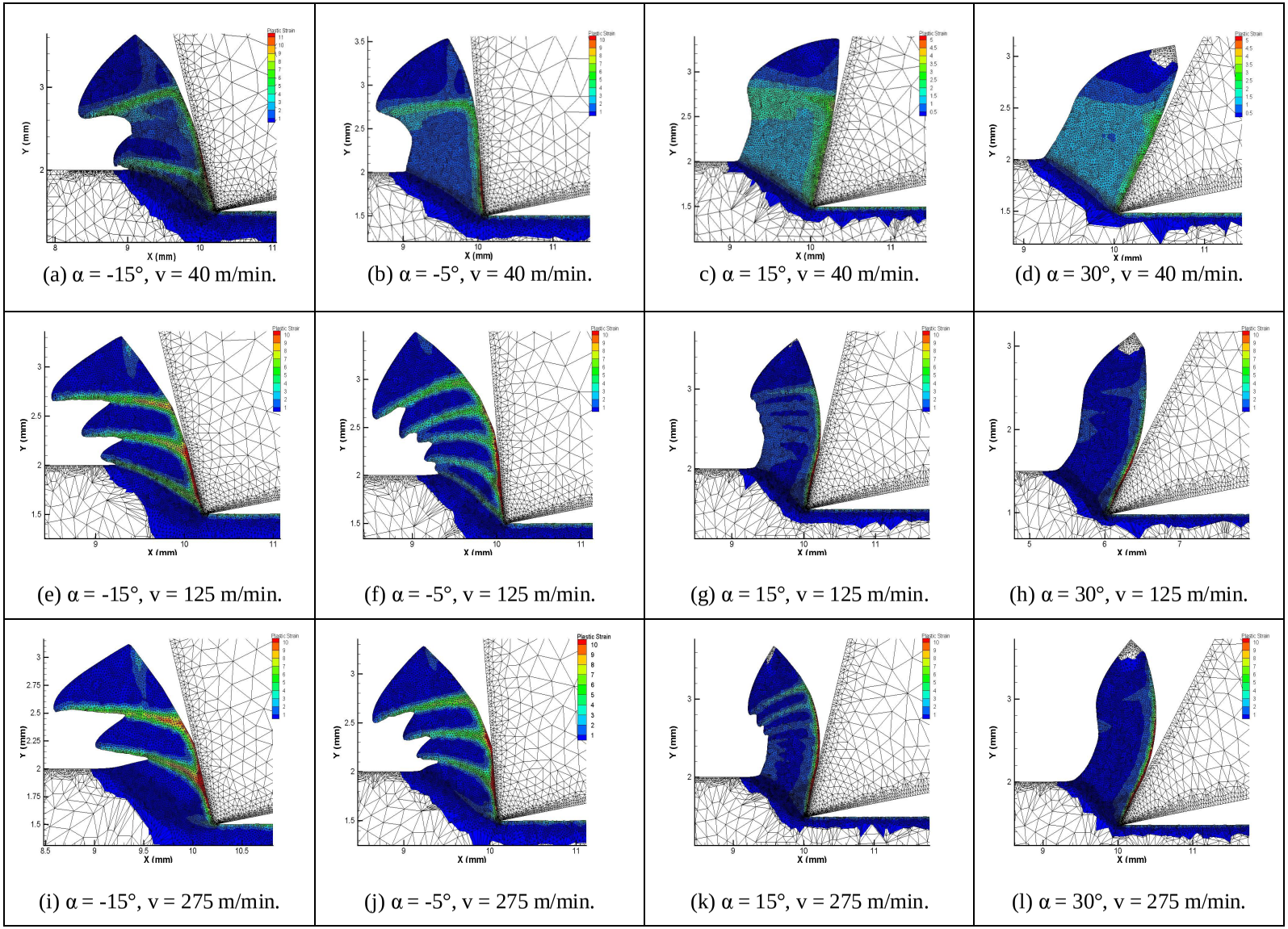

(a) α = -15°, v = 40 m/min. (b) α = -5°, v = 40 m/min. c) α = 15°, v = 40 m/min. (d) α = 30°, v = 40 m/min.

(e) α = -15°, v = 125 m/min. (f) α = -5°, v = 125 m/min. (g) α = 15°, v = 125 m/min. (h) α = 30°, v = 125 m/min.

(i) α = -15°, v = 275 m/min. (j) α = -5°, v = 275 m/min. (k) α = 15°, v = 275 m/min. (l) α = 30°, v = 275 m/min.

Fig 6.6.1 Effect of rake angle on chip formation in the machining of AISI 4340 steel (325 BHN) at different cutting speeds

chip formed continued to be continuous. A cutting speed of 125 m/min and tool rake angle of -15° produced shear-localized chips. With further increase in rake angle (from negative to positive), the chip morphology changed from shear-localized to continuous. Chips produced were from inhomogeneous shear-localized with -5° rake angle, initial wavy then continuous with a 15°, to continuous with 30° rake angle. A similar trend in change in chip morphology was observed when cutting speed was changed to 275 m/min.

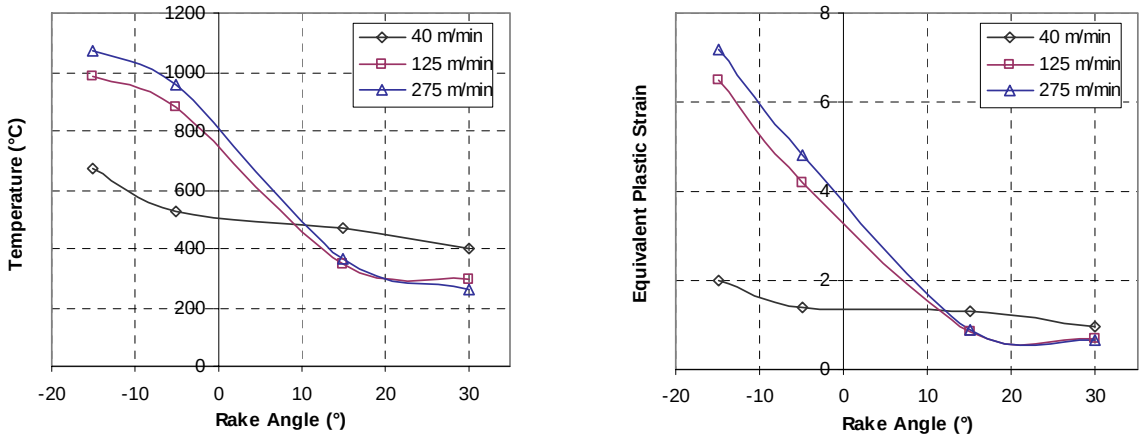

(a) Temperature (b) Equivalent plastic strain

Fig. 6.6.2 (a) Temperature and (b) equivalent plastic strain in the shear zone in the machining of AISI 4340 steel (325 BHN)

Important observations in temperature and equivalent plastic strain in the shear zone for different cutting speeds used in the machining AISI 4340 steel (325 BHN) can be made from the Fig. 6.6.2. Temperature and equivalent plastic strain generated in the shear zone also depends on the cutting speed. More importantly, it also depends on the chip thickness ratio in continuous chip formation process. From Fig 6.6.2 (a), at a cutting speed of 40 m/min, the temperature in the shear zone was observed to be about 690°C for a rake angle -15°. It reduces to about 545°C for a rake angle -5°, then 500°C for a rake angle of 15°, and finally to about 420°C for a rake angle of 30°. When the speed was

increased to 125 m/min, the instability has already set in. The work done in the process is more and therefore the temperature in shear zone was found to increase to about 980°C for a -15° rake angle. Then with increase in the rake angle to positive values, the temperature in the shear zone was found to decrease. A similar trend was observed at a cutting speed of 275 m/min.

Here, an important observation regarding the shear zone temperature can be made. Larger difference was found in the shear zone temperature when machined with tools with negative rake angles at different cutting speeds. This can be attributed to the extent of the segmentation with increasing cutting speed and decreasing rake angle. At the cutting speed of 275 m/min and rake angle of -15°, the amount of segmentation is more than at cutting speed of 125 m/min and 40 m/min. Due to which the shearing between the segments is more and hence the temperature rise. But with the tool with 15° and 30° rake angles, the difference in the shear zone temperature was observed to be less as compared to when machined with negative rake angles. This can be due to the continuous chip formation at all the cutting speeds when machined with tools with positive rake angles.

The observation in the shear zone equivalent plastic strains followed a similar trend as the shear zone temperature, at different cutting speeds [Fig. 6.6.2(b)]. An important thing to be noted here is that, when the shear instability sets in at cutting speed of 125 m/min, the shear zone temperature and equivalent plastic strain shoots up for -15° and -5° rake angle tools. With further increase in cutting speed to 275 m/min, where complete shear-localization is observed, raise in the temperature and equivalent plastic strain in the shear zone is relatively less. This shows that the dynamic shear strength of

the material tends to become insensitive to strain rate when catastrophic shear is developed. This is in agreement with the observation by Recht [8].

The temperature and equivalent plastic strain trend lines for different cutting speeds crosses within the range of ±2° of tool rake angle. The reason for this can be due to difficulty in measuring the average temperature and equivalent plastic strain along the shear zone.

Fig. 6.6.3 shows the tool rake face temperature in the machining of AISI 4340 steel (BHN 325). The tool rake face temperature was observed to be higher for -15° rake

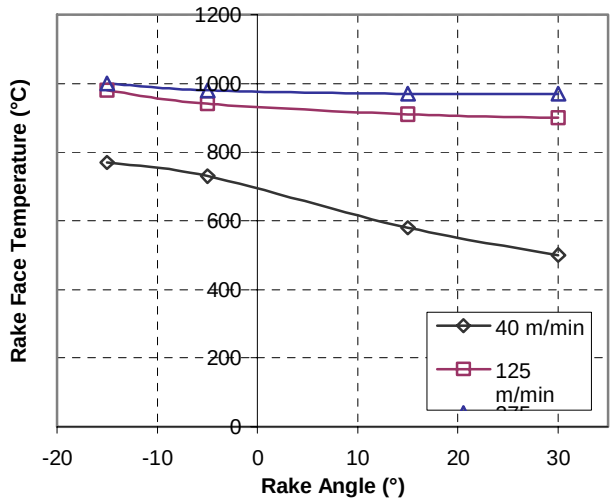

Fig. 6.6.3 Tool rake face temperature in the machining of AISI 4340 steel (325 BHN).

angle tool at all cutting speeds. The tool rake face temperature was observed to be of relatively less decreasing trend for cutting speeds at 125 m/min and 275 m/min than at cutting speed of 40 m/min for rest of the rake angles (-5°, 15°, and 30°). The rake face temperature mainly depends on the friction coefficient and the work done at the tool-chip interface. The higher temperature limits the metal removal rate in machining and hence affects the tool life significantly.

For the cutting speed of 275 m/min, the rake face temperatures were observed to be higher than at cutting speeds of 125 m/min and 40 m/min for all the rake angles. At a cutting speed of 40 m/min, the plastic strain in the secondary shear zone is less as compared to cutting speeds of 125 m/min and 275 m/min (see Fig. 6.6.1). Therefore, the temperature gradients established are less at 40 m/min with any rake angle tool. The decreasing nature of rake face temperature plot for 40 m/min with increase in rake angle (from negative to positive) can be attributed to the type of chip produced. In the continuous chip, strain-hardening is predominant and therefore the shear deformation is distributed throughout the material. Along with this, the temperature gradients at the tool-chip interface are lower at this cutting speed. On the whole, the work done goes on decreasing with increase in the tool rake angle. Therefore, the rake face temperatures decrease with increase in the tool rake angle at cutting speed of 40 m/min. But, at the cutting speeds of 125 m/min and 275 m/min the chip morphology changes from shear-localized to continuous with increase in the rake angle (from negative to positive). The rake temperature with the continuous chip is almost same with the shear-localized chip because the rake face temperature is determined by averaging elemental temperature over the entire contact length and due to which the effect of the high temperature shear zone at the interface is significantly lessen. Whereas, the rake face temperature distribution is almost constant along the entire contact length with the continuous chip except at the tool tip. Therefore, this can be the reason for almost constant average rake face temperature with negative as well as positive rake angles at the cutting speeds of 275 m/min and 125 m/min.

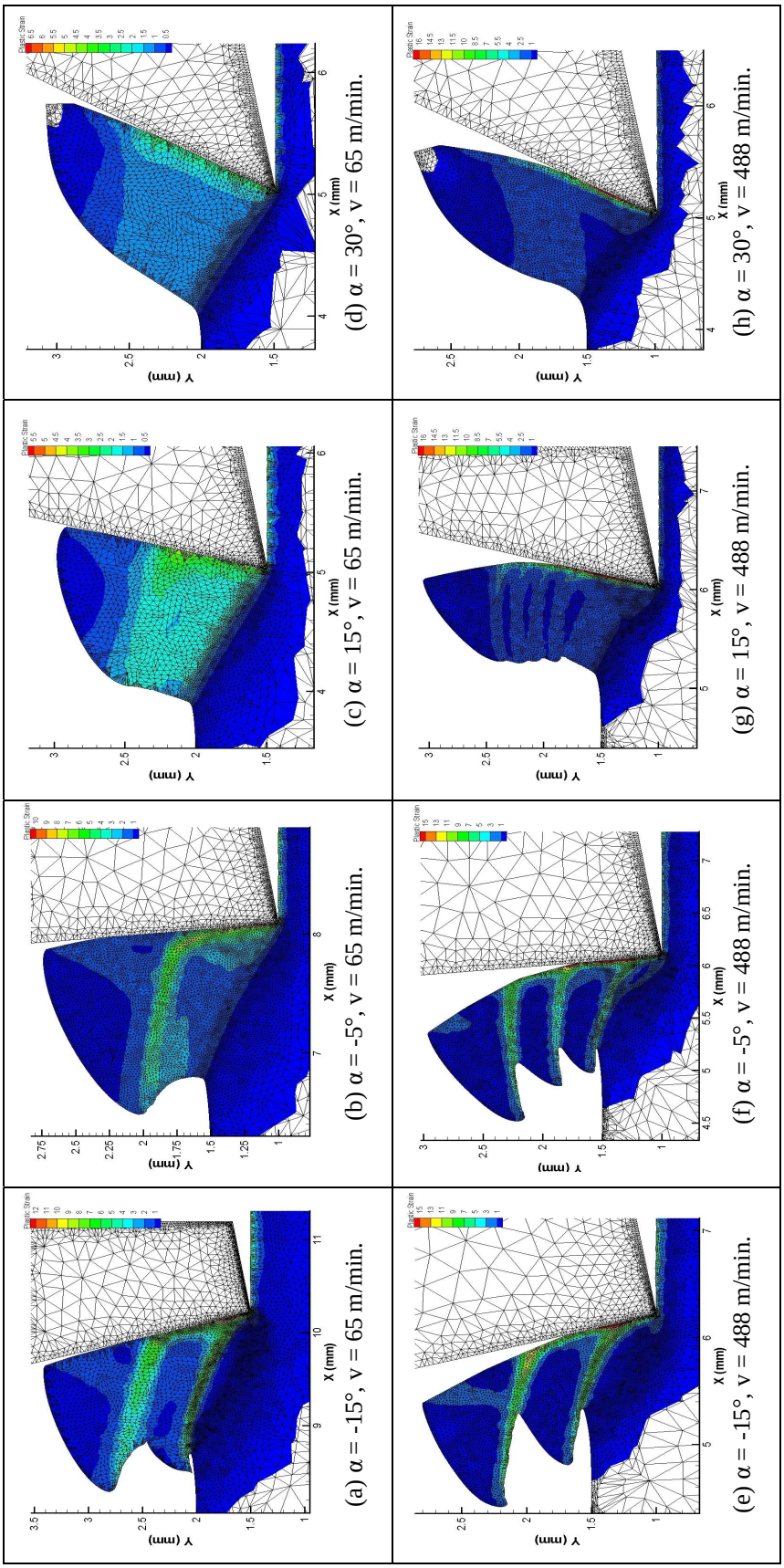

Fig 6.6.4 Rake angle effect on chip formation in the machining of AISI 4340 steel (215 BHN) at two cutting speeds, i.e. 65 m/min and 488 m/min

The change in chip morphology observed when machining AISI 4340 steel (215 BHN) was similar to one observed in AISI 4340 steel (325 BHN) (Fig. 6.6.4). At a cutting speed of 65 m/min and a rake angle of -15°, a wavy chip was observed with minimum shear-localization. As the rake angle was increased to -5°, the chip morphology has resulted in the generation of continuous chip as explained in the previous section. With further increase in the tool rake angle to 15° and 30°, the chip produced continued to be continuous. When machined at a cutting speed of 488 m/min and -15° rake angle, intense shear-localization is observed. Greater amount of work is done in the shear zone. When the rake angle was changed to -5°, shear-localized chip was continued to be observed, but the work done was found to be less. Rake angle of 15°, initial chip morphology was observed to be a little wavy followed by a continuous chip. A rake angle of 30° produced continuous chip.

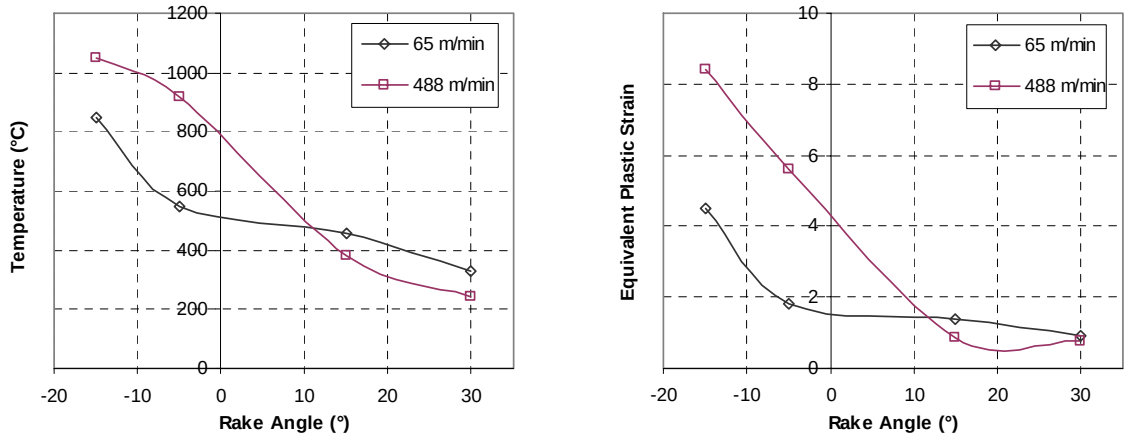

(a) Temperature (b) Equivalent plastic strain

Fig 6.6.5 (a) Temperature and (b) equivalent plastic strain in the shear zone in the machining of AISI 4340 steel (215 BHN)

The trend in the shear zone temperature [Fig. 6.6.5(a)] and equivalent plastic strain [Fig. 6.6.5(b)] for a cutting speed of 65 m/min was observed to be very similar to that at 40 m/min in cutting AISI 4340 steel (325 BHN). For a cutting speed of 488 m/min, variation in temperature and equivalent plastic strain in the shear zone in machining AISI 4340 steel (215 BHN) were observed to be almost constant for all the rake angles. The temperature and equivalent plastic strain trend lines for different cutting speeds crosses within the range of ±2° of tool rake angle. As explained earlier for the case of AISI 4340 steel (325BHN), the reason for this can be due to difficulty in measuring the average temperature and equivalent plastic strain along the shear zone.

Shear-localized chip was formed when machining with a -15° rake angle at the two cutting speeds (65 m/min and 488 m/min) and with a -5° rake angle. In shear-localized chip, the material is plastically deformed in the shear zone, due to which heat is generated locally causing temperature gradients to establish. These temperature gradients soften the material causing catastrophic shear between the segments i.e. in the shear zone. This can be the reason for higher values of temperature and equivalent plastic strain in the shear zone.

With a change in chip morphology from shear-localized to continuous, rake angle, the temperature and equivalent plastic strain in the shear zone was observed to be drop significantly. This can be attributed to the dissipation of temperature and distribution of strain throughout the material. The variation in the temperature and equivalent plastic strain in the shear zone is similar to that observed in machining of AISI 4340 steel (325 BHN).

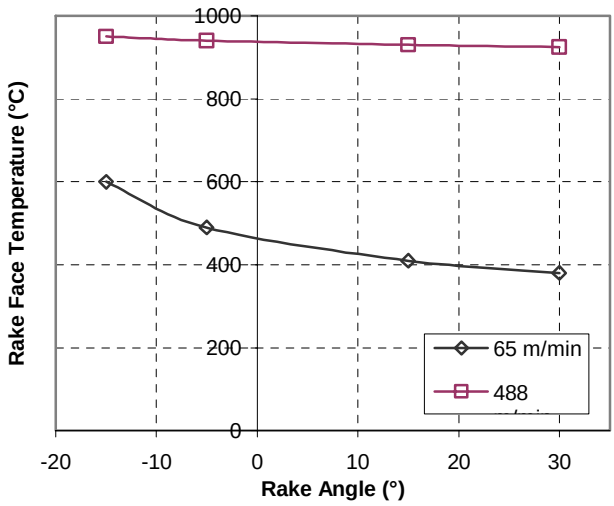

Fig 6.6.6 Tool rake face temperature when machining AISI 4340 steel (215 BHN) with different rake angles (-15°, -5°, 15°, and 30°)

The tool rake face temperature in the machining of AISI 4340 steel (215 BHN) was observed to gradually decrease from the highest value with a -15° rake angle (~ 600°C) to 30° rake angle (~ 380°C) for cutting speed of 65 m/min. At cutting speed of 488 m/min, it was observed to be almost constant for all the rake angles. This trend in the rake face temperature is similar to that observed in the machining of AISI 4340 steel (325 BHN). The decreasing trend of the rake face temperature with change in rake angle from negative to positive at 65 m/min can also be attributed to the amount of work done in the secondary shear zone. Similar explanation for the variation in the rake face temperature can be given for the machining of AISI 4340 steel (215 BHN) as for the machining of AISI 4340 steel (325 BHN), that is the average temperature measured at the tool rake face when shear-localized chip is produced is close to the average temperature measured when continuous chip is produced at the cutting speed of 488 m/min.

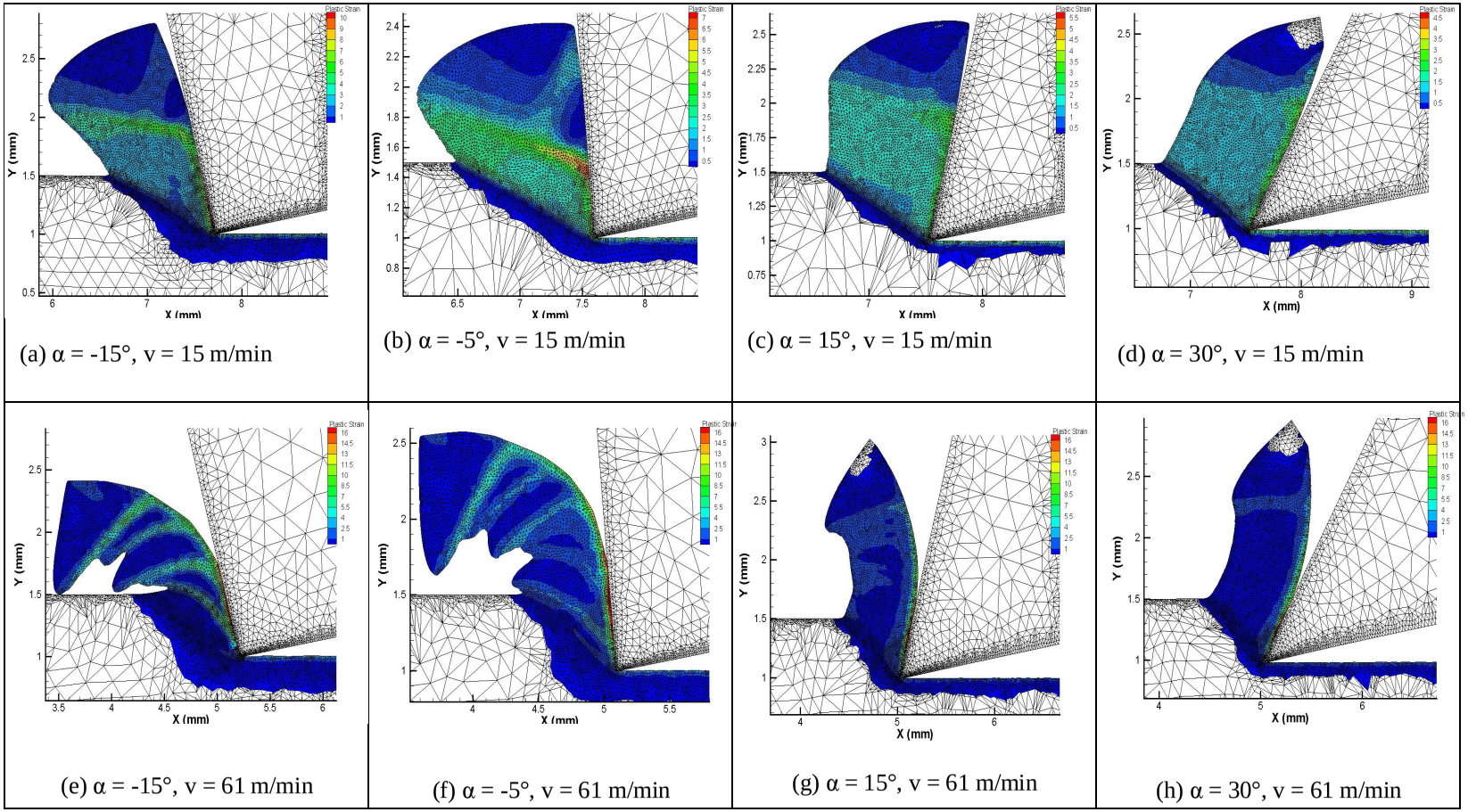

(a) α = -15°, v = 15 m/min

(b) α = -5°, v = 15 m/min

(c) α = 15°, v = 15 m/min

(d) α = 30°, v = 15 m/min

(e) α = -15°, v = 61 m/min

(f) α = -5°, v = 61 m/min

(g) α = 15°, v = 61 m/min

(h) α = 30°, v = 61 m/min

Fig. 6.6.7 Rake angle effect on chip segmentation in the machining of AISI 4340 Steel (520 BHN) at two cutting speeds, namely, 15 m/min and 61 m/min

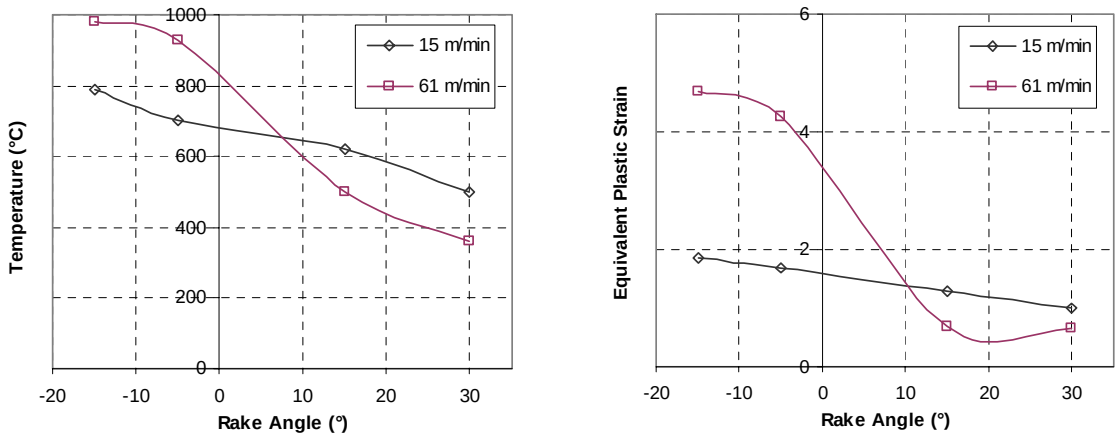

(a) Temperature (b) Equivalent plastic strain

Fig. 6.6.8 (a) Temperature and (b) equivalent plastic strain in the shear zone in the machining of AISI 4340 steel (520 BHN)

A very similar trend in chip morphology (transition) from shear-localized to continuous was observed in AISI 4340 steel of hardness 520 BHN similar to that observed in other two material hardness values (215 BHN and 325 BHN) (see Fig. 6.6.7).

Fig. 6.6.8 shows the variation in the temperature and equivalent plastic strain in the shear zone in the machining of AISI 4340 steel (520 BHN) with rake angles of -15°, -5°, 15°, and 30° at cutting speeds of 15 m/min and 61 m/min, respectively. The variation in the temperature and equivalent plastic strain in the shear zone for all rake angles was observed to be similar to the observations in AISI 4340 steel (325 BHN). Same explanation for the transition in chip morphology with change in rake angle can be given here.

Fig. 6.6.9 shows the tool rake face temperature when machining AISI 4340 steel of hardness 520 BHN with different rake angles -15°, -5°, 15°, and 30°. A similar trend was observed in machining AISI 4340 steel (325 BHN and 215 BHN). Same explanation

for the machining of AISI 4340 steel (325 BHN and 215 BHN) applies to the trend of the rake face temperature plot obtained in the machining AISI 4340 steel (520 BHN).

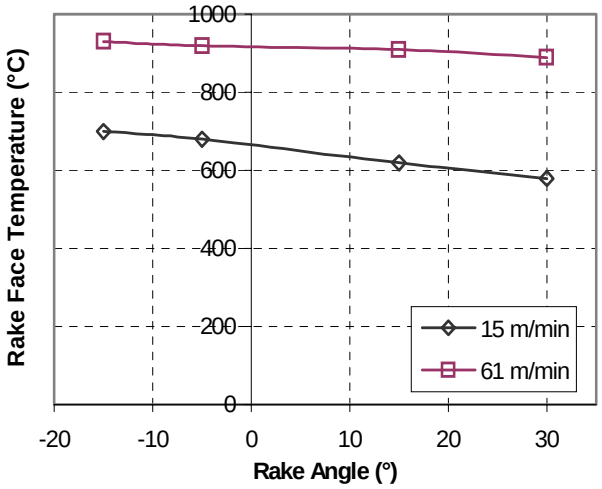

Fig. 6.6.9 Variation of the tool-rake face temperature with rake angles of -15°, -5°, 15°, and 30° in the machining AISI 4340 steel (520 BHN) at cutting speeds of 15 m/min and 61 m/min

6.7 Effect of Contact Length on Chip Segmentation in the Machining of AISI 4340 Steel

Shear-localized chip is mainly formed due to instabilities in the primary shear zone as a result of thermo-mechanical response of AISI 4340 steel when machining at high cutting speeds. Along with this, the chip formation process is influenced by various factors, such as the rake angle, material hardness, and cutting speed as seen in the previous sections. Another factor that can influence the chip formation process discussed the in literature is the contact length between the tool and the chip [3]. To eliminate the shear-localization in the machining of AISI 4340 steel, an attempt was made to artificially change the contact length between the tool and the chip by modifying the tool geometry.

The tool was modified in such a way that the chip will not come in contact with the curved surface once it leaves the rake surface (see Fig. 6.7.1). The rake angle used was -5° and the length of contact was 0.25 mm. The material used was AISI 4340 steel (325 BHN), machined at a cutting speed of 275 m/min and depth of cut of 0.5 mm.

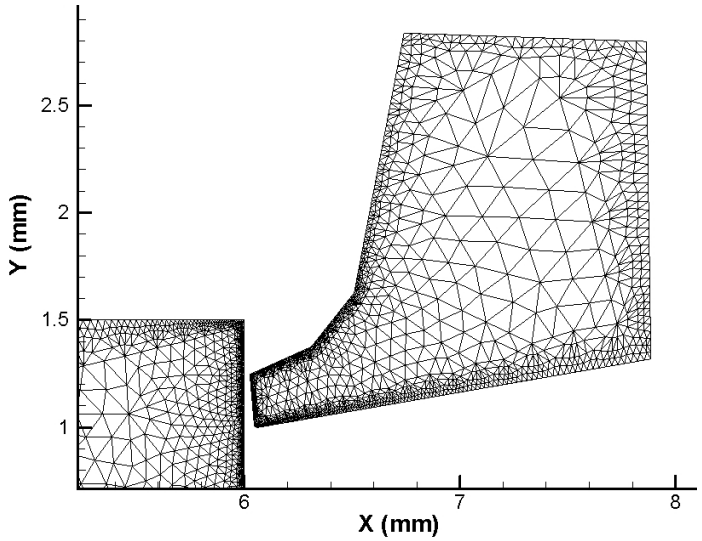

Fig. 6.7.1 Modified tool geometry of reduced contact length between the tool and the chip

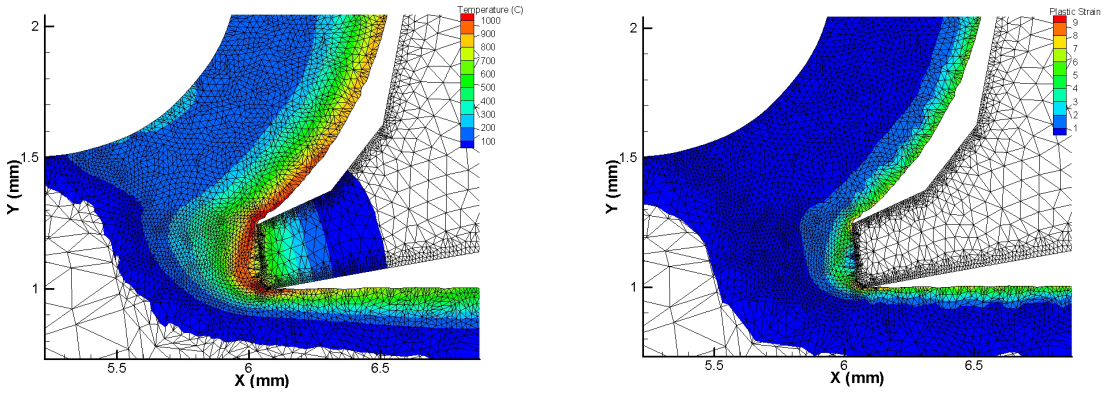

(a) Temperature contours (b) Equivalent plastic strain contours.

Fig. 6.7.2 (a) Temperatures and (b) equivalent plastic strains contours in the machining of AISI 4340 steel (325 BHN) with a controlled contact length tool (α = -5°, v = 275 m/min)

The resultant chip was observed to be continuous (see Fig. 6.7.2) unlike the shear-localized chip [see Fig. 6.4.1 (c) and (d)] obtained with normal tool geometry and similar machining conditions. In this simulation, the contact length was changed from 0.5 mm to 0.25 mm until the shear-localized chip was completely eliminated. This was done by reducing the contact length from 0.5 mm to 0.25 mm in steps of 0.05 mm. During the process, material was observed to form a stagnant built-up surface (accumulation of the material) along the rake face. This made the tool to cut the material with the blunt surface formed in front of the rake face (see Fig. 6.7.3). The material was found to flow around this built-up material along the rake face. Due to the accumulation of material in front of the rake face, the cutting appeared to take place with a positive rake angle instead of original negative rake angle. As the contact between the tool and chip was limited, the chip flow was without any shear-localization in the primary shear zone. Shearing action

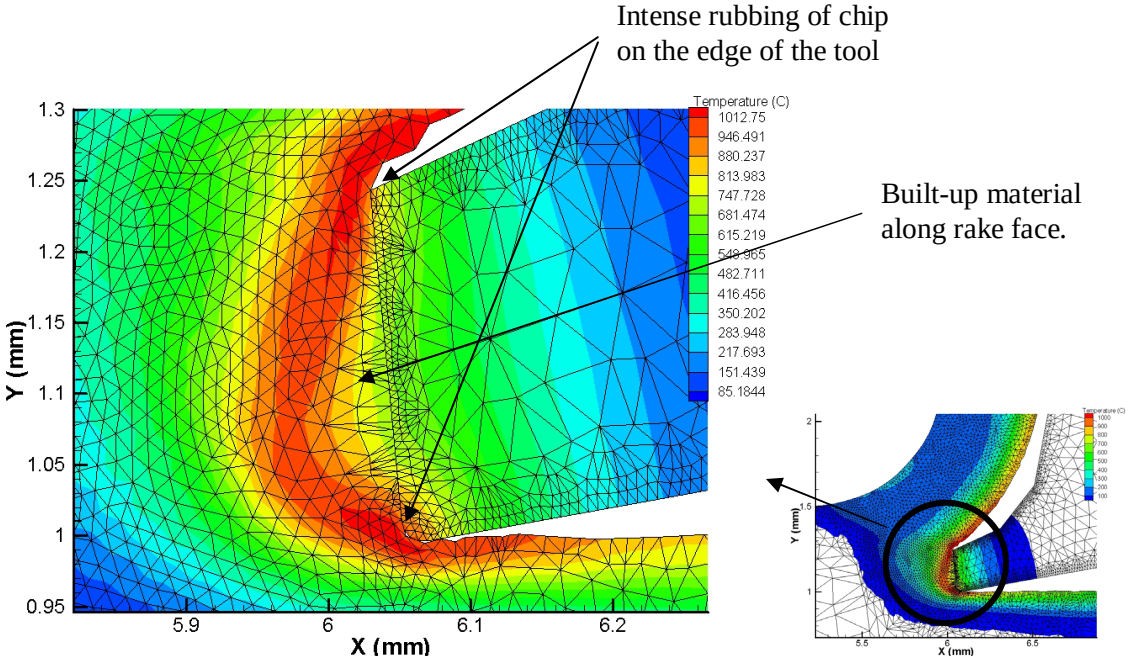

Fig. 6.7.3 Work material built up along the rake face in the machining of AISI 4340 steel (325 BHN) with a controlled contact length tool (α = -5°, v = 275 m/min)

was observed only in the secondary shear zone around the built up material formed in front of the rake face. This can be the reason for the continuous chip formation due to reduced contact length.

Building up of material along the rake face can be helpful in avoiding direct rubbing of the chip on the rake face and hence facilitate in reducing the tool wear. But it can also significantly increase the wear due to intense rubbing action of the chip at the top edge of the rake face and at the tool tip (see Fig. 6.7.3). As the contact area is small at the top edge of the rake face and tool tip, the wearing would be rapid. This can reduce the rake face area, further reducing the strength of the tool with eventual fracturing the tool tip. Therefore, even though this method of eliminating the shear-localized chip with a controlled contact length tool is successful, it requires thorough investigation on the part of tool life.

Chapter 7

CONCLUSIONS

The formation of shear-localized chip due to catastrophic shear instability is the fundamental characteristic of hardened AISI 4340 steel when machined at high cutting speeds. To study this characteristic, a commercial explicit, Lagrangian 2D finite element code *AdvantEdge*™ was used. To model the material behavior Johnson-Cook's constitutive model was employed. A criterion for catastrophic thermo-plastic shear developed by Recht was used as a failure criterion. A user-subroutine was developed to incorporate the Johnson-Cook's constitutive model and Recht's failure criterion. To handle large plastic strains, high strain rates, and high temperatures in the process, continuous remeshing and adaptive meshing was used. The results of the model were compared with experimental results published in the literature [9] and results from another finite element program, ABAQUS. The observations made in the machining simulations of AISI 4340 steel with different hardness values under different conditions were compared with the observations reported in the literature [2, 3, 12, and 19]. With reference to the simulation results and analysis, the following conclusions may be drawn:

1. To simulate the shear-localization phenomenon, Johnson-Cook's material model and Recht's failure criterion were incorporated in the finite element

code through a user-subroutine. The thermoplastic shear instability in the machining process was successfully simulated using *AdvantEdge*™ explicit, Lagrangian finite element code.

2. The use of Johnson-Cook's material model and Recht's failure criterion enabled the simulations to display change in chip morphology with change in cutting speed and rake angle in the machining of AISI 4340 steel for different hardness values.
3. The cutting forces from simulations agree with the experimental results. The maximum difference found was 11%. The temperature and equivalent plastic strain in the shear zone and at the chip-tool interface were also in agreement with the results obtained from ABAQUS analyzed with Johnson-Cook's material model and Johnson-Cook's damage model. The maximum difference found in both temperature and equivalent plastic strain was ~ 6.5% at both the locations.
4. The mechanism of shear-localization in the machining of AISI 4340 steel at high cutting speed was in agreement with the mechanism of shear-localization elucidated by Komanduri *et al.* [2, 3, 12, and 19].
5. Significant influence of material hardness was observed on chip formation process when machining AISI 4340 steel. AISI 4340 steel (215 BHN) showed fully developed shear-localized chip at a cutting speed of 488 m/min, AISI 4340 steel (325 BHN) at 275 m/min, and AISI 4340 steel (520 BHN) at 61 m/min.

6. At high cutting speeds, the plastic deformation was observed to be rapid, causing heat to be generated in the shear zone and establishing temperature gradients in the chip. This resulted in local deformation in the shear zone till the weakening of the material due to temperature rise was equals to or higher than the strengthening of the material due to strain-hardening.
7. With a rake angle of -5° and depth of cut of 0.5 mm, AISI 4340 steel (215 BHN) at a cutting speed of 65 m/min produced continuous chips and at 488 m/min produced shear-localized chips. AISI 4340 steel (325 BHN) produced continuous at cutting speed of 40 m/min, inhomogeneous chips at 125 m/min and fully developed shear-localized chips at 275 m/min. Whereas, AISI 4340 (520 BHN) produced continuous chips at 15 m/min and shear-localized chips at 61m/min. This was in reasonable agreement with the observations reported in the literature [2 and 12].
8. The qualitative comparison of the chip morphology in the machining of AISI 4340 steel (215 BHN), showed a good agreement with the experimental results. Therefore the extrapolated properties for AISI 4340 steel (215 BHN) can be considered to be reasonable valid.
9. When the change in chip morphology from continuous to inhomogeneous was observed with the change in speed, the temperature and equivalent plastic strain in the shear zone were observed to rise steeply. Once shear-localization was set in, it was observed to rise slowly with the cutting speed. This was observed for all hardness values of AISI 4340 steel.

10. The cutting and thrust force from simulation showed a decreasing trend with increase in cutting speed. This trend can be attributed to the localized adiabatic heating in the shear-localized chips. This is due to thermal softening dominating in this region, the material loses strength and thus the force require to cut the material is low.
11. The power required for machining AISI 4340 steel of all the material hardness values showed a linear increase with the cutting speed, regardless of the type of chip formed.
12. The tool with a rake angle -15° produced shear-localized chip for all the cutting speeds and material hardness values in all simulations. With the change in speed from lower to higher with a constant rake angle of -5°, the chip morphology changed from continuous to shear-localized. With a rake angle of 15°, the initial chip morphology is somewhat wavy followed by continuous for all the cutting speeds and material hardness values. Finally, with a rake angle of 30°, the chip produced is continuous regardless of cutting speed and material hardness value. Of course, this would not be possible in practice as the tool would fracture with such a high rake angle.
13. For higher cutting speeds, the temperature and equivalent plastic strain in the shear zone decreases at higher rate than at lower cutting speeds with increase in rake angle from negative to positive (-15°, -5°, 15 and 30).
14. The rake face temperature at higher cutting speed increases slightly as the rake angle is varied from -15° to -5° after which it remained constant from -5° to 30° rake angle.

Future Work

1. A user-subroutine incorporating Johnson-Cook's constitutive model and Recht's classical model for catastrophic failure can be developed for ABAQUS. After successful implementation of the user-subroutine in ABAQUS, the results reported in this investigation can be verified.
2. If the Johnson-Cook's constants for AISI 4340 with hardness of 215 BHN are made available, the results with extrapolated constants for 215 BHN can be verified.
3. Discontinuous chip formation process can be studied by developing a new user-subroutine with enhanced capability of elements deletion for crack initiation and propagation.

REFERENCES

1 Ernst, H., "Physics of Metal Cutting," Machining of Metals, American Society of Metals, Cleveland, Ohio, 1938; (Also Cincinnati Milacron, Inc. Publication No. A-138).

2 Komanduri, R., Schroeder, T., Hazra, J., Von Turkovich, B. F. and Flom, D. G., "On the Catastrophic Shear Instability in High-Speed Machining of an AISI 4340 Steel," Trans. ASME, J. Eng. Ind., 104 (1982) 121-131.

3 Komanduri, R. and Brown, R. H., "The Mechanics of Chip Segmentation in Machining," Trans. ASME J. of Eng. for Ind., 103(1) (1981) 33-51.

4 Kalhori, V., "Modeling and Simulation of Mechanical Cutting," Doctoral Thesis. Lulea University of Technology, Lulea, Sweden, 2001.

5 Shaw, M. C., "Metal Cutting Principles," (3rd Edition) Clarendon Press, Oxford.

6 Childs, T. H. C., Maekawa, K., Obikawa, T., and Yamane, Y., Metal Machining – Theory and Applications, Arnold Publisher, London, 2000.

7 Shaw, M. C., Duke, S. O., Smith, P. A., Cook, N. H., Loewen, E. G., and Yang, C. T., "Machining Titanium," MIT Rep., (1954) (Massachusetts Institute of Technology).

8 Recht, R. F., "Catastrophic Thermoplastic Shear," Trans. ASME Journal of Applied Mechanics, 86 (1964) 189-193.

9 Barry, J., Byrne, G., and Lennon, D., "Observations on Chip Formation and Acoustic Emission in Machining Ti-6Al-4V Alloy" Int. J. of Machine Tools & Manufacturing, 41 (2001) 1055–1070.

10 Semiatin, S. L. and Rao, S. B., “Shear Localization during Metal Cutting,” Mat. Sci. and Engg., 61 (1983) 185-192.

11 Xie, J. Q., Bayoum, A. E., and Zbib, H. M., “A Study on Shear Banding in Chip Formation of Orthogonal Machining,” Int. J. Mach. Tools Manufact., 36(7) (1996) 835-847.

12 Hou, Z. B. and Komanduri, R., “Modeling of Thermomechanical Shear Instability in Machining,” Int. J. of Mechanical Science, 39(11) (1997) 1273-1314.

13 Matsumoto, Y., Barash, M. M., and Liu, C. R., “Cutting Mechanism during Machining of Hardened Steel,” Mat. Sci. and Tech., 3 (1987) 299-305.

14 Lemaire, J. C. and Backofen, W. A., “Adiabatic Instability in the Orthogonal Cutting Steel,” Metall. Trans., 3 (1972) 477-481.

15 Komanduri, R., Flom, D. G., and Lee, M., “Advance Machining Research Program,” Techincal Information Series Report 84 CRD 169, July 1984, By GE Corporate Research and Development, Schnectady, NY.

16 Eu-Gene Ng, El-Wardany, T. I., Dumitrescu, and Elbestawi, M. A., “Physics Based Simulation of High Speed Machining,” International Workshop on Modeling of Machining Operations, 2002.

17 Marusich, T. D. and Ortiz, M., “Modeling and Simulation of High-Speed Machining,” ASME Symposium on Mechanics in Materials Processing and Manufacturing, AMD194: 137-149.

18 Guo, Y. B. and Yen, D. W., “A FEM Study on Mechanisms of Discontinuous Chip Formation in Hard Machining,” Journal of Materials Processing Technology, 2004, Article in Press.

19 Komanduri, R. and von Turkovich, B. F., “New Observation on Mechanism of Chip Formation When Machining Titanium Alloys,” Wear, 69 (1981) 179–188.

20 Strenkowski, J. S. and Carroll III, J. T., “A Finite Element Model of Orthogonal Metal Cutting,” Trans. ASME J. of Engineering For Industry, 107 (1985) 349-354.

21 Carroll III, J. T. and Strenkowski, J. S., “Finite Element Models of Orthogonal Cutting with Application to Single Point Diamond Turning,” Int. J. Mech. Sci., 30 (1988) 899-920.

22 Shi, G., Deng, X. and Shet, C., “A Finite Element Study of the Effect of Friction in Orthogonal Metal Cutting,” Finite Elements in Analysis and Design, 38 (2002) 863-883.

23 Kalpakjian, S., “Manufacturing Processes for Engineering Materials,” 3rd Edition, Menlo Park, Addison-Wesley, California, 1997.

24 Shih, A. J. and Yang, H. T. Y., “Experimental and Finite Element Predictions of the Residual Stresses due to Orthogonal Metal Cutting,” Int. J. Num. Meth. Eng., 36 (1993) 1487–1507.

25 Shih, A. J., “Finite Element Simulation of Orthogonal Metal Cutting,” Trans. ASME J. Eng. Ind., 117 (1995) 84–93.

26 Shih, A. J., “Finite Element Analysis of Orthogonal Metal Cutting Mechanics,” Int. J. Mach. Tools Manuf., 36 (1996) 255–273.

27 Shih, A. J., “Finite Element Analysis of the Rake Angle Effects in Orthogonal Metal Cutting,” Int. J. Mech. Sci., 38 (1996) 1–17.

28 Tyan, T., and Yang, W. H., “Analysis of Orthogonal Metal Cutting Processes,” Int. J. Num. Meth. Eng., 34 (1992) 365–389.

29 K. Komvopoulos and S.A. Erpenbeck, “Finite Element Modeling of Orthogonal Metal Cutting,” Trans. ASME J. Eng. Ind., 113 (1991) 253–267.

30 Huang, J. M. and Black, J. T., “An Evaluation of Chip Separation Criteria for the FEM Simulation of Machining,” Trans. ASME J. of Manufacturing Sci. Engg. (1996) 118-545.

31 Shirakashi, T. and Maekawa, K., “Recent Progress of Computer Aided Simulation of Chip Flow and Tool Damage in Metal Machining,” Proc. of I. Mech. E., J. of Engineering Manufacture, (1996) 233-242.

32 Shirakashi, T. and Obikawa, T., “Recent Progress and Some Difficulties in Computational Modeling of Machining,” Machining Science and Technology, 2(2) (1998) 277-301.

33 Obikawa, T. and Usui, E., “Computational Machining of Titanium Alloy–Finite Element Modeling and a Few Results,” Trans. ASME J. Of Manufacturing Sci. Engg., 118 (1996) 208-215.

34 Obikawa, T., Sasahara, H., Shirakashi, T. and Usui, E., “Application of Computational Machining Method to Discontinuous Chip Formation,” Trans. ASME J. of Manufacturing Science and Engineering, 119 (1997) 667-674.

35 Chao, B. T. and Trigger, K. J., “Controlled Contact Cutting Tool,” Trans. of ASME, 81 (1959) 139-151.

36 Komanduri, R., “Some Clarifications on Mechanics of Chip Formation When Machining Titanium Alloys,” Wear, 78 (1982) 15-34.

37 Schroeder, T. A., “High Speed Machining of Some Aircraft Alloys,” Advanced Machining Research Program Semiannual Technical Report (SRD-81-018) Prepared for Air Force Systems Command by General Electric Co., (1981) Schenectady, NY, 3.1.1-3.3.17.

38 Camacho, G. T. and Ortiz, M., “Adaptive Lagrangian Modeling of Ballistic Penetration of Metallic Targets,” Computer Methods in Applied Mechanics and Engineering, 142 (1997) 269-301.

39 Lemonds, J. and Needleman, A., “Finite Element Analyses of Shear Localization in Rate and Temperature Dependent Solids,” Mechanics of Materials, 5 (1986) 339-361.

40 Lemonds, J. and Needleman, A., “An Analysis of Shear-Band Development Incorporating Heat Conduction,” Mechanics Of Materials, 5 (1986) 363-373.

41 Needleman, A., “Dynamic Shear-Band Development in Plane Strain,” Trans. ASME J. of Applied Mechanics, 56 (1989) 1-9.

42 Zhou, M., Needleman, A., and Clifton, R. J., “Finite Element Simulations of Shear Localization in Plane Impact,” J. of Mech. Phys. Solids, 42(3) (1994) 423-458.

43 Baker, M., Rosler, J., and Siemers, C., “A Finite Element Model of High Speed Metal Cutting with Adiabatic Shearing,” Computers and Structures, 80 (2002) 495-513.

44 Baker, M., Rosler, J., and Siemers, C., “The Influence of Thermal Conductivity on Segmented Chip Formation,” Computational Materials Science, 26 (2003) 175-182.

45 Baker, M., “An Investigation of the Chip Segmentation Process using Finite Elements,” Technische Mechanik, 23(1) (2003) 1-9.

46 Baker, M., “The Influence of Plastic Properties on Chip Formation,” Computational Material Science, 28 (2003) 556-562.

47 Hibbitt, Karlsson, and Sorenson Inc, 2002, ABAQUS^{TM} Theory Manual Version 6.3, Providence, RI.

48 Komanduri, R. and Hou, Z. B, “On Thermoplastic Shear Instability in the Machining of a Titanium Alloy (Ti-6Al-4V),” Metallurgical and Material Trans. A, 33A (2002) 2995-3010.

49 Hua, J. and Shivpuri, R., “Influence of Crack Mechanics on the Chip Segmentation in Machining of Ti-6Al-4V,” Advances in Concurrent Engineering, (2002) 357-365.

50 Shivpuri R. and Hua, J., “Prediction of Chip Morphology and Segmentation during the Machining of Titanium Alloys,” J. of Mat. Proc. Tech., 150 (2004) 124-133.

51 Nakayama, K., “The Formation of Saw Tooth Chips,” Proc. Int. Conf. on Prod. Engg., Tokyo, (1974) 572-577.

52 Eu-Gene Ng and Aspinwall, D. K., “Modeling of Hard Part Machining,” Journal of Materials Processing Technology, 5756 (2002) 1-8.

53 Eu-Gene Ng, Aspinwall, D. K., Brazil, D., and Monaghan, J., “Modeling of Temperature and Forces When Orthogonally Machining Hardened Steel,” International Journal of Machine Tools and Manufacture, 39 (1999) 885-903.

54 Third Wave AdvantEdge Theoretical Manual, Version 3.3., 1998.

55 Johnson, G. R. and Cook, W. H., "A Constitutive Model and Data for Metals Subjected to Large Strains, High Strain Rates and High Temperatures," Proc. of the Seventh International Symposium on Ballistic, The Hague, The Netherlands, (1983) 541-547.

56 Liang, R. and Khan, A. S., "A Critical Review of Experimental Results and Constitutive Models for BCC and FCC Metals over a Wide Range of Strain Rates and Temperatures," Int. J. of Plasticity, 15 (1999) 963-980.

57 Poulachon, G., Moisan, A. and Jawahir, I. S., "On Modeling the Influence of Thermo-Mechanical Behavior in Chip Formation During Hard Turning of 100Cr6 Bearing Steel," Annals of the CIRP, 50/1 (2001) 31-36.

58 Metals Handbook, Desk Edition, Second Edition, ASM International.

59 Alcaraz, J. L., Lorenzo, I., and López L. N., "Thermomechanical Analysis of a Chip Machining Process," ABAQUS User's Conference 2003.

60 Shirakashi, T., "New Trends on Machining Theory," Int. J. Jpn. Soc. Proc. Engg., 27 (1993) 299-311.

61 Komanduri, R., and Schroeder, T.A., "On shear instability in machining a Nickel-Iron base superalloy," Transactions of ASME, Journal of Engineering for Industry 108 (1986) 93-100.

APPENDIX

User subroutine developed in this study for applying Johnson-Cook material model and Recht's criterion for thermoplastic shear instability.

```
c**********************************************************************
*
      SUBROUTINE MAT_USER(sig,dtime,temperature,ql,epsl,d,deps)
c
      implicit real*8 (a-h,o-z)
c
c        Defomation tensor * dtime (strain increment)
c       deps(1,1) = Dxx*dtime, deps(1,2)=Dxy*dtime, deps(2,2)=Dyy*dtime
c
c                 Material propeties are read from _wp.twm file
c
c                 Researved parameters
c                 d(2)           Densitiy (scaled)
c                 d(5)           lambda (Lame's constant)
c                 d(6)           mu (Lame's constant)
c                 d(7)           SIGMA0 (Yield stress)
c                 d(24)

c                 User parameters
c                 d(25)          E
c                 d(26)          xnu
c                 d(27)          sigma0
c                 d(28)          epsl0
c                 d(29)          A
c                 d(30)          B
c                 d(31)          C
c                 d(32)          dn
c                 d(33)          dm
c                 d(34)          epsldot0 : reference plastic strain
rate
c                 d(35)          epsldotcutoff :cutoff plastic strain
rate
c                 d(36)          Tm : Melting Temperature
c                 d(37)          Tr : Room Temperature
c                 d(38)          f : feed rate in m
c                 d(39)          thc : thermal conductivity
c                 d(40)          cp : heat capacity
c
c                 Reserved parameters
c
c                 d(83)          DENSITY
c                 d(84)          HEAT CAPACITY
c                 d(98)          Conductivity
c                 d(100)         Density (thermal)
c
c**********************************************************************
*

c                 Radial Return method  elastic perfect-plastic
material
c
      real*8 sig(3,3),dtime,epsl(3,3),d(100),ql(15),deps(3,3)
```

```
      real*8 temperature
      real*8 sigtr(3,3),sigdiv(3,3),q(3,3)

        parameter ( zero = 0.d0, one = 1.d0, two = 2.d0, three = 3.d0,
     *       third = one / three, half = 0.5d0, twothds = two / three,
     *       op5 = 1.5d0 )

            e           = d(25)
            xnu         = d(26)
            sigma0      = d(27)
            epsl0             = d(28)
            A           = d(29)
            B           = d(30)
            C           = d(31)
            dn          = d(32)
            dm          = d(33)
            epsldot0    = d(34)
            epsldotcutoff     = d(35)
            Tm          = d(36)
            Tr          = d(37)
            f           = d(38)
            thc         = d(39)
            cp          = d(40)

            d2mu        = e / ( one + xnu )
            d3mu        = 1.5 * d2mu
                  dLambda     = d2mu * xnu / ( one - two * xnu )

c**********************************************************************
*
c     Initialize plastic work (heat generation)
        ql(3)= 0.0d0
        deltaLamTotal = 0.0d0

c************************************************************
       epsldotstar = ql(4) / epsldot0

c     Elastic stress increment
        tm1 = dLambda*(deps(1,1)+deps(2,2)+deps(3,3))
        sigtr(1,1) = sig(1,1) + d2mu*deps(1,1)+tm1
        sigtr(2,2) = sig(2,2) + d2mu*deps(2,2)+tm1
        sigtr(3,3) = sig(3,3) + d2mu*deps(3,3)+tm1
        sigtr(1,2) = sig(1,2) + d2mu*deps(1,2)
        sigtr(2,1) = sigtr(1,2)

50    continue
c************************************************************

c     Calculate Deviatoric stress
        call umat_div_stress(sigtr,sigdiv)

c     Calculate deviatroic stress norm
        sigma_e = umat_sigdiv_norm(sigdiv)

c************************************************************

c      If plastic strain rate is below cut off, set
```

```
c       approximation
c      to cut off no strain rate hardening will occur

       Tstar = (temperature - Tr)/(Tm - Tr)

c      Yield stress
       sigmaJC= (A+B*ql(1)**dn)*(1-
*           Tstar**dm)*(1+C*dlog(epsldotstar))

c**********************************************************************
       Ep= (dn*B*ql(1)**(dn-1))*(1-Tstar**dm)*(1+C*dlog(epsldotstar))

       if(ep .ge. e)then
       ep = e - 1
       endif

       dH = (Ep * e)/(e - Ep)

c**********************************************************************
c      Strain increment (Radial return method)
       denom = d2mu*(1.0d0+dH/(d3mu))
       deltaLam =(sigma_e-dsqrt(2.0d0/3.0d0)*sigmaJC)/denom

      if (deltaLam.le.0.0d0 .or. deltaLam.lt.1.0e-12) goto 100

c**********************************************************************
c     Case of plasticity
       factor = 1.0d0/sigma_e

       q(1,1)= factor*sigdiv(1,1)
       q(2,2)= factor*sigdiv(2,2)
       q(3,3)= factor*sigdiv(3,3)
       q(1,2)= factor*sigdiv(1,2)
       q(2,1)= factor*sigdiv(1,2)

       deltaLamTotal = deltaLamTotal + deltaLam

c      Updated  stress

       sig(1,1) = sigtr(1,1)-deltaLam*d2mu*q(1,1)
       sig(2,2) = sigtr(2,2)-deltaLam*d2mu*q(2,2)
       sig(3,3) = sigtr(3,3)-deltaLam*d2mu*q(3,3)
       sig(1,2) = sigtr(1,2)-deltaLam*d2mu*q(1,2)
       sig(2,1) = sig(1,2)

       sigtr(1,1)=sig(1,1)
       sigtr(2,2)=sig(2,2)
       sigtr(3,3)=sig(3,3)
       sigtr(1,2)=sig(1,2)
       sigtr(2,1)=sig(1,2)

       goto 50

100   continue

c**********************************************************************
```

```
c        Plastic strain
        ql(1)=ql(1) + deltaLamTotal * ((2/3)**0.5)

c       Plastic strain rate
        ql(4)= deltaLamTotal/dtime

c       Plastic work rate (heat generation)
        ql(3)= deltaLamTotal * sigmaJC/dtime

c        Updated  stress
        sig(1,1) = sigtr(1,1)
        sig(2,2) = sigtr(2,2)
        sig(3,3) = sigtr(3,3)
        sig(1,2) = sigtr(1,2)
        sig(2,1) = sigtr(1,2)
c
c*********************************************************************
c     for Pure RECHT formulation

        tau = sigma0 / dsqrt(3.0d0)

c     common terms


      constant = 1 / (2 * 4.1868 * dsqrt(3.1428*d(83)*thc*cp))


      DNUM = (dn*B /3)*(ql(1)**(dn-1))*(1- Tstar**dm)


      DENOM1 = (1/dsqrt(3.0d0)) * (A + B * (ql(1)**dn))
     *                  *(- dm/ (temperature - Tr)) * (Tstar**dm)

      DENOM2 = constant * tau * f * dsqrt (ql(4)/(ql(1)- epsl0))


      R = -DNUM / ( DENOM1 * DENOM2 )

      if(R .gt. 0.0d0 .and. R .lt. 1.0d0) then
           sig(1,1) = 0.d0
           sig(2,2) = 0.d0
           sig(3,3) = 0.d0
           sig(1,2) = 0.d0
           sig(2,1) = 0.d0
      end if
c*********************************************************************
       END SUBROUTINE
c*********************************************************************

      double precision function umat_sigdiv_norm(sigdiv)
c
c     Calculate diviatoric stress norm
c
      real*8 sigdiv(3,3)
      real*8 sigma_norm
c
       sigma_norm = sigdiv(1,1)*sigdiv(1,1)
```

```
     1             +sigdiv(2,2)*sigdiv(2,2)
     1             +sigdiv(3,3)*sigdiv(3,3)
     1       +2.0d0*sigdiv(1,2)*sigdiv(1,2)

      umat_sigdiv_norm = dsqrt(sigma_norm)
      return
      end

c**********************************************************************

      SUBROUTINE umat_div_stress(sig,sigdiv)
c
c     Calculate Deviatoric stress
c
        real*8 sigdiv(3,3),sig(3,3),pressure
        pressure = (sig(1,1)+sig(2,2)+sig(3,3))/3.0d0
        sigdiv(1,1) = sig(1,1)-pressure
        sigdiv(2,2) = sig(2,2)-pressure
        sigdiv(3,3) = sig(3,3)-pressure
        sigdiv(1,2) = sig(1,2)
        sigdiv(2,1) = sig(2,1)

      return
      end

c**********************************************************************
```

VITA

Parag Purshottam Konde

Candidate for the Degree of

Master of Science

Thesis: FINITE ELEMENT ANALYSIS OF SHEAR-LOCALIZATION IN HIGH-SPEED MACHINING OF AISI 4340 STEEL

Major Field: Mechanical Engineering

Biographical:

Personal Data: Born in Pune, India, On December 22, 1978, the son of P. S. Konde and M. P. Konde.

Education: Received Bachelor of Engineering degree in Mechanical Engineering from University of Pune, India in November 2000. Completed the requirements for the Master of Science degree with a major in Mechanical Engineering at Oklahoma State University in December 2004.

Experience: Graduate Research Assistant in Mechanical and Aerospace Engineering Department, Oklahoma State University, Stillwater, Oklahoma, from August 2002- present.

Name: Parag Konde Date of Degree: December, 2004

Institution: Oklahoma State University Location: Stillwater, Oklahoma

Title of Study: FINITE ELEMENT ANALYSIS OF SHEAR- LOCALIZATION IN HIGH SPEED MACHINING OF AISI 4340 STEEL

Pages in Study: 121 Candidate for the Degree of Master of Science

Major Field: Mechanical Engineering

Scope and Methodology of Study: Hardened AISI 4340 steel is one of the difficult-to-machine materials. As the cutting speed increases, the chip morphology changes from discontinuous chip, to continuous chip, to shear-localized chip. At speeds above this, the shear-localized chips continue to form except that instead of continuous series of segments in the chips, the segments get isolated. As the hardness of the workmaterial increases, these transitions occur at much lower speeds. To understand the mechanism of chip formation in high-speed machining of AISI 4340 steel, finite element analysis is used. It is a Lagrangian explicit finite element code available commercially (*AdvantEdge*^{TM}). To overcome the problems associated with extensive element distortion, adaptive meshing and remeshing are used. Johnson-Cook's material model that is capable of giving flow stresses at various strains, strain rates, and temperature is used along with Recht's catastrophic shear failure criterion. A user-subroutine (UMAT) is developed to incorporate Johnson-Cook's material model and Recht's catastrophic shear failure criterion in the finite element code. Effects of workmaterial hardness, cutting speed, tool rake angle, and contact length on the chip morphology, temperature, strains, forces, and power are investigated.

Findings and Conclusions: Finite element analysis of the machining of AISI 4340 steel is studied for different hardness values, viz., 215 BHN, 325 BHN, and 520 BHN. The cutting speed used are 65 m/min and 488 m/min to machine AISI 4340 steel (215 BHN), 40 m/min, 125 m/min, and 275 m/min to machine AISI 4340 steel (325 BHN), 15 m/min and 61 m/min to machine AISI 4340 steel (520 BHN). The tool rake angles used for all the simulations are -15°, -5°, 15°, and 30° and the depth of cut used is 0.5 mm. The model is validated by comparing the simulation results with the experimental results published in the literature and also with the results from another finite element code, ABAQUS for which conventional method of Johnson-Cook's constitutive and damage model was used. The results of the present investigation agree reasonably with the experimental results published in the literature (difference less than 11%). Also, the shear-localization process agrees closely with the process published in the literature.

ADVISOR'S APPROVAL: Dr. Ranga Komanduri